Czech Technical University in Prague

Faculty of Electrical Engineering

Doctoral Thesis

August 2019

Pavel Puričer

Czech Technical University in Prague

Faculty of Electrical Engineering
Department of Radioelectronics

ADS–B Signal Processing Improvement in Difficult Environment

Doctoral Thesis

Pavel Puričer

Prague, August 2019

Ph.D. Programme: P2612 Electrical Engineering and Information Technology
Branch of study: 3708V017 Air Traffic Control

Supervisor: ***Doc. Dr. Ing. Pavel Kovář***

Abstract

The presented thesis is aimed on identification and description of basic principles related to radar signal detection, reception, and processing with special focus on ADS–B system signals, using Mode S extended squitter format. The reception of such signals is analyzed here for difficult propagation environment, typical for airport area, where signal blockage and multipath propagation occurs due to presence terrain and manmade obstacles and structures. The impact to airplanes and vehicles position determination is presented in the document, either by affecting detection and decoding of position message data or by increase of TDoA solution error in multilateration systems. The analysis of the TdoA based multilateration position computation is provided with thecomputed Cramer-Rao lower bound for arbitrary 3D positions of stations. There is proposed an enhancement of ADS–B system performance using second order correlation detector and radio channel modeling with use of radio channel equalization. The proposed methods are supported by simulations and results of application on real measured ADS–B data.

Keywords: ADS–B; Mode S; multipath propagation; signal detection; equalization; radio channel model

Anotace

Předkládaná práce se zaměřuje na stanovení a popis základních principů detekce, příjmu a zpracování radarových signálů se zvláštním zaměřením na signály systému ADS-B vysílané ve formátu Mode S extended squitter. Příjem takových signálů je zde analyzován pro případ šíření ve složitém prostředí typickém pro pozemní plochy letiště. Pro toto prostředí jsou běžné jevy jako blokování přímé cesty signálu nebo mnohacestné šíření signálu způsobené terénem nebo překážkami a strukturami. Ve studii je uveden jejich vliv na určení polohy letadel a vozidel, a to jako zhoršení možnosti detekce a dekódování dat polohové zprávy nebo jako zvýšení chyby řešení hyperbolické navigační úlohy pro multilateraci. Je provedena anlayza způsobu určení polohy při řešení TDoA úlohy a vypočtena Cramer-Raova dolní mez pro obecný počet stanic v trojrozměrném prostoru. V práci je předložen návrh zlepšení parametrů ADS–B systému použitím detekce založené na korelaci druhého řádu a modelování a ekvalizace rádiového kanálu. Navržené metody jsou podpořeny simulacemi a výsledky získanými aplikací na měřeních reálných ADS–B signálů.

Klíčová slova: ADS–B; Mode S;mnohacestné šíření; detekce signálu; ekvalizace; model rádiového kanálu

Acknowledgment

I would like to thank Pavel Kovář for his intensive care, guidance, and support during my work on the thesis and also for a provision of opportunity to work on projects in the area of signal processing and radio reception.

I would like to thank professor František Vejražka for bringing me to the area of radionavigation, satellite navigation, and radar and for the possibility to participate on the research lead by his person.

Iwould like to deeply thank to my family for the unlimited support and love throughout my whole study and life.

Table of Contents

List of acronyms and abbreviations

AA – Address Announced
ACAS – Airborne collision avoidance system
ACF – Autocorrelation function
ADS–B – Automatic dependent surveillance – broadcast
ADS–R – Automatic dependent surveillance – rebroadcast
AF – Application Field (CA equivalent for DF19 reply)
AoA – Angle of arrival
ATC – Air traffic control
CA – Capability Field
CDF – Cumulative distribution function
CF – Capability Field (CA equivalent for DF18 reply)
CRC – Cyclic redundancy check
CRLB – Cramer–Rao lower bound
DF – Downlink format
DoA – Direction of arrival
DOP – Dilution of precision
EHS – Enhanced surveillance
ELM – Extended length message
FIM – Fisher information matrix
GDOP – Geometrical dilution of precision
GLRT – General likelihood ratio test
GNSS – Global navigation satellite system
GPS – Global positioning system
HAE – Height above ellipsoid
HDOP – Horizontal dilution of precision
ICAO – International Civil Aviation Organization
IFF – Identification Friend or Foe
LOS – Line-of-sight
LS – least squares
MIMO – Multiple input, multiple output
ML – Maximum likelihood
MLAT – Multilateration
MMSE – Minimum mean square error
MSE – Minimum square error
NAC – Navigation Accuracy Category
NIC – Navigation Integrity Category
NLOS – Non-line-of-sight
OOK – On-Off keying
PDF – Probability density function
PI – Parity identification
PPM – Pulse position modulation
RMS – Root mean square
RSS – Received signal strength
RTT – Round trip travel

SDR – Software defined receiver
SFU – Solar flux unit
SIL – Surveillance Integrity Level
SLM – Standard length message
SMGCS – Surface Movement Guidance and Control System
SMR – Surface movement radar
SNR – Signal to noise ratio
SSR – Secondary surveillance radar
TDoA – Time difference of arrival
TIS–B – Traffic information service – broadcast
ToA – Time of arrival
TSS – Target state and status
WLAN – Wireless local area network
WSS – Wide sense stationary
WSSUS – Wide sense stationary uncorrelated scattering

1 Introduction

As global transport increases both in personal and cargo sectors, the rapid growth of air transport is its integral part. According to EUROCONTROL prognosis [1] for ESRA (EUROCONTROL Statistical Reference Area) the growth of global air traffic between 2013 and 2035 will increase by factor 1.8 which will lead to more than 17 million of IFR flights in 2035 throughout the Europe. The similar numbers (approx. doubled amount of travelers between 2014 and 2034) are presented by IATA for world passengers' air traffic [2].

The natural traffic bottleneck is then close vicinity to airport and its ground area (runways, taxiways, apron). The density of the traffic is further increased by presence and movements of supporting vehicles ("follow-me" cars, passenger buses, fuel and maintenance cars, cargo operation vehicles, emergency and rescue units, etc.). Such situation brings new challenges to air traffic control operations and supporting systems.

The key task for ATC is to ensure a safe spacing between aircrafts and vehicles in aerodrome movement area (usually stated by the term airport airside area) and to avoid or significantly reduce amount of incidents that can in such area occur. The complications for such task can include the increasing number of operations that are made under low visibility conditions, the already mentioned growth of traffic, and complex layout of modern airports.

General movement and operations at an airport airside area rely on air traffic controllers, pilots, and drivers using visual-based observations to evaluate the mutual positions of aircraft and vehicles. Pilots and vehicle drivers further use visual aids provided by airport infrastructure (light systems, markings, and signs) to guide them along their assigned routes and to identify intersections and holding positions. In case of low visibility conditions the air traffic controllers rely on pilot's and driver's reports and data from surface movement radar to monitor moving objects positions and spacing to identify and avoid potential conflicts. The efficiency of the operation under such low visibility conditions is decreasing and thus the capacity of the airport is lowered as well.

The airport infrastructure that helps to plan and realize movements on the surface of the aerodrome is called Surface Movement Guidance and Control System (SMGCS). It consists of guidelines, signs, taxiway lines, and stop bars providing guidance to aircrafts and vehicles for all airside area of the airport. The plan of movements is then controlled by orders of ATC. The augmentation of surveillance information for low visibility conditions is ensured usually by surface movement radar (SMR). This system is based on primary radar principle in X to Ka frequency bands (i.e. 10-40 GHz) and provides an image of the airport area with typical refresh rate of 1 second. The primary radar operation principle however does not provide joint identification of imaged object and its performance is still affected by signal transmission environment (terrain, obstacles, interference, multipath propagation).

These described aids and systems are called non-cooperative surveillance systems because their operation does not require special equipment on board of an aircraft or a vehicle. They are at present airports combined with cooperative surveillance system that collect information about the aircraft of vehicle from an active element of the transponder equipment. This technique allows collecting more moving object parameters than the non-cooperative surveillance, for instance the aircraft or vehicle identity. The typical representatives of such cooperative system are a secondary surveillance sadar (SSR) in Modes A/C/S or its modification, ADS-B system. The combination is then called Advanced Surface Movement Guidance and Control System (A-SMGCS) and is more and more often installed at present airports. The ADS-B system seems to be now the most prospective technology for surveillance and ATC purposes and is planned to be fully implemented in the civil aviation sector at last in the 2020 [3], [4].

Such advanced systems enable to increase efficiency in traffic surveillance and control and thus enhance the capacity of airport or maintain current capacity under low visibility conditions. Although the benefits are significant, the performance of these systems is still affected by signal propagation and reception difficulties due to interference and environment impacts. The research of the methods that can bring an improvement to the quality of service these systems can provide in the difficult environment is in the focus of many present research activities and is the task that works this thesis as well.

1.1 Scope of the thesis

Since the ADS–B signal can be used for position determination in air traffic management in several ways, the information oriented way, using the ADS–B message content, and the radio signal way, using the ADS–B signal as a pattern for surveillance methods, the aim of the thesis is to analyze and determine the mean influences on the ADS–B signal from both points of view with focusing on the environment, typical for airport area and its close vicinity. The content of the thesis should propose a approach, how to positively influence the signal processing to improve performance of ADS–B signal use. The main work is focused on ADS–B signal detection and processing in a difficult environment.

1.2 Contributions

The contributions I have made in the frame of this thesis can be summarized to following points:

- In the section concerning the use of ADS–B signal for multilateration based of time difference of arrival (TDoA), I have calculated Cramer-Rao lower bound extended from standard published 2D case to the full 3D case for arbitrary number of stations and arbitrary location of the stations. The values were then demonstrated by simulations for selected constellations.

- In the section concerning detection of ADS–B signal I have proposed a detection solution based on second order correlation between received signal and the replica and compared its performance with conventional detectors used in radar based on integration or matched filter. The proposed detector has shown better or at least comparable performance to the matched filter and provided successful detection and determination of signal relative delay in simulated channel with multipath propagation.
- In the section concerning ADS–B channel estimation and equalization I have applied the equalization algorithm on the signal received through difficult environment, mainly characteristic by multipath propagation and verified this approach, known from communication systems but not commonly applied to the ADS–B signal, both on simulated and real data.

1.3 Other activities related to the theme of the thesis

During the work on the thesis, I have participated on several research project that were coherent with the thesis topic or related to the principles the thesis discusses about. The most significant activities were as follows

- In the frame of the project TA01030722 "*ADS-B/TIS-B*" of The Technological agency of the Czech Republic I have participated on the measurement campaign for estimation of parameters for ADS–B channel parameters at the Prague Vaclav Havel airport and worked on processing of measured data with estimation of channel impulse response [5].
- In the frame of the research project of EC (European Commission) CZ.02.1.01/0.0/0.0/15_003/0000481 "*Center of Cosmic Rays and Radiation Events in the Atmosphere*" I have participated on the design, development, and signal processing of specialized software receiver in the frequency band 1–2 GHz for the registration and evaluation of interference caused by solar radio bursts in the operation band of Mode S radar and global navigation satellite systems (GNSS) [6].
- In the frame of the project of Ministry of Interior of CR VI20172019090 "S*trategic infrastructure protective system detecting illegal acts affecting GNSS signals*" I have participated on the design of positioning algorithms for localization of interfering radio source.

1.4 Outline of the thesis

The thesis is separated to several thematic chapters. Each chapter includes in text an information about current state of art together with references to the relevant literature.

The Chapter 2 describes the approaches used for position determination and surveillance used in the air transportation with focus on radar and more closely, on secondary surveillance radar.

The Chapter 3 informs in detail about the subclass of secondary surveillance radar services, the Automatic Dependent Surveillance–Broadcast (ADS–B), a main object of the thesis. There is described a message format and content and definition of signal in space.

The Chapter 4 provides an overview about the methods that are generally used for position determination. The principle of each method is provided together with current state of art.

The Chapter 5 describes the multilateration concept, at present popular method of determination of position based on time difference of arrival. The more detailed description of the method is provided together with the calculations of Cramer-Rao bound for TDoA, a theoretical limit that can be reached with optimal system. The impact of the stations constellation is discussed in this chapter as well with provision of dilution of position parameter. Then the several approaches for TDoA position solution task are presented, both iteration based and direct solution and their benefits and drawbacks are discussed.

In the Chapter 6 are presented main approaches to the radio channel description and modeling, the models based on statistical parameters and theoretical calculations are summarized with the intent of provision of base information about channel models that will be used for signal detection and estimation operations in following chapters.

The Chapter 7 is focused on mechanisms related to the ADS–B signal detection and decoding. The general approach to decoding of radio signal is introduced and the typical detector solutions are provided based on current state of art. The other kind of detector based on second order of correlation is proposed here and its performance is compared with previously provided detectors. The main intent is dedicated to the environment with multipath propagation which is typical for area with obstacles and can occur at the airport.

The Chapter 8 presents the methods of channel estimation and equalization, provides the typical solution for wide sense uncorrelated scattering channel model with derivation of equalizer solution and performance metric. The chosen equalization algorithm is evaluated on simulated data related to signal in environment typical with multipath propagation. The evaluated algorithm is then tested on real ADS–B data and compared with third party solutions.

The Conclusions and Outlook chapter summarizes achieved results and provides a discussion about possible ways to further development af activities in the investigated research area.

2 Position determination in air transportation

2.1 The secondary surveillance radar

The necessity to reduce ambiguity in tracked airborne targets bring the call for enhancement of classical primary radar technology. The preliminary trials came already in the time of Second World War with the introducing system of identification “Friend or Foe”[7]. Such enhancement in identification was valuable also in the following progress of civilian air transport and the air traffic control connected with it. The answer was secondary radar bringing the change in operation principle from plain echolocation to work with cooperative targets [8]. In this chapter, the brief description of such system will be provided as it forms a structural background to the signals processed in the thesis.

The secondary surveillance radar (SSR) is a ground based position determination and surveillance system working on principle of two-way communication with cooperating target (airplane, vehicle, stationary station).

It consists of two basic elements: the ground station that executes uplink interrogations (questioning) to the targets in operation range of system and the downlink replying targets equipped with proper responding devices (transponders). The targets generate replies as an reaction to interrogation in predefined manner, varying according to the mode of operation and capability of the on-board transponder. The interrogations and the replies are transmitted on separate frequencies, 1030 MHz (uplink) and 1090 MHz (downlink), respectively, to reduce clutter and false targets generated by possible reflections.

Since classical SSR system uses narrow beam rotating antenna and is very often coupled with primary radar it is capable to estimate target distance and azimuth using standard radar techniques (i.e. time of travel for sent pulse signals). The data provided by transponder reply then enhance information about particular target by the extents varying with used modes of operation. The basic modes for civilian use of SSR are A, C, S, and intermode. In case of SSR mode A, the transponder sends in the reply identification of the airplane, so called “squawk code”, in SSR mode C, the reply contains the encoded barometric altitude of the responsing plane. In both modes A and C, the replies come form all targets that are in the reception range of interrogation from the ground station. The mode S differs by format of the reply and also by the fact, that the target is interrogated selectively and thus only single airplane replies. Moreover, the content of the reply can differ. The intermode operation enables to request replies from combination of transponders with different modes, intermode A/C all-call interrogation causes replies from transponders working in mode A or mode c and suppress replies from Mode S transponders, intermode A/C/S provides all-call interrogation enabling all the transponders to reply according its particular modes, so it initiates responses from mode A, mode C and also from mode S transponders.

Since the processing of the signals in this thesis is focused on the downlink frequency 1090 MHz, the interrogation signals, their description, format, and content will be omitted and the description will be aimed to reply signals. Nevertheless, the description of interrogations can be found for example in [9].

2.1.1 Mode A/C

The interrogation in mode A or mode C emits the reply in appropriate mode. The signal in space format is common for both modes and is in the form of sequence of pulses as depicted on Figure 2.1.

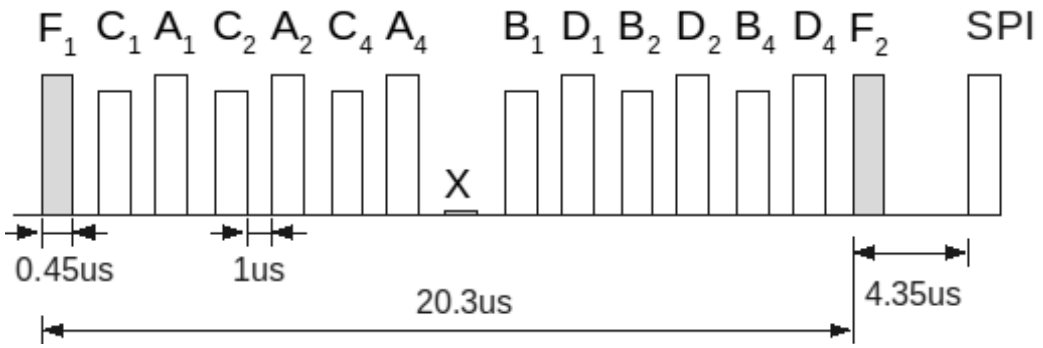

Figure 2.1 SSR Mode A/C reply signal in space format

The message is defined by two framing pulses, F_1 and F_2, that are separated by interval 20.3 μs and present in every reply. The data pulses in between framing pulses have common width of 0.45 μs with tolerance ±0.1 μs and their positions are in increments of 1.45 μs counted from the first framing pulse F_1 with tolerance ±0.1 μs. Special position identification pulse (SPI) is transmitted only for Mode A reply and as a result of manual (pilot) selection and shall be spaced at an interval of 4.35 microseconds following the last framing pulse. A pulse rise time shall lay between 0.05 and 0.1 microsecond, a decay time between 0.05 and 0.2 microsecond and the pulse amplitude variation of one pulse with respect to any other pulse in a reply shall not exceed 1 dB.

The data bits then represent either four-digit octal identification of airplane for Mode A or encoded pressure altitude in 100 ft increments with respect to standard pressure settings as defined in [9]. Since the message content is not an object of the signal processing of this thesis, the more detailed description can be omitted as the described signal in space acts here as a possible source of interference to evaluated ADS–B messages.

2.1.2 Mode S

The Mode S signals [10] differ both by signal format and the content of the message. The biggest difference from the previous modes is its addressing intent because the interrogation addresses a particular target and only this target generates a reply.

Each Mode S reply (Figure 2.2) starts with a preamble identifying the Mode S itself to differ it from Mode A/C replies as it uses same frequency. The preamble consists of four pulses with width of 0.5 μs each formed to two pairs. The pulses are transmitted in multiples of 0.5 μs, namely 1.5 μs, 3.5 μs, and 4.5 μs, counted from the beginning of the first pulse.

The message part then starts in interval 8 μs from the first pulse of the preamble. The data message bits are transmitted using pulse position modulation (PPM) with duration of 1 μs per each bit. The PPM is applied by different levels in the first and second half of bit interval. Data bit "0" represents low in first half and high in second half, data bit "1" is the inverse case.

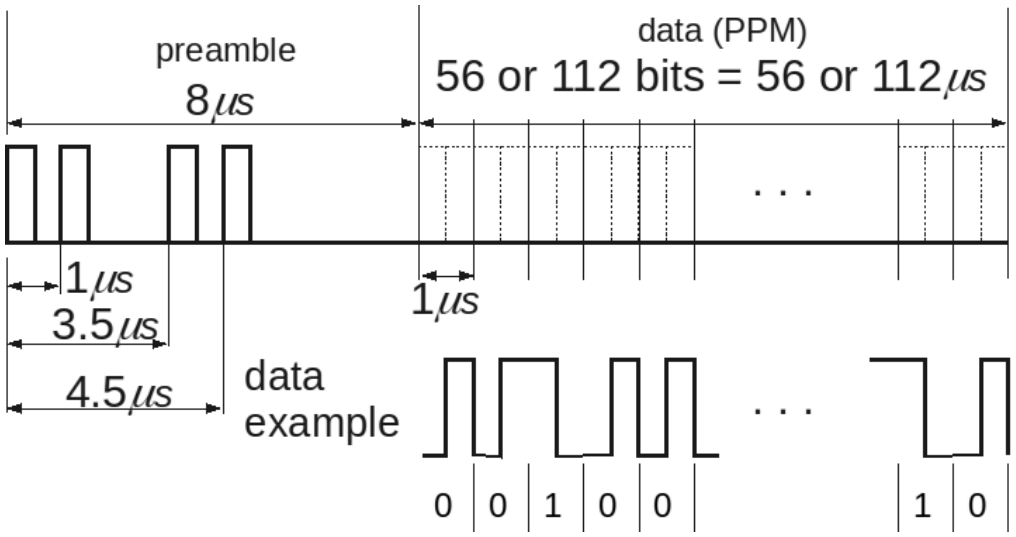

Figure 2.2: SSR Mode S reply signal in space format

The total signal length and the message format vary according to the type of Mode S protocol with three basic groups:

- surveillance message
- standard length message (SLM)
- extended length message (ELM)

The surveillance and SLM messages can exist in its short or long form (Figure 2.3). The short form consists from 5 bits of Downlink Format (DF) block specifying the type of reply (Table 2.1), 27 bits of surveillance and communication control block and 24 bits of combined parity and unique ICAO assigned aircraft address [11]. The long form includes another 56 bits of message data between surveillance and communication control block and parity+ICAO address block. So total duration of the Mode S reply is 64 (short form) or 120 μs (long form) including 8 μs of preamble.

The extended length message (ELM) is a special case of multi-frame message with DF 24 separated to several consecutive replies with 80 bits capacity each capable to transmit the total size of data up to 1 280bits. Since ELM message is only reply with DF binary representation starting 11…, the DF header is reduced to these two bits and the remaining bits are used for purposes of identifying the messages sequence order (Figure 2.4).

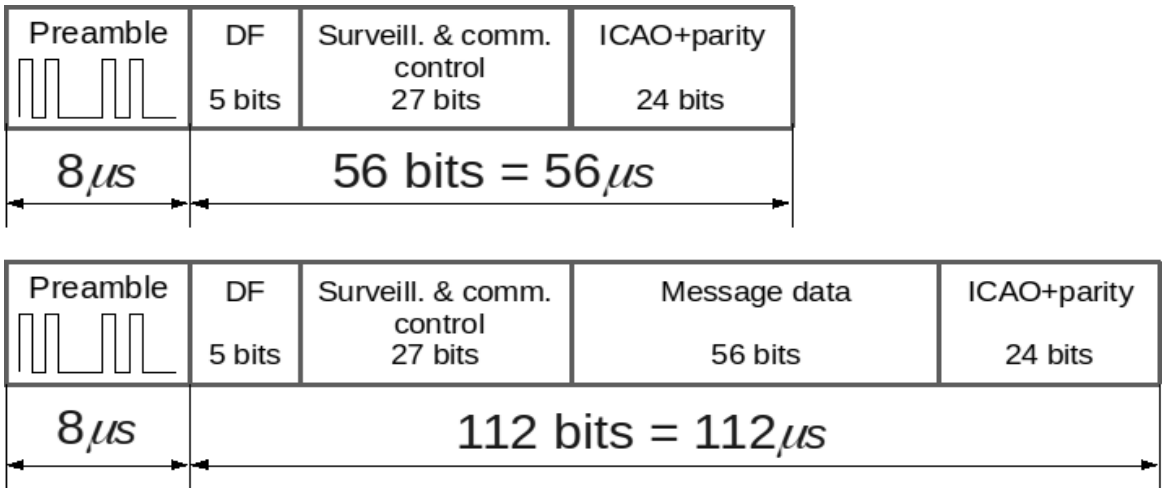

Figure 2.3: Mode S Surveillance and SLM messages format: short (upper) and long (lower)

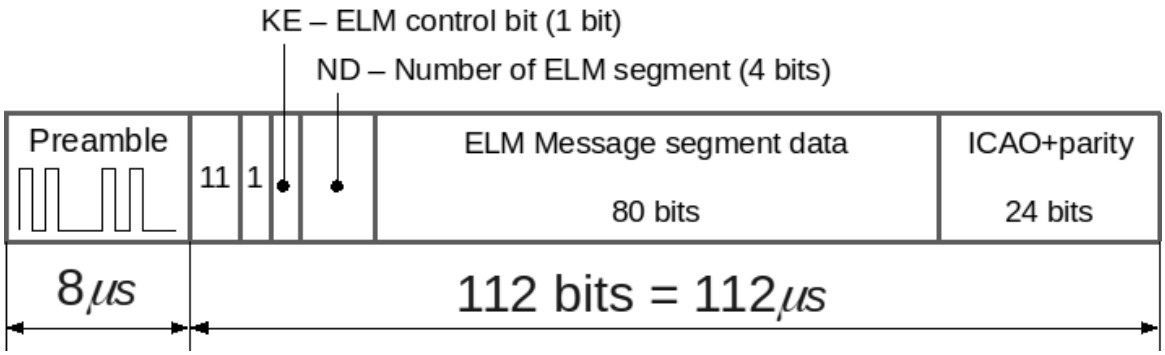

Figure 2.4: Mode S ELM message segment format

The special kind of messages are the ones with DF 17, DF 18, and DF 19. They represent long form of Mode S messages and are called “Extended Squitter”, very often abbreviated as 1090ES. The squitting term here means that these messages are broadcast unsolicited, i.e. without prior interrogation. They also represent messages of ADS-B system that will be described in following chapter and whose signals will be a primary interest of this thesis.

Table 2.1: Types of Mode S replies according to DF field value

DF value	Type of message, content	Format
0	Short ACAS message	SLM short
4	Altitude reply to individual iterrogation (roll-call)	Surveillance short
5	Identification reply to individual iterrogation (roll-call)	Surveillance short
11	Identification reply to Mode S all-call interrogation	Surveillance short
16	Long ACAS message	SLM long
17	1090 Extended Squitter	SLM long
18	1090 Extended Squitter (complementary)	SLM long
19	Military Extended Squitter	SLM long
20	EHS Comm-B+altitude	SLM long
21	EHS Comm-B+identification	SLM long
24	ELM data message	ELM

3 ADS-B

The current chapter will focus on description of the the Mode S SSR replies with DF 17 and DF 18 belonging to messages of Automatic Dependent Surveillance–Broadcast (ADS–B) or Traffic Information System-Broadcast (TIS–B) [12]. It will cover basic structure of signals and data format and content with main interest to provide time independent content of messages. The messages use common Mode S reply structure and can be distinguished by DF block value, where DF 17 represents ADS–B message from Mode S equipment and DF 18 is a TIS–B message (from ground or airborne source) or ADS–B message from equipment that cannot be interrogated. The reply with DF 19 is a military version of ADS–B message. All these messages are broadcast automatically in regular intervals without interrogation.

3.1 ADS–B message format

The message structure respects Mode S long SLM reply with specific population of data parts as depicted in Figure 3.1.

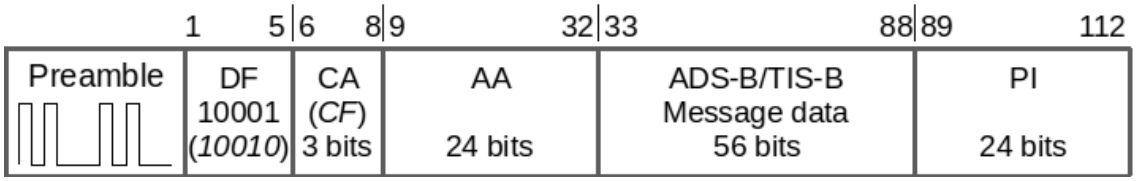

Figure 3.1: ADS–B/TIS–B Message structure (DF =17, DF = 18)

The field DF=17 (10001 binary) specifies ADS-B message from equipment capable to respond to standard Mode S interrogations. Its surveillance and communication control field consist from two parts, CA – Capability Field and AA – Address Announced. The CA field represented by bits 6–8 of message specifies, inter alia, level of transponder [9] and flight status (airborne or on the ground).

The AA field represented by bits 9–32 of message is a specification of address of source of reply providing unique identification as shown in Table 3.1. It can be ICAO address assigned to an aircraft or vehicle or other appropriate identification information, e.g. Mode A ID address or arbitrary “anonymous” address.

In the similar manner, the DF=18 (10010 binary) is a specification of either ADS–B message from source that cannot reply to Mode S interrogation, TIS–B message or ADS–R message, i.e. rebroadcast of an ADS–B message obtained by other link. The determination of type of reply is done by content of CF field, place in the same bit position as CA field in DF 17 type of reply.

It has to be mentioned that there exists also reply with the DF=19 (10011 binary) representing a military application of extended squitter transmission where ADS–B type message is stated by AF field = 0 at the bit positions of CA field in DF 17 reply.

The parity block (PI) with length 24 bits contains the parity information computed according to [9], [13]. In the case of ADS–B messages the parity is not overlaid with interrogator or aircraft address as is made for standard Mode S replies.

Table 3.1: ADS–B, TIS–B, ADS–R messages overview

DF	**CA/ CF/ AF**	**AA**	**Message type**
17	0–7	24 bit ICAO address	ADS–B message
18	0	24 bit ICAO address	ADS–B message
	1	Anonymous address or ground vehicle address or fixed obstacle address	
	2	24 bit ICAO address/12 bit Mode A code and track file number	TIS-B message
	3	24 bit ICAO address/12 bit Mode A code and track file number	
	4	Management information	TIS-B and ADS–R Management Messages
	5	24 bit non-ICAO Address	TIS-B message
	6	24 bit ICAO address	Rebroadcast of an ADS–B Message from an alternate data link
	7	Reserved	
19	0	24 bit ICAO address	ADS–B message
	1–7	Reserved for military applications	

The next crucial classification of nature and character of ADS–B message is the value of TC – Format Type Code, the first five bits of ADS–B message data body, i.e. bits 33–37. They specify the type of message content, fully specified in [14], briefly summarized in Table 3.2. The term “Baro altitude” means barometric pressure altitude, relative to a standard pressure of 1013.25 millibars. The term “GNSS HAE” means Height Above the Ellipsoid obtained using GNSS navigation equipment. Let’s also note that each message type is transmitted with appropriate rate which can be used for estimation of radio channel traffic.

Table 3.2: ADS–B message type content and update rates

TC	Message data type content	Broadcast update intervals [second]		
		On the ground (not moving)	**On the ground (moving)**	**Airborne**
0	Airborne Position or Surface Position (Baro Altitude or no altitude information)	4.8 – 5.2	0.4 – 0.6	0.4 – 0.6
1-4	Aircraft Identification and Category	9.8 – 10.2	4.8 – 5.2	4.8 – 5.2
5-8	Surface Position (no altitude information)	4.8 – 5.2	0.4 – 0.6	N/A
9-18	Airborne Position (Baro Altitude)	N/A	N/A	0.4 – 0.6
19	Airborne Velocity (Difference between Baro Altitude‖ and GNSS HAE)	N/A	N/A	0.4 – 0.6
20-22	Airborne Position (GNSS HAE)	N/A	N/A	0.4 – 0.6
23	Test Message	N/A		
24	Surface System Status (status of elements of surface surveillance systems, e.g. MLAT)	N/A		
25-26	Reserved	N/A		
27	Reserved for Trajectory Change	N/A		
28	Extended Squitter Aircraft Status	0.7 – 0.9 (status change), 4.8 – 5.2 (no status change)		
29	Target State and Status (TSS)	N/A	N/A	1.2 – 1.3
30	Reserved	N/A		
31	Aircraft Operational Status	4.8 – 5.2	0.7 – 0.9 (NIC/NAC/SIL change), 2.4 – 2.6 (no change)	0.7 – 0.9 (TSS not broadcast & NIC/ NAC/SIL change), 2.4 – 2.6 (other cases)

To estimate average messages generated by one aircraft per second, we can assume that according to are transmitters limited to 2 event-driven messages (TSS, status message, etc.) per second. Therefore, in case of airborne target, we can count with 2 airborne position messages, 2 airborne velocity messages, 0.2 identification message, and 2 status and other

event-driven messages per second, which yield 6.2 messages per second for one aircraft. In case of ground movement, there will be combination of 2 surface position messages and 2 event-driven messages, which yields 4 messages per second for one aircraft. It can be considered as an upper limit, whereas the real rate is usually lower depending on rate of transmission of status and event-driven messages.

3.2 ADS–B Signal in space definition and model

The current signal in space description will be source for further considerations about signal detection and decoding in various kinds of environment, therefore the time and frequency parameters will be reviewed here according to standards for the ADS–B signal. The signal is transmitted on the carrier frequency f_C = 1090 MHz with tolerance ±1 MHz. It consist from sequence of pulses representing preamble and message content as described in previous chapter. The pulse amplitude variations shall not exceed in emitted signal 2 dB. The pulse rise time shall not be less than 0.05 μs or greater than 0.1 μs and the decay time shall not be less than 0.05 μs or greater than 0.2 μs. The related frequency mask for spectrum occupancy according to [9] is shown in Table 3.3 where f_t represents carrier frequency of transmitted signal that can vary from nominal f_c by tolerable deviation as described above.

Table 3.3: ADS-B signal spectrum level mask

Frequency deviation	**Relative drop of spectrum power level**
$f \le f_t + 1.3\,MHz$	0 dB
$f_t + 1.3 < f \le f_t + 7\,MHz$	3 dB
$f_t + 7 < f \le f_t + 23\,MHz$	20 dB
$f_t + 23 < f \le f_t + 78\,MHz$	40 dB
$f_t + 78\,MHz < f$	60 dB

The ADS–B signal model then can be defined as

$$s_{ADS-B}(t) = d(t) \cdot \cos\left(2\pi(f_c + \Delta f)t\right) \quad , \tag{3.1}$$

where f_c = 1090 MHz, Δf is possible carrier frequency deviation in range ±1 MHz (restricted by [9] to ±3 MHz but nowadays receivers are usually working with the 1MHz tolerance), and *d(t)* the data signal

$$d(t) = \sum_{i=0}^{T_D - 1} s_D(i)\, p(t - i \cdot T_p) \quad , \tag{3.2}$$

where T_D = 240 (half microsecond multiple of ADS–B signal duration 120 μs), *p(t)* is pulse shape in accordance to parameters stated in this chapter according to [9] with duration of T_p, $s_D(i)$ is half microsecond sequence with values according to message content with respect to PPM data bit definition, i.e. starting 1010000101000000…. which represents four pulses of preamble in 8 μs interval. The spectrum then represents typical form of pulse-like signal spectra, as seen on Figure 3.2.

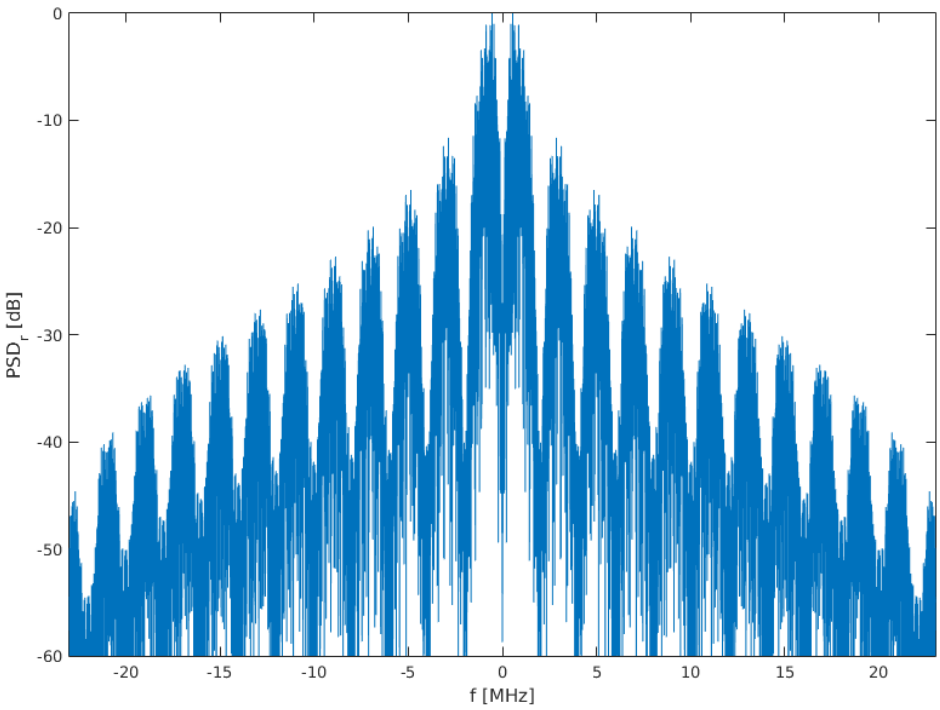

Figure 3.2: Power spectral density of ADS–B signal (frequency axis is depicted relative to carrier frequency)

The frequency deviation brings the reminder of carrier frequency after demodulation, which can be for complex envelope of the signal be represented as consecutive phase change component $e^{j2\pi\Delta ft}$ multiplying the original signal envelope, resulting in rotation of complex envelope of signal as depicted at Figure 3.3 and necessity to accommodate it in the signal processing algorithms. The possible carrier frequency deviation is also usually taken into account for setup of low-pass filter in the receiver to suppress an out-of-band interference.

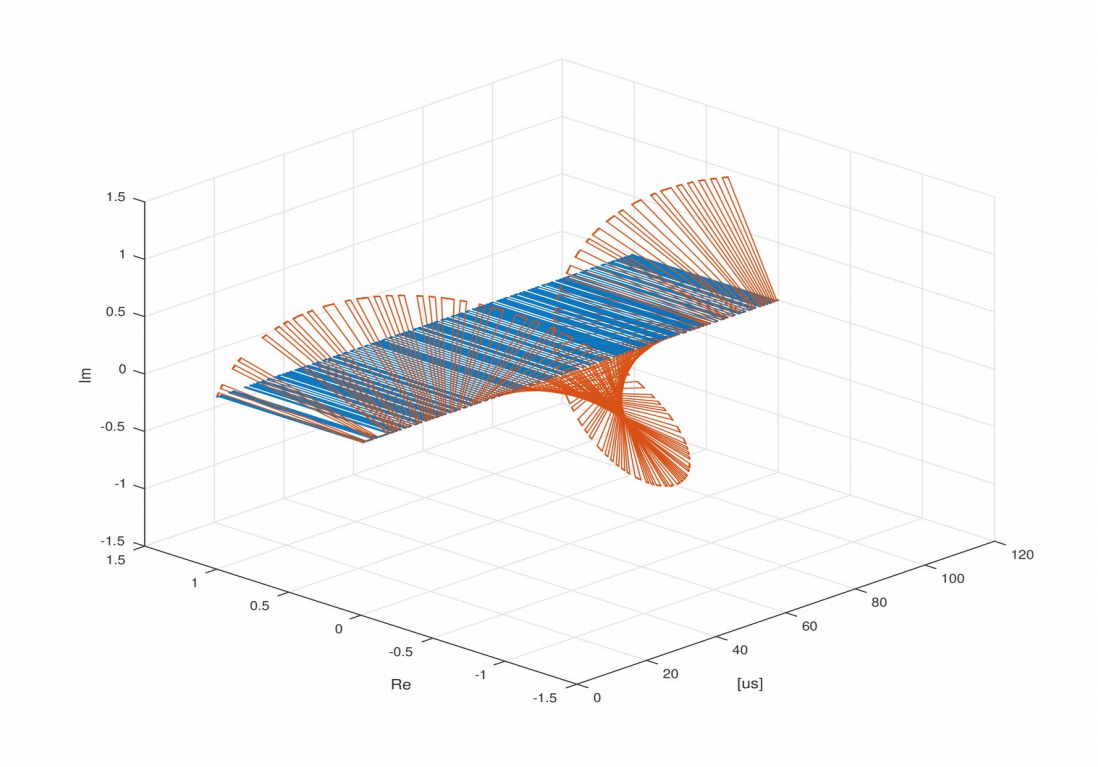

Figure 3.3: Impact of carrier frequency deviation (Δf=10 kHz) to ADS–B signal complex envelope

4 Position determination techniques

The airplane position determination methods described in Chapter 2, are standard conservative applications of a radar technology. They use, in its pure form, a single station providing transmission of ranging signal and also receiving and processing echoes in case of primary radar or replies in case of secondary radar. Such approach uses processing of determined signals excited by the ground station and it is not suitable for processing of unsolicited replies provided by ADS–B system. In this chapter, the methods, working with processing of the transmitted signal by a set of independent or synchronized receivers, and their current state of art will be summarized and described.

The position determination techniques can be classified according to the kind of information that is for the position algorithm used:

- direction of arrival (DoA) or angle of arrival (AoA)
- received signal strength (RSS) based on channel modeling or location pattern matching methods
- time of arrival (ToA) including round trip travel (RTT) method
- time difference of arrival (TDoA)

4.1 Direction or angle of arrival (AoA)

The DoA/AoA, also known as an angulation, is based on evaluation of an angle of incidence for received signal incoming to a points with known location and orientation. In case of determination of angle of incidence for at least two receiving stations, the estimation of relative position to the stations can be calculated (Figure 4.1). This principle is well known and was realized in numerous variant of radio goniometers and direction finders since World War II [15].

The angular information can be obtained for example by direction antenna steered in evaluated plane and evaluation of signal strength dependence on bearing of antenna boresight. The beam steering can be realized either mechanically or by using multiple elements array and use the combinations of the elements together with signal processing to produce desired pattern[16], [17]. Another common method is the use of an antenna phased array that can provide angular information relative to array baseline from comparison of phase changes of incoming waves to elements of array or by measurement of incoming signal delay (de facto similar to TDoA method) which is a basic principle of interferometer instruments[18], [19].

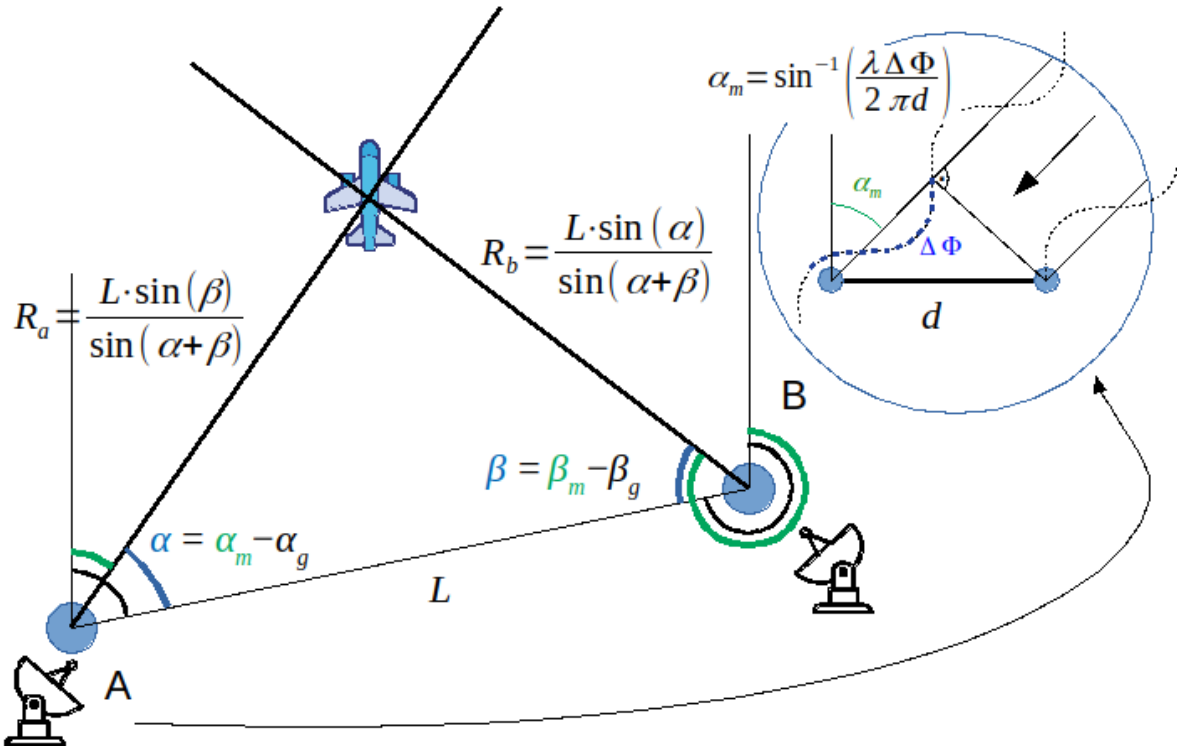

Figure 4.1: Angle of arrival (AoA) principle. (Depicted 2D case for sake of clarity)

The precision of such method is dependent on a precision of angle evaluation, so it is directly proportional to beam resolution of used antennas. The better performance can be achieved by phased arrays, where the angular resolution can be enhanced by a change of baseline distance. The precision however naturally decreases with the increase of the distance of the signal source from the reception stations. Moreover, the performance of the AoA system is affected by line of sight blockage and by multipath propagation[20], which complicates its use in environments with possible obstructed view to a signal source [21], [22].

4.2 Received signal strength (RSS)

The RSS methods use the information about strength of signal related to distance of a transmitter from the receivers[23], [24]. The most simple approach works with the fact that free space loss of radio path is proportional to the square of distance between the source and the target. The distance estimation obtained from signal attenuation is then used for lateration calculations yielding the position of signal source (Figure 4.2). The RSS method is quite often used in wireless telecommunication networks due to the fact that most of chipsets of mobile devices are now equipped with provision of received signal strength indicator (RSSI) i.e. a measured power of received radio signal.

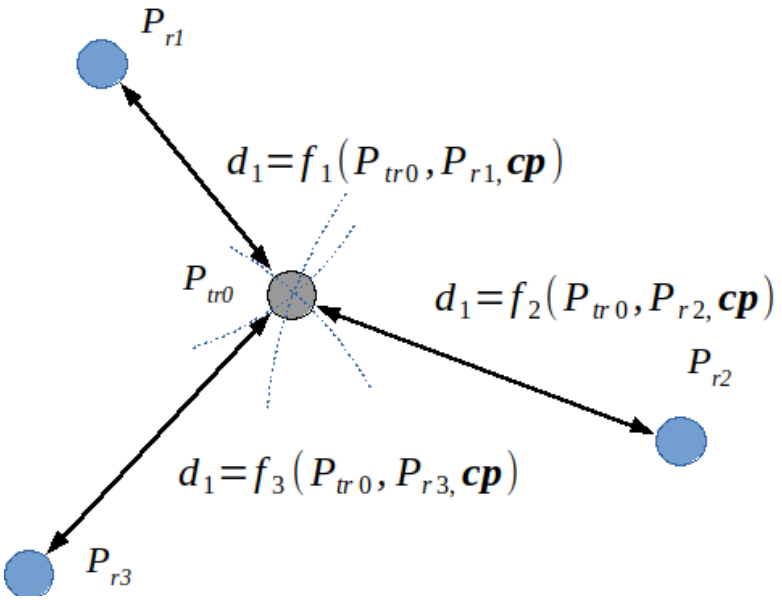

*Figure 4.2: Received signal strength (RSS) based localization, using Power of transmitter P_t, received powers P_{ri} and channel parameters **cp** to determine position of source (grey). (Depicted 2D case for sake of clarity)*

The dependence on relationship between signal strength and distance however complicates the use of such method in case of more complex propagation environment, e.g in case of obstacles, bringing blockage of line of sight and reflections which results in multipath propagation and fading. These phenomena that can occur in the area of application mean the necessity of a very accurate propagation attenuation models which brings a loss of precision and increases the algorithm complexity [25]. The another common option is to map the signal strength for evaluated area[26], [27] which removes the impact of propagation model but the precision usually does not increase due to general time variance of signal distribution and it brings signal map validity constraint to only limited area and thus often used only indoors [24]. Moreover, the location pattern matching algorithms, that are often used for such map construction, are based on extensive filtration use (e.g. extended Kalman filter, particle filter, Rao-Blackwelized particle filter [28]) and therefore the desired reduction of complexity is practically not achieved.

4.3 Time of arrival (ToA)

One of the methods that work with time of signal propagation is a time of arrival (ToA) evaluation. That method is well known from global navigation satellite systems (GNSS) [29]–[33] or WLAN positioning [34]–[37] and measures detection time of signal initiated from the transmitter and coming to the receiver. There can obviously be two variants of the system topology: either the coordinates of several transmitters is known and the position of single

receiver is computed or vice versa, the unknown position of transmitter is computed from measurements made by several receivers with known positions. The estimated delay of signal travel is then proportional to distance between transmitter and receiver and thus the task of positioning can be transformed to a lateration, i.e. geometrical solution. The obtained distances form a set of circles (for 2D solution) or spheres (for 3D solution) with centers in known positions of stations (either receivers or transmitters) and position of unknown station is estimated as an intersection of these geometrical objects (Figure 4.3).

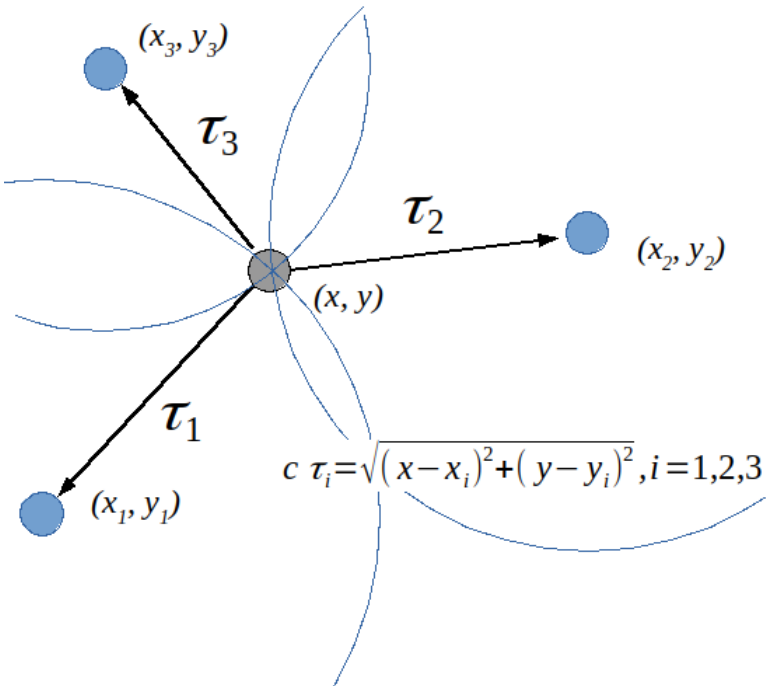

Figure 4.3: Time of arrival (ToA) based localization. We assume an unknown position of transmitter (x,y) and known positions of receivers (x_i,y_i). (Depicted 2D case for sake of clarity)

The positioning task can be described as a set of equations to be solved. Let's assume the transmitter at unknown coordinates (x, y, z) transmitting omni-directional radio signal, that is received by a set of stations with known coordinates (x_i, y_i, z_i). The measured time of arrival for i-th station TOA_i is then equal to

$$TOA_i = \Delta_{T-R_i} + \frac{1}{c} \cdot \sqrt{(x-x_i)^2+(y-y_i)^2+(z-z_i)^2} + e_i \quad , \tag{4.1}$$

where Δ_{T-R_i} represents difference of clocks between transmitter and i-th receiver, c is a velocity of signal propagation (usually a speed of light for radio signals), and e_i represents TOA measurement error.

The parameter representing clocks offset brings unwanted rise of degrees of freedom for positioning task, so to be able to obtain finite set of solutions, a precise synchronization of receivers and transmitter is necessary. The requirement to the precision of time synchronization is in this case at least as hard as the requirement on position accuracy. Since there is usually no practical way to achieve such general coherence, the realized synchronization is reduced to the set of receivers. Then the offsets become an common value for all receivers $\Delta_{T-R_i} = \Delta_{T-R}$ and the set of positioning equations can be solved by overdetermination of the set of equations producing target coordinates and offset between transmitter and system of receivers.

The synchronization requirement is in several cases resolved by use of round trip travel (RTT) approach, when the signal travels from station with known position to the located target and back. The delay is then measured between signal transmit and received reply in the same manner as in classical radar operation. The obtained value then represents twice the signal travel time plus time during which the sent signal is processed in located target to generate reply back to the station. The advantage of the removal of the unknown clock offset between transmitter and receiver is paid by need of precise determined processing time of interrogating signal which can bring another challenge to the clock stability and thus attainable precision[25]. Generally, resolving the problem of unknown clock offset brings ToA and RSS systems to the same level and same positioning algorithms can be applied.

The solutions of the set of positioning equations can be achieved by various known methods, either in the form of direct algebraic solution or as an iterative process. The closed form of positioning equation [38]–[40] usually produces direct solution but either with some ambiguity of several possible positioning solutions that have to be further resolved [39] or using transformation of non-linear equations to its linear form [38] that brings necessity of overdetermination of the task (i.e. the need of additional stations in the system). Nevertheless, they are more appropriate choice in case on unknown initial conditions or bad geometry of system (the impact of stations geometric topology will be presented in chapter concerning details of multilateration concept). The iteration based methods usually go by way of least squares error minimization [41], e.g. using Gauss-Newton method or Levenberg-Marquardt method [42] (they will be described more in detail in chapter concerning TDoA) leading usually to Kalman filter [43]. The advantage of such approach is no need of overdetermination to produce unique solution and keeping the simplicity of linear iterative convergence rate. The drawback of these methods can be seen in its dependence on initial estimate for iterative process which can affect a number of necessary iterations or complicate convergence. That problem becomes more significant in small scale of the system. Recent approaches often use a combination of classical least squares estimator approach but use an direct form for obtaining a promising initial estimate and modify the weighting function of an iterative process to improve the algorithm performance [44]–[46].

4.4 Time difference of arrival (TDoA)

The need of knowledge of the origin time of transmission in the ToA system is removed in a another well known approach which uses the time-difference of arrival (TdoA) for signals received by a pair of measuring stations (Figure XXX). The synchronization is then needed only for measuring units, usually by common time information (e.g. common view GNSS time distribution) or by one or more reference transponders placed at known positions.

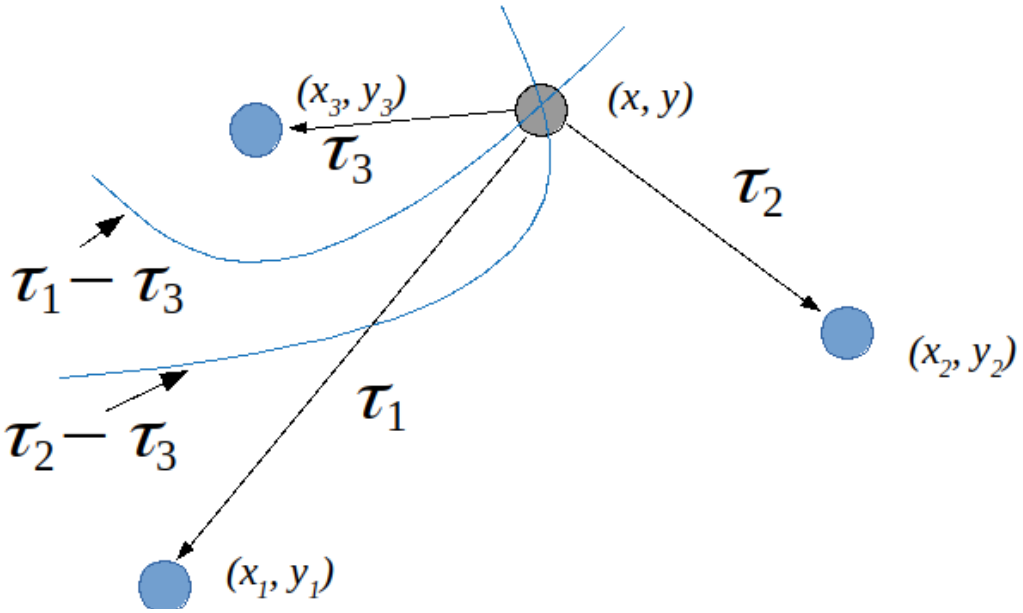

Figure 4.4: Time difference of arrival (TDoA) based localization. The differences of delays are expressed with respect to station with coordinates (x_3, y_3). (Depicted 2D case for sake of clarity)

The positioning task then forms a set of non-linear hyperbolic equations in the form of

$$TDoA_{i,j} = \frac{1}{c}\left(\sqrt{(x-x_i)^2+(y-y_i)^2+(z-z_i)^2} - \sqrt{(x-x_j)^2+(y-y_j)^2+(z-z_j)^2}\right) + e_{i,j} \quad , \qquad (4.2)$$

where $TDoA_{i,j}$ is a time difference between a signal arrival from the transmitter to i-th measuring station with coordinates (x_i, y_i, z_i) and j-th measuring station with coordinates (x_j, y_j, z_j), c is a speed of light, and $e_{i,j}$ is a TDoA measurement error. The solutions then represent hyperbolas (in 2D case) or hyperboloids (in 3D case) with foci in measuring stations and the target placed on the calculated curve or surface, respectivelly. The TDoA method is applied in widely used hyperbolical navigation systems e.g. Gee, Omega, Chayka, Loran C in history [47], [48] (before it was overcome by ToA based GNSS) and in present wireless network

systems [49] (in the same manner as described in ToA method) and it is also a core for multilateration system that will be described more in detail in the following chapter together with similar review of state of art of position solutions as was done in part concerning time of arrival approach.

4.5 Combined methods

There is a logical step in use of the above described method to their combination and mutual exploitation. The first natural combination is using AoA angulation together with ToA(RTT) lateration [50] as can be seen in classical radar approach, hereby using a network with an array of antennas for angle determination and RTT measurement for distance information to be combined [51], [52]. The similar approach is also used for RSS/AoA combinations [53]. The problem of multipath propagation can be in some suitable applications (e.g. multifrequecy Wi-Fi networks) partially suppresed by using combination of space and frequency diversity for DoA methods [54].

The next common (from the application point of view) is a combination of TDoA and AoA methods [55]. The typical problems nowadays solved are the optimal algebraic or iterative solution of combination of AoA and TDoA measurements [56]–[58], the optimal placement of measuring sensors [59], [60], or using processing of single sensor measurement in different time instances for TDoA task construction [61]. The location of moving targets also implies an use of combination of TDoA and FDoA (Frequency difference of arrival – due to the Doppler effect) methods for position solution [62]–[64].

5 Multilateration concept of operation

Multilateration (MLAT) systems are generally a kind of positioning system, using a set of measuring stations to determine position of unknown (usually mobile) unit through reception and processing transmitted signal with application of any of methods described in Chapter 4.

The most common and for our case reference solution will be an hyperbolic positioning system using time difference of signal arrival (TDoA) from target for calculations of target's position as described principally in Chapter 4.4.

The conventional hyperbolic navigation is based on set of fixed stations with known locations that broadcast synchronously signals that are received by aircraft or other object. The related parameters of received signals are then measured, typically a time of arrival or a phase. The MLAT systems differ from that by inverse mechanism of propagation. The signal is only one and it is broadcast by an aircraft or other object that is in the focus of the surveillance system. This signal is then received by (usually) ground stations of the system and centrally processed. The stations position is known and their measurements are made in synchronized way.

The time differences are evaluated for pairs of measuring stations with one chosen as a reference station and they then can be expressed using (4.2). The result of a set of equations is an intersection of hyperboloids with foci in stations' positions as indicated on Figure 5.1. The possible methods for solution of position task is provided further by review and analysis of positioning algorithms.

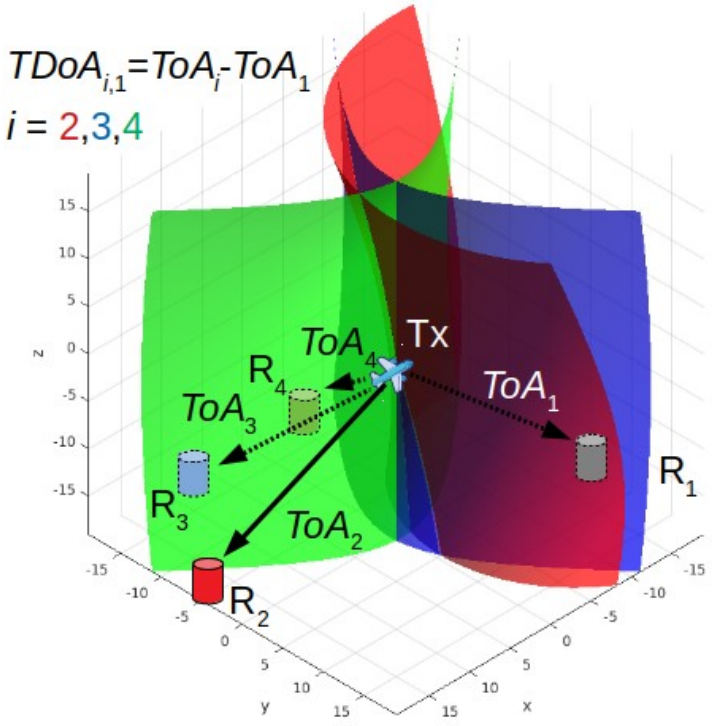

Figure 5.1: Solution of TDoA task as an intersection of hyperboloids. The reference station is station R_1 (grey). For sake of clarity, stations hidden behind hyperboloids surfaces are depicted by dashed lines

5.1 The TDoA positioning algorithms

A set of hyperbolic equations based on 4.2 consist of known parameters (typically measured delay differentials and positions of measuring stations), the unknown parameters of interest, i.e. target position to be computed, and unknown parameters representing measurement errors. The estimation of the unknown parameters is usually done by searching an extreme (maximum or minimum) of objective criterion. Such criteria can be squared residuals, likelihood functions, posteriori density function s of risk functions. There will be presented general classification and brief description of relevant methods to provide background for considerations about impact of delay measurement error to final position estimation.

The maximizing a likelihood function (ML) and minimizing least squares of errors (LS) are two most common approaches for parameters estimation, that's why we will further focus on them.

Their common property is that using an inverse covariance matrix of measurement errors as an weighting factor for parameters estimation the variance for a case of normally distributed ranging errors attains the Cramer-Rao lower bound (CRLB) which is a common theoretical measure for estimator performance [65]. Such behaviour works well for a plain case of line-of-sight (LOS) signal only, however the situation complicates with non-line-of-sight (NLOS) cases and for more complicated radio channel configuration , e.g. in case of multipath.

The positioning algorithm uses for both approaches expression of measurements as

$$\boldsymbol{d} = f(\boldsymbol{u}, \boldsymbol{b_u}) + \boldsymbol{e} \quad , \tag{5.1}$$

where $\boldsymbol{d}$ represents m-dimensional vector of measurements, $\boldsymbol{u}$ is n-dimensional unknown parameter (in our case target coordinates x_t, y_t, z_t), $\boldsymbol{b_u}$ m-dimensional parameter of measurement, and $\boldsymbol{e}$ m-dimensional parameter representing measurement errors. The function $f(.)$ then provides a non-linear mapping of $\mathbb{R}^n \rightarrow \mathbb{R}^m$, n is a dimension of unknown parameters and m is a dimension of set of measurements.

5.1.1 Cramer-Rao lower bound for TDoA position estimation

Cramer-Rao lower bound [65] can provide theoretical bound for asymptotically achievable error covariance of unbiased estimator. It is defined as an inverse of Fisher information matrix (FIM) $\mathfrak{I}_o$. In case of estimates $\hat{u}$ of unknown parameter u from measurements d the error variance fulfills the bound

$$\mathbf{E}[(\hat{u}-u)(\hat{u}-u)^T] \geq \mathfrak{I}_0^{-1} \quad , \tag{5.2}$$

Where **E**[.] is an expectation.

Assuming the transmitter $\boldsymbol{u}$ at unknown position $\boldsymbol{u} = (x_u, y_u, z_u)^T \in \mathbb{R}^3$ ans set of M sensors $\boldsymbol{u}_i$ with known positions $\boldsymbol{u_i} = (x_i, y_i, z_i)^T \in \mathbb{R}^3, i = 1, \ldots, M$ the distance range can be expressed as

$$r_i = \|\boldsymbol{u} - \boldsymbol{u}_i\| = \sqrt{(x_u - x_i)^2 + (y_u - y_i)^2 + (z_u - z_i)^2}, \quad i = 1, \ldots, M \quad . \tag{5.3}$$

Then TDoA range differences as a function of unknown position $\boldsymbol{u}$ are

$$RD(\boldsymbol{u})_{ij} = r_i - r_j \quad , \quad i, j \in \{1, \ldots, M\} \cap i \neq j \quad . \tag{5.4}$$

Assuming measurement errors as additive random values uncorrelated from each time instant to other time instant and uncorrelated between sensor measurements, the u_i and u_j as known parameters of measurement, we obtain a set of $M-1$ measurements

$$d_{ij} = RD(\boldsymbol{u})_{ij} + n_{ij} \quad , \quad i \in \{1, \ldots, M\} \quad , \quad j \in \{2, \ldots, M\} \quad , \quad j > i \quad , \tag{5.5}$$

where n_{ij} is a normally distributed zero mean random process with variance $\sigma_i^2 + \sigma_j^2$ created from sum of noises for measurements by station $\boldsymbol{u}_i$ and station $\boldsymbol{u}_j$.

Let's evaluate a case of minimal number of station, i.e. four stations for full 3D evaluation and put a station $\boldsymbol{u}_1=(x_1, y_1, z_1)^T$ as a reference station for range differences. Then there will be a vector $\boldsymbol{d}_{u1}$ of measured range differences

$$\boldsymbol{d}_{\boldsymbol{u}1}=(d_{12}, d_{13}, d_{14})^T \tag{5.6}$$

and measurement function $\boldsymbol{RD}_{\boldsymbol{u}1}$

$$\boldsymbol{RD}_{\boldsymbol{u}1}=(RD_{12}, RD_{13}, RD_{14})^T \tag{5.7}$$

with elements according to (5.4).

If we extend the set of measurements choosing possible station pairs without respect to single fixed station as reference, we get vector of full set of measurements

$$\boldsymbol{d}_{full}=(d_{12}, d_{13}, d_{14}, d_{23}, d_{24}, d_{34})^T \tag{5.8}$$

and measurement function

$$\boldsymbol{RD}_{full}=(RD_{12}, RD_{13}, RD_{14}, RD_{23}, RD_{24}, RD_{34})^T \quad . \tag{5.9}$$

The likelihood function is under assumptions about measurements above for case of single fixed reference station $\boldsymbol{u}_1$

$$p(\boldsymbol{d}_{\boldsymbol{u1}}|\boldsymbol{u})=\frac{1}{\sqrt{2\pi\mathbf{R}_{\mathbf{u1}}}}\exp\left(-\frac{1}{2}\left(\boldsymbol{d}_{\boldsymbol{u1}}-\boldsymbol{RD}_{\boldsymbol{u1}}(\boldsymbol{u})\right)^T\mathbf{R}_{\mathbf{u1}}{}^{-1}\left(\boldsymbol{d}_{\boldsymbol{u1}}-\boldsymbol{RD}_{\boldsymbol{u1}}(\boldsymbol{u})\right)\right) \quad , \tag{5.10}$$

where $\mathbf{R}_{\mathbf{u}1}$ is covariance matrix of measurements. Because of the use of common sensor in the measurement, the measurements are correlated [66] and variance for a single pair *i* and *j* is $\sigma_{ij}^2=\sigma_i^2+\sigma_j^2$. The covariance matrix of measurements for system of four stations with the station $\boldsymbol{u}_1$ as a reference station has a form

$$\mathbf{R}_{\boldsymbol{u1}}=\begin{pmatrix}\sigma_1{}^2+\sigma_2{}^2 & \sigma_1{}^2 & \sigma_1{}^2\\ \sigma_1{}^2 & \sigma_1{}^2+\sigma_3{}^2 & \sigma_1{}^2\\ \sigma_1{}^2 & \sigma_1{}^2 & \sigma_1{}^2+\sigma_4{}^2\end{pmatrix} \quad . \tag{5.11}$$

Analogically, the likelihood function for a full set of measurements (using all station pairs) is

$$p(\boldsymbol{d}_{full}|\boldsymbol{u})=\frac{1}{\sqrt{2\pi\mathbf{R}_{full}}}\exp\left(-\frac{1}{2}\left(\boldsymbol{d}_{full}-\boldsymbol{RD}_{full}(\boldsymbol{u})\right)^{T}\mathbf{R}_{full}^{-1}\left(\boldsymbol{d}_{full}-\boldsymbol{RD}_{full}(\boldsymbol{u})\right)\right) \tag{5.12}$$

and measurement covariance matrix

$$\mathbf{R}_{full}=\begin{pmatrix}\sigma_1^2+\sigma_2^2 & \sigma_2^2 & 0 & \sigma_1^2 & \sigma_2^2 & \sigma_1^2\\ \sigma_2^2 & \sigma_2^2+\sigma_3^2 & \sigma_3^2 & \sigma_3^2 & \sigma_2^2 & 0\\ 0 & \sigma_3^2 & \sigma_3^2+\sigma_4^2 & \sigma_3^2 & \sigma_4^2 & \sigma_4^2\\ \sigma_1^2 & \sigma_3^2 & \sigma_3^2 & \sigma_1^2+\sigma_3^2 & 0 & \sigma_1^2\\ \sigma_2^2 & \sigma_2^2 & \sigma_4^2 & 0 & \sigma_2^2+\sigma_4^2 & \sigma_4^2\\ \sigma_1^2 & 0 & \sigma_4^2 & \sigma_1^2 & \sigma_4^2 & \sigma_1^2+\sigma_4^2\end{pmatrix}. \tag{5.13}$$

Then the Fisher information matrix for CRLB from (5.2) is [65]

$$\mathfrak{I}_0=-\mathbf{E}\left[\frac{\partial^2 \ln p(\boldsymbol{d}|\boldsymbol{u})}{\partial \boldsymbol{u}^2}\right], \tag{5.14}$$

so for our case of set of stations with reference station $\boldsymbol{u}_1$ and likelihood function from (5.10) it can be expressed as

$$\mathfrak{I}_0=\left(\frac{\partial \boldsymbol{RD}_{\boldsymbol{u}1}(\boldsymbol{u})}{\partial \boldsymbol{u}}\right)^{T}\mathbf{R}_{\boldsymbol{u}1}{}^{-1}\left(\frac{\partial \boldsymbol{RD}_{\boldsymbol{u}1}(\boldsymbol{u})}{\partial \boldsymbol{u}}\right) \tag{5.15}$$

where $\mathbf{R}_{\mathbf{u}1}$ has a form expressed in (5.11) with its inversion like

$$\mathbf{R}_{\boldsymbol{u}1}{}^{-1}=\frac{1}{|\mathbf{R}_{\boldsymbol{u}1}|}\begin{pmatrix}\left(\sigma_1\sigma_4{}^2+\sigma_1{}^2\sigma_3{}^2+\right.\\ \left.+\sigma_3{}^2\sigma_4{}^2\right)\end{pmatrix} & -\sigma_1{}^2\sigma_4{}^2 & -\sigma_1{}^2\sigma_3{}^2\\ -\sigma_1{}^2\sigma_4{}^2 & \begin{pmatrix}\sigma_1{}^2\sigma_2{}^2+\sigma_1{}^2\sigma_4{}^2+\\ +\sigma_2{}^2\sigma_4{}^2\end{pmatrix} & -\sigma_1{}^2\sigma_2{}^2\\ -\sigma_1{}^2\sigma_3{}^2 & -\sigma_1{}^2\sigma_2{}^2 & \begin{pmatrix}\sigma_1{}^2\sigma_2{}^2+\sigma_1{}^2\sigma_3{}^2+\\ +\sigma_2{}^2\sigma_3{}^2\end{pmatrix}\end{pmatrix}, \tag{5.16}$$

where $|\mathbf{R}_{\mathbf{u}1}|$ is a determinant of $\mathbf{R}_{\mathbf{u}1}$ and Jacobian matrix of $\boldsymbol{RD}_{\boldsymbol{u}1}$ has a form

$$\frac{\partial \boldsymbol{RD}_{\boldsymbol{u}1}(\boldsymbol{u})}{\partial \boldsymbol{u}}=\begin{pmatrix} \frac{\partial RD_{12}(\boldsymbol{u})}{\partial x} & \frac{\partial RD_{12}(\boldsymbol{u})}{\partial y} & \frac{\partial RD_{12}(\boldsymbol{u})}{\partial z} \\ \frac{\partial RD_{13}(\boldsymbol{u})}{\partial x} & \frac{\partial RD_{13}(\boldsymbol{u})}{\partial y} & \frac{\partial RD_{13}(\boldsymbol{u})}{\partial z} \\ \frac{\partial RD_{14}(\boldsymbol{u})}{\partial x} & \frac{\partial RD_{14}(\boldsymbol{u})}{\partial y} & \frac{\partial RD_{14}(\boldsymbol{u})}{\partial z} \end{pmatrix} \tag{5.17}$$

where elements of the Jacobian matrix have a form

$$\begin{aligned} \frac{\partial RD_{ij}(\boldsymbol{u})}{\partial x}&=\frac{x-x_i}{r_i}-\frac{x-x_j}{r_j} \\ \frac{\partial RD_{ij}(\boldsymbol{u})}{\partial y}&=\frac{y-y_i}{r_i}-\frac{y-y_j}{r_j} \\ \frac{\partial RD_{ij}(\boldsymbol{u})}{\partial z}&=\frac{z-z_i}{r_i}-\frac{z-z_j}{r_j} \end{aligned} \quad . \tag{5.18}$$

Since the inversion of measurements covariance matrix is diagonally symmetrical matrix, the Fisher information matrix has also a diagonally symmetrical form with size 3×3 and the elements on main diagonal are

$$\Im_{0(11)}=\frac{1}{|\mathbf{R}_{\boldsymbol{u}1}|}\sum_{i=1}^{4}\sum_{\substack{j=1\\ j\neq i}}^{4}\sum_{\substack{k=j+1\\ k\neq i}}^{4}\sigma_j^{\,2}\sigma_k^{\,2}\left(\frac{x-x_i}{r_i}\right)^2-\frac{2}{|\mathbf{R}_{\boldsymbol{u}1}|}\sum_{i=1}^{4}\sum_{\substack{j=i+1\\ j\neq i}}^{4}\sigma_v^{\,2}\sigma_w^{\,2}\left(\frac{x-x_i}{r_i}\right)\left(\frac{x-x_j}{r_j}\right) \tag{5.19}$$

$$v,w\in\{1,2,3,4\}-\{i,j\} \quad , \quad v<w$$

respectively

$$\Im_{0(22)}=\frac{1}{|\mathbf{R}_{\boldsymbol{u}1}|}\sum_{i=1}^{4}\sum_{\substack{j=1\\ j\neq i}}^{4}\sum_{\substack{k=j+1\\ k\neq i}}^{4}\sigma_j^{\,2}\sigma_k^{\,2}\left(\frac{y-y_i}{r_i}\right)^2-\frac{2}{|\mathbf{R}_{\boldsymbol{u}1}|}\sum_{i=1}^{4}\sum_{\substack{j=i+1\\ j\neq i}}^{4}\sigma_v^{\,2}\sigma_w^{\,2}\left(\frac{y-y_i}{r_i}\right)\left(\frac{y-y_j}{r_j}\right)$$

$$\Im_{0(33)}=\frac{1}{|\mathbf{R}_{\boldsymbol{u}1}|}\sum_{i=1}^{4}\sum_{\substack{j=1\\ j\neq i}}^{4}\sum_{\substack{k=j+1\\ k\neq i}}^{4}\sigma_j^{\,2}\sigma_k^{\,2}\left(\frac{z-z_i}{r_i}\right)^2-\frac{2}{|\mathbf{R}_{\boldsymbol{u}1}|}\sum_{i=1}^{4}\sum_{\substack{j=i+1\\ j\neq i}}^{4}\sigma_v^{\,2}\sigma_w^{\,2}\left(\frac{z-z_i}{r_i}\right)\left(\frac{z-z_j}{r_j}\right) \tag{5.20}$$

$$v,w\in\{1,2,3,4\}-\{i,j\} \quad , \quad v<w$$

and elements outside the main diagonal are

$$\mathfrak{I}_{0(12)}=\mathfrak{I}_{0(21)}=\frac{1}{|\mathbf{R}_{\boldsymbol{u}1}|}\sum_{i=1}^{4}\sum_{\substack{j=1\\j\neq i}}^{4}\sum_{\substack{k=j+1\\k\neq i}}^{4}\sigma_j^{\,2}\,\sigma_k^{\,2}\left(\frac{x-x_i}{r_i}\right)\left(\frac{y-y_i}{r_i}\right)-$$
$$-\frac{1}{|\mathbf{R}_{\boldsymbol{u}1}|}\sum_{i=1}^{4}\sum_{\substack{j=1\\j\neq i}}^{4}\sigma_v^{\,2}\,\sigma_w^{\,2}\left(\frac{x-x_i}{r_i}\right)\left(\frac{y-y_j}{r_j}\right)$$

$$\mathfrak{I}_{0(13)}=\mathfrak{I}_{0(31)}=\frac{1}{|\mathbf{R}_{\boldsymbol{u}1}|}\sum_{i=1}^{4}\sum_{\substack{j=1\\j\neq i}}^{4}\sum_{\substack{k=j+1\\k\neq i}}^{4}\sigma_j^{\,2}\,\sigma_k^{\,2}\left(\frac{x-x_i}{r_i}\right)\left(\frac{z-z_i}{r_i}\right)-$$
$$-\frac{1}{|\mathbf{R}_{\boldsymbol{u}1}|}\sum_{i=1}^{4}\sum_{\substack{j=1\\j\neq i}}^{4}\sigma_v^{\,2}\,\sigma_w^{\,2}\left(\frac{x-x_i}{r_i}\right)\left(\frac{z-z_j}{r_j}\right) \qquad (5.21)$$

$$\mathfrak{I}_{0(23)}=\mathfrak{I}_{0(32)}=\frac{1}{|\mathbf{R}_{\boldsymbol{u}1}|}\sum_{i=1}^{4}\sum_{\substack{j=1\\j\neq i}}^{4}\sum_{\substack{k=j+1\\k\neq i}}^{4}\sigma_j^{\,2}\,\sigma_k^{\,2}\left(\frac{y-y_i}{r_i}\right)\left(\frac{z-z_i}{r_i}\right)-$$
$$-\frac{1}{|\mathbf{R}_{\boldsymbol{u}1}|}\sum_{i=1}^{4}\sum_{\substack{j=1\\j\neq i}}^{4}\sigma_v^{\,2}\,\sigma_w^{\,2}\left(\frac{y-y_i}{r_i}\right)\left(\frac{z-z_j}{r_j}\right)$$

$$v,w\in\{1,2,3,4\}-\{i,j\}\quad,\quad v<w$$

To consider an impact of stations number and position, the set of simulations were made. The set of scenarios worked with set of three (for possibility to compare achievable TDoA CRLB also for 2D case), four and five stations. All stations were placed to same z-coordinates to model the most probable placement in real applications.

The first scenario (Figure 5.2) shows development of CRLB with different height of the transmitter. The CRLB was calculated in a grid of positions in 3D with step 100 m. The figures show values of theoretically achievable variance of TDoA position for heights 0 up to 3 km. The value of sigma for single measurement was set to 30m, which corresponds to error of detection of delay of 1 nanosecond. For the all further presented graphs are common following parameters: distance shown in km, colorbar represents value of standard deviation in km, values higher than 1000m were cut for sake of readability.

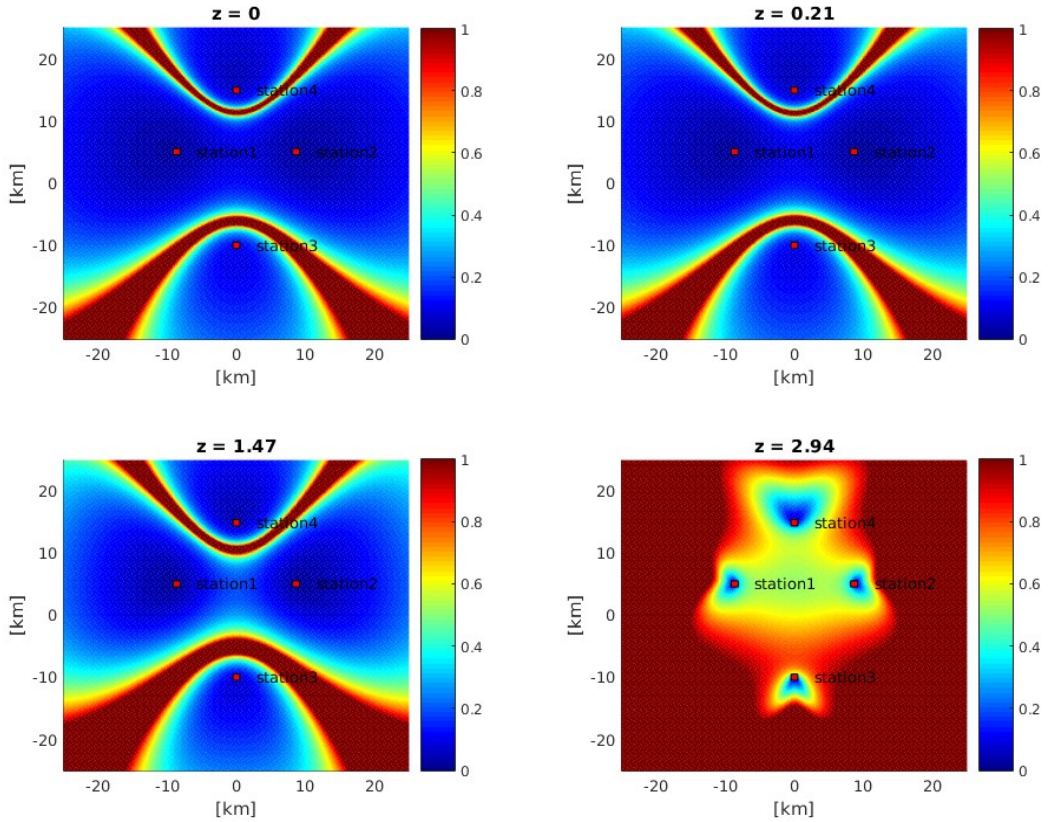

Figure 5.2: CRLB values of the 3D position for TDoA measurement with a set of 4 stations. Pictures represent horizontal slices for z values 0, 210 m 1.47 km and 2.94 km. The positions of stations are marked by red rectangles

The images above also show the influence of the placement of the sensors in the regular geometry, which can lead to Fisher matrix to be singular of close to singular for some positions of transmitter. In the graphs it represent hyperbolic belts e.g. around station 4 and station 3.

The comparison was made also for case of 2D measurements to correlate the results with those published in other works [67]. The Figure 5.3 therefore shows comparison of 2D measurement scenario with 3 stations and 4 stations. Since the calculations are made in two dimensions only, there are different dimensions of matrices and therefore the values for 4 stations differ from values obtained by full 3D calculations. Nevertheless, the impact of additional station is clearly visible in both cases (2D version and 3D version) by widening of areas with low values of CRLB.

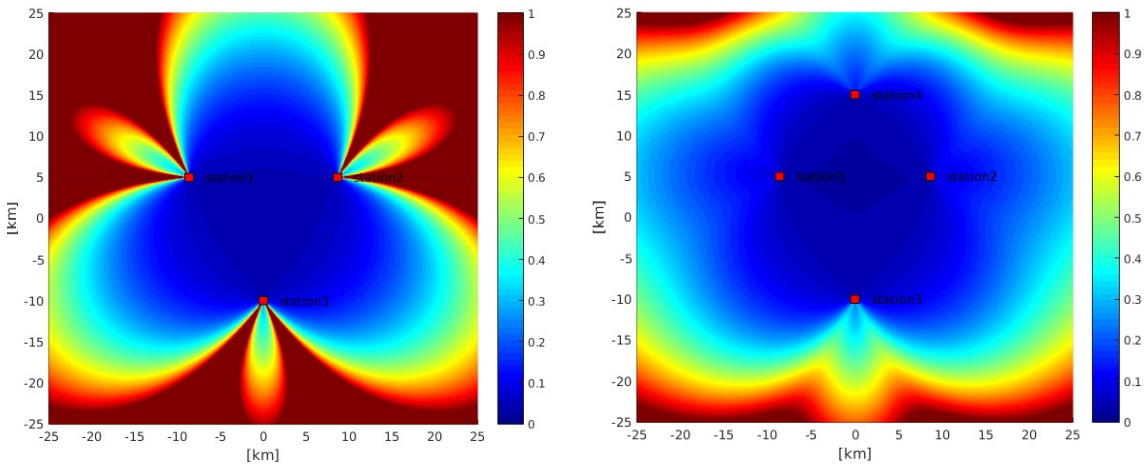

Figure 5.3: CRLB plots for 2D TDoA position for use of minimal set of 3 stations (a) and set with one additional station (b)

The same impact is observable for case of 3D scenario, where was the set of four stations from Figure supplemented by an additional station, the results can be seen at Figure 5.4.

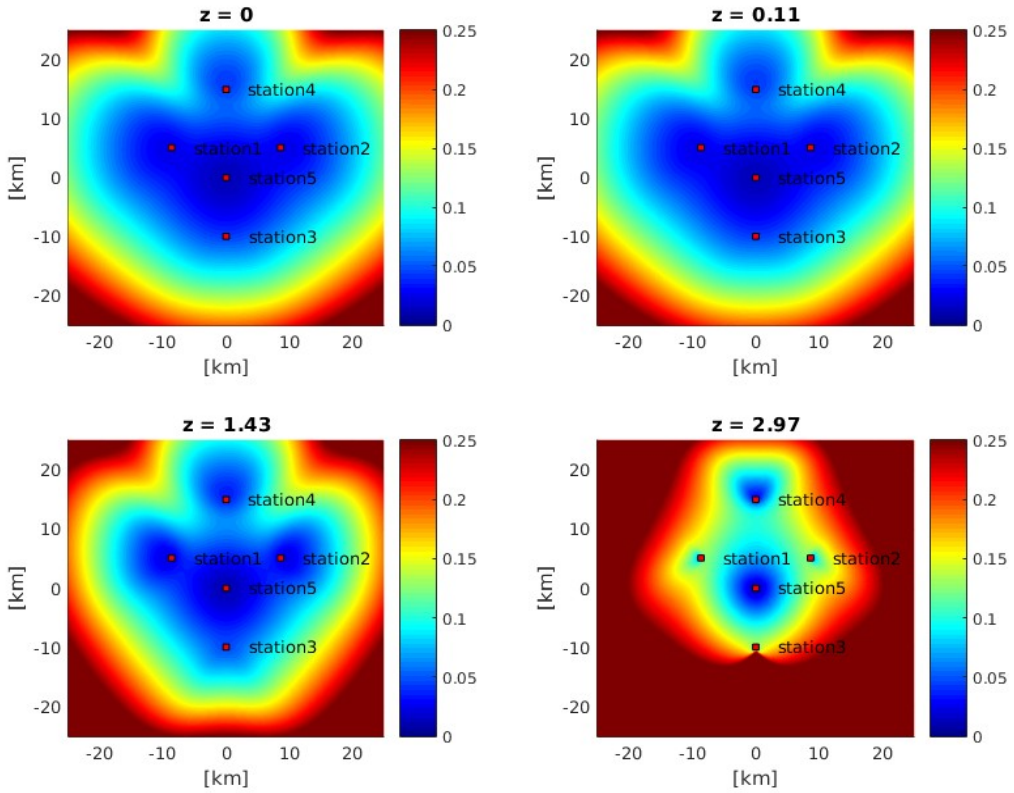

Figure 5.4: CRLB plot for 5 stations. (Note: the colorbar has 4 times smaller range than in the case of 4 stations)

The expression of FIM in (5.19)-(5.21) also respects the non-uniform values of variance for the individual mesaurements, this impact to the CRLB can be demonstrated at the Figure 5.5, where sigma value for station 4 was set to be 3 times bigger than for the rest of stations. It is also logical, that biggest impact to the results will have the error variance of measurements of reference station.

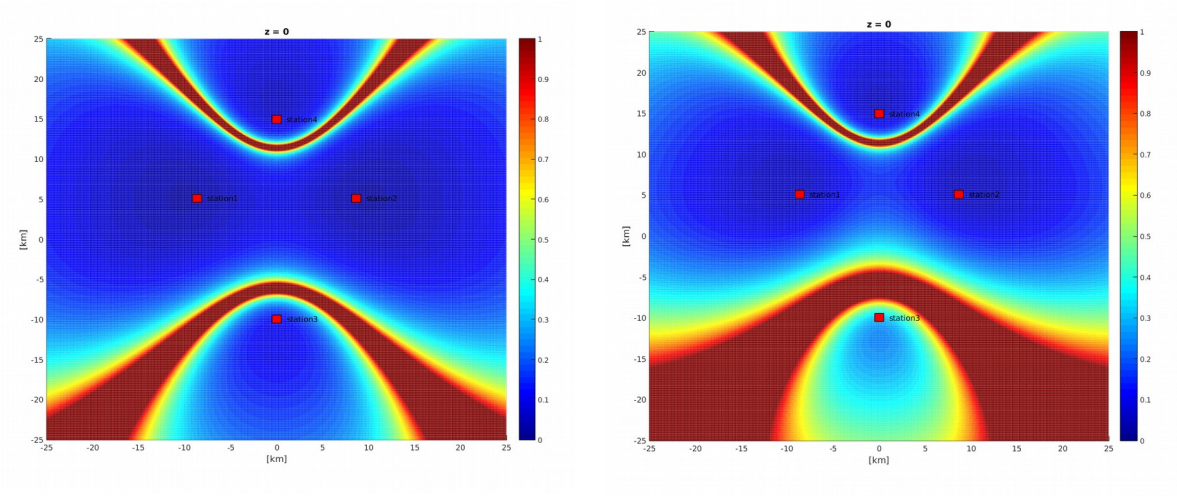

(a) (b)

Figure 5.5: CRLB plot for uniform (a) and non-uniform (b) values of measurement error variance

To be able to consider influence only of the geometrical configuration, the Fisher information matrix is expressed without the part representing the covariance of single range(or related delay) measurement error and (5.15) becomes to a form of matrix of dimensionless coefficients representing the impact of angles for mutual vectors between transmitter and receiving stations. It can be easily demonstrated graphically on following picture Figure 5.6.

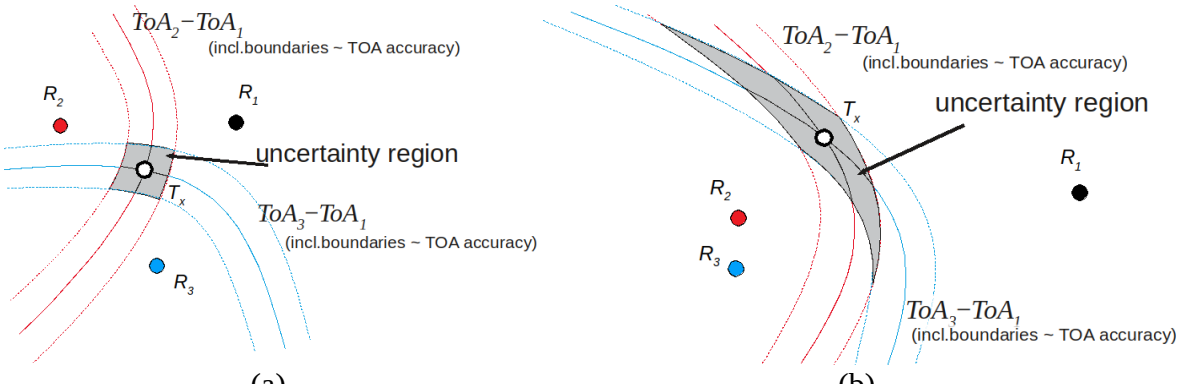

(a) (b)

Figure 5.6: Impact of TOA measurement errors for TDoA solution for good constellation of stations (a) and bad constellation of stations (b)

Since individual range measurements (equivalent to ToA measurements) are affected by errors, the TDoA solution (which consists from a pair of ToA measurements) forms not single hyperbola but it can be imagined as a stripe (in 2D) or tube (in 3D) with boundaries representing uncertainties in measurement. The intersection of these stripes or tubes forms region where the target position is expected. The size and shape of this region is affected by mutual position of receivers and target transmitter[59].

The parameter, related to the influence of mutual constellation of transmitter and receivers has then form of inverse dimensionless Fisher information matrix

$$\boldsymbol{DOP} = \left(\frac{\partial \boldsymbol{RD}_{\boldsymbol{u1}}(\boldsymbol{u})}{\partial \boldsymbol{u}} \right)^{T} \left(\frac{\partial \boldsymbol{RD}_{\boldsymbol{u1}}(\boldsymbol{u})}{\partial \boldsymbol{u}} \right)^{-1} \tag{5.22}$$

and is called Dilution of precision (DOP). The impact of geometry in 3D x,y,z space is expressed as GDOP (Geometrical dilution of precision) [68] and has form of

$$GDOP = \sqrt{\mathrm{tr}\left(\boldsymbol{DOP}\right)} \tag{5.23}$$

The following figures present values of HDOP coefficient (i.e. DOP coefficient calculated for 2D case) for Prague Vaclav Havel airport obtained during measuring capaign of MLAT transponders.

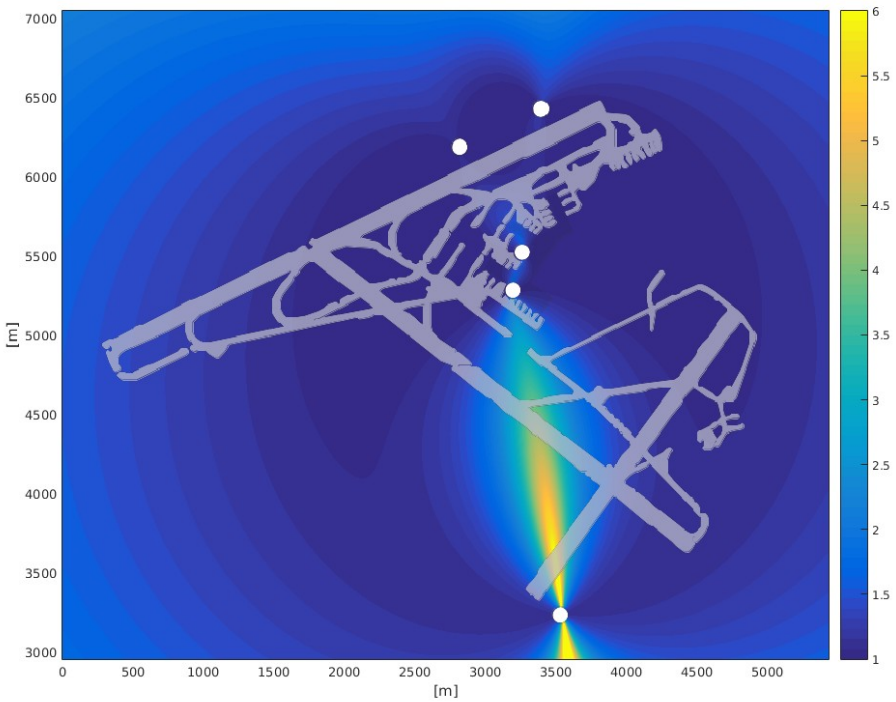

Figure 5.7: HDOP for Prague Vaclav Havel airport for system with 5 stations

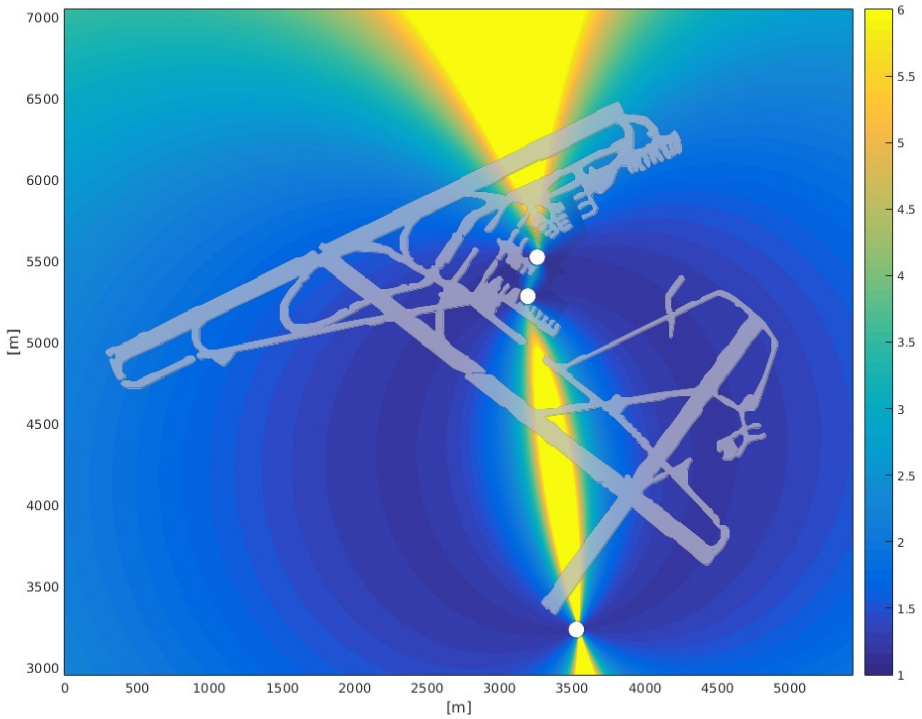

Figure 5.8: HDOP for Prague Vaclav Havel airport for system with minimal configurations of 3 stations

It is evident from CRLB values and formulation that TDoA measurement variance is dependent on single range measurement variance σ_i^2 for particular sensor. The CRLB for single delay estimate in AWGN is according to [65]

$$\sigma_i^2 \geq \frac{1}{SNR_i \cdot B^2} \quad , \tag{5.24}$$

where SNR_i is signal to noise ratio of signal measured by station $\boldsymbol{u}_i$ and B is signal bandwidth. Therefore, it is further necessary (and it will be discussed in the next chapter) to make considerations of signal processing during delay estimation.

Moreover, the impact of SNR can be alleviated by an increase of the noise background due to radio interference, which can be to some extent avoided, but also by noise produced by e.g. solar bursts in radio spectrum that are extremely wide-band and can from steady quiet state of Sun represented by radiations of about 100 SFU (Solar flux units) reach during a burst the intensities of about 100 000 SFU which means in common receiver with 3 dB antenna gain a drop of SNR by 15 dB [6], [69].

5.1.2 ML based position estimation methods

Although the mentioned CRLB provides estimate variance for general TDoA measurements, the concrete solution of hyperbolic equations can vary. The ML methods use the probabilistic description of the relationship between unknown parameters that are estimated and measured values. So, if the joint probability density function (PDF) of measured data $\boldsymbol{d}$ is available and can be expressed as conditional probability $p(\boldsymbol{d}|\boldsymbol{u})$ dependent on unknown parameter $\boldsymbol{u}$ (that is estimated), ML estimation can be then stated a maximization of of the formed likelihood function across possible values of $\boldsymbol{u}$

$$\hat{\boldsymbol{u}} = \underset{\mathrm{u}}{\arg\max}\left(p\left(\boldsymbol{d}|\boldsymbol{u}\right)\right) \quad . \tag{5.25}$$

The estimate calculation is clearly dependent on the quality of description of the likelihood function, which can strongly vary according to the environment, time-variance of the signals, transmission medium, and possible interference. Therefore the available research works are not very frequent and usually restrain to a simple assumption of a signal in AWGN (additive white Gaussian noise) channel case [67], [70]–[72], where the character of normal distribution of uncorrelated additive noise simplifies an evaluation of log-likelihood function and solution of such created non linear equations by implementing various (usually iterative) methods, e.g. unscented Kalman filter [73] or Gaussian sum approximation [74]. Moreover, the ML approach is usually exhaustive in search space during the process of the calculation of values of likelihood function and therefore puts stress on numerical resources [74].

5.1.3 LS based position estimation methods

The advantage of LS based methods in comparison to ML approach is no need of apriori knowledge of the measurement probability density function (PDF) in the simple unweighted approach (and for approaches with weighting transformation matrices the knowledge of second order moments is usually sufficient [75]). It can be demonstrated [76] that ToA and TDoA measurements can be transformed to each other and still keep the full information necessary for position computation, so the algorithms developed purely for ToA cases can be also used for TDoA measurements. We will focus on algorithms, primary developed for TDoA cases.

The LS based methods can be classified to two main groups: the methods using some direct form of expression of hyperbolic equations solution and the methods using iterative steps to reach a position solution. For the single measurement of delay (ToA) we get measured pseudorange

$$d_i = \|\boldsymbol{u} - \boldsymbol{u_i}\| + b_i + e_i \qquad i = 1, \ldots, m \quad , \tag{5.26}$$

where $\boldsymbol{u}_i$ denotes position of *i*-th receiver, b_i represents difference between receiver and transmitter clocks weighted by speed of light and $\|\boldsymbol{u}-\boldsymbol{u}_i\|$ operation represents as same as in section of CRLB derivation

$$\|\boldsymbol{u}-\boldsymbol{u}_i\|=\sqrt{(\boldsymbol{u}-\boldsymbol{u}_i)^T(\boldsymbol{u}-\boldsymbol{u}_i)}=\sqrt{(x_t-x_i)^2+(y_t-y_i)^2+(z_t-z_i)^2} \quad . \tag{5.27}$$

In case of synchronization of measuring stations (receivers) the parameter b_i is constant and for the range differences that are used for TDoA equations construction is this clock offset canceled. The distance differences equations with respect to a reference receiver $\boldsymbol{u}_r$ are

$$d_i-d_r=\|\boldsymbol{u}-\boldsymbol{u}_i\|-\|\boldsymbol{u}-\boldsymbol{u}_r\|+e_i-e_r \qquad i=1,\ldots,m-1 \quad . \tag{5.28}$$

It is then desired task to find a set of coordinates $\boldsymbol{u}$ in a such way that the function *f(.)* fits best to the measured data d in terms of minimizing (generally weighted) sum of squares of residuals

$$\hat{\boldsymbol{u}}=\arg\min_{\mathbf{u}}\left(\sum_{i=1}^{m-1} w_i r_i^2\right) \quad , \tag{5.29}$$

where residuals r_i are

$$r_i=d_i-d_r-\|\boldsymbol{u}-\boldsymbol{u}_i\|-\|\boldsymbol{u}-\boldsymbol{u}_r\| \quad , \tag{5.30}$$

or using (5.1)

$$\hat{\boldsymbol{u}}=\arg\min_{\mathbf{u}}\left([\boldsymbol{d}-f(\hat{\boldsymbol{u}})]^T\boldsymbol{W}[\boldsymbol{d}-f(\hat{\boldsymbol{u}})]\right) \quad , \tag{5.31}$$

where $\boldsymbol{W}$ is a weighting matrix respecting cases of non-consistent set of measurements.

The minimum occurs when the gradient of the term inside brackets in (5.29) is zero. The number of unknown parameters *n* then determines a number of gradient equations that have to be evaluated (for sake of simplicity assuming consistent measurements, hence $\boldsymbol{W}$ = **I**)

$$2\sum_{i=1}^{m-1} r_i\frac{\partial r_i}{\partial u_j}=0 \qquad j=1,\ldots,n \tag{5.32}$$

or

$$\mathbf{J}^T \boldsymbol{r} = \mathbf{0} \quad , \tag{5.33}$$

where $\boldsymbol{r}$ is an $(m-1)$ residuals matrix and **J** a Jacobian matrix with elements $J_{i,j} = \frac{\partial r_i}{\partial u_j}$.

Since there is not a rigorous closed solution of the above gradient equations the algebraic forms of solution or the iteration mechanism is usually introduced. The initial estimation for iteration case $\hat{\boldsymbol{u}}_0$ is made and then the unknown parameters are estimated interactively using in each step evaluation of general form of differences

$$_{k+1}\hat{\boldsymbol{u}} = {}_k\hat{\boldsymbol{u}} - \boldsymbol{Q}(\hat{\boldsymbol{u}})\Delta \boldsymbol{u} \quad , \tag{5.34}$$

where $\boldsymbol{\Delta u}$ are residuals obtained by previous iteration step, k is the iteration step, and $\boldsymbol{Q}(.)$ is arbitrary but positive definite matrix.

The next operation of iteration algorithms that is executed in every iteration step is a linearization of the measurement term ${}_k\boldsymbol{d}$ around estimated solution using first a form of Taylor expansion

$$_k\boldsymbol{d} = f({}_k\hat{\boldsymbol{u}}) + \partial_{\boldsymbol{u}^r} f({}_k\hat{\boldsymbol{u}})(\boldsymbol{u} - {}_k\hat{\boldsymbol{u}}) + o(\boldsymbol{u} - {}_k\hat{\boldsymbol{u}}) + {}_k e \quad , \tag{5.35}$$

where $\partial_{\boldsymbol{u}^r} f(\boldsymbol{u})$ denotes Jacobian matrix of ***f(u)*** and $o(\boldsymbol{u} - {}_k\hat{\boldsymbol{u}})$ is the Landau order term representing the remainder in the Taylor expansion which can be further considered negligible for $\hat{\boldsymbol{u}}$ colse to $\boldsymbol{u}$. So the problem of set on non-linear equations is transformed to to solution of a set of linear equations in each iteration step to produce differences in the form of residuals and use them for the next step estimate to minimize the estimation error [77]–[79].

There exist various approaches to reach the minimal residual error for the above linearized term. The most popular method is a Gauss–Newton algorithm [77] solving in every step k a set of normal equations created from Taylor expansion

$$\sum_{i=1}^{m-1} \sum_{q=1}^{n} J_{ij} J_{iq} \Delta u_q = \sum_{i=1}^{m-1} J_{ij} \; {}_k r_i \qquad j = 1, \ldots, n \quad , \tag{5.36}$$

where

$$J_{ij} = -\frac{\partial r_i}{\partial u_j} \quad , \quad \mathrm{J}_{\mathrm{iq}} = -\frac{\partial r_i}{\partial u_q} \quad , \quad {}_k r_i = d_i - f\left({}_k u_i\right) \quad , \tag{5.37}$$

or in equivalent matrix form

$$\left(\mathbf{J}^T \mathbf{J}\right) \boldsymbol{\Delta u} = \mathbf{J}^T \boldsymbol{r} \quad . \tag{5.38}$$

The expressed correction of $\boldsymbol{\Delta u}$ in (5.38) is in its weighted form applied to (5.34) as correction for new iteration step

$${}_{k+1}\hat{\boldsymbol{u}} = {}_k\hat{\boldsymbol{u}} - \left({}_k\mathbf{J}^T \boldsymbol{W}\, {}_k\mathbf{J}\right)^{-1} {}_k\mathbf{J}^T \boldsymbol{r}\left({}_k\hat{\boldsymbol{u}}\right) \quad . \tag{5.39}$$

The other common used method is a Levenberg-Marquardt algorithm [42] that modifies the Gauss–Newton method using correction factor for iteration step for (5.34) as

$$\boldsymbol{Q}\left({}_k\boldsymbol{u}\right) = \left({}_k\mathbf{J}^T \boldsymbol{W}\, {}_k\mathbf{J} + {}_k\alpha \boldsymbol{S}\right)^{-1} \quad , \tag{5.40}$$

where ${}_k\alpha$ is a non-negative scalar and **S** is a positive definite matrix. The presence of coefficient α enables a change of the length and direction of the shift in consecutive steps and therefore ease the convergence towards final solution.

The other recent methods that come to play go within the process of linearization of residual equations through the way of orthogonal decomposition, for example QR decomposition executing the expansion of Jacobian matrix in gradient equations **J**=**QR** to orthogonal matrix **Q** and upper triangular matrix **R** using some orthogonalization algorithm (e.g. Gram–Schmidt algorithm [80]) or singular value decomposition producing QR decomposition with additional column pivoting which works well for cases of rank deficient matrix that has to be decomposed [81]. All these cases are then solvable in the form of a set of linear equations.

Although the iteration methods provide asymptotically precise solution within their convergence region, their computational demands, need of an initial estimate, and convergence constraints bring an attraction to the direct methods that try to transform equations (5.29) and (5.31) to the approximate or equivalent linear form that can be analytically solved. However, every so far used transformation approach bring some from of loss of information in determined task therefore the result is more or less close approximation.

The first approach used an approximation of hyperbolic surfaces by the set of spheres and resolved the root search as a spherical intersections [82]. The process of approximation of hyperboloids by spheres is used in similar manner using spherical interpolation instead of intersection expressing measurement error by its quadratic form and then transforming it into set of linear equations multiplied by weighting matrix. It can be geometrically described as an

search of origin of sphere (estimated coordinates of target) that passes through an reference sensor and the distances of its surface to other sensors are the most close to measured range differences [44], [83]. The similar approach using linear equations to describe coordinates of intersections of true hyperbolic curves appears in [75], [84].

Many methods use an linearization approach based on squaring the positioning equations and therefore removal the square root from (5.27) which enables the transformation of minimization of squares of residuals from a problem of non-linear LS solutions to a linear LS case and intermediate non-linear variable. The non-linear measurement equation (5.1) is transformed to new form

$$\boldsymbol{d} = \boldsymbol{A}\,\boldsymbol{u} + \boldsymbol{B}\,\boldsymbol{b}_u + \boldsymbol{C}\,\chi(\boldsymbol{u}) + \boldsymbol{e} \quad , \tag{5.41}$$

where $\boldsymbol{A}$, $\boldsymbol{B}$, $\boldsymbol{C}$ are known matrices and $\chi(\boldsymbol{u})$ is non linear function of $\boldsymbol{u}$. The general solution [75]is then

$$[\hat{\boldsymbol{u}}, \hat{\boldsymbol{b}_u}, \hat{\chi}]^T = \underset{\mathbf{u}, \mathbf{b}_u, \chi}{\operatorname{argmin}} \left([\boldsymbol{d} - \boldsymbol{A}\,\boldsymbol{u} - \boldsymbol{B}\,\boldsymbol{b}_u - \boldsymbol{C}\,\chi(\boldsymbol{u})]^T \boldsymbol{W} [\boldsymbol{d} - \boldsymbol{A}\,\boldsymbol{u} - \boldsymbol{B}\,\boldsymbol{b}_u - \boldsymbol{C}\,\chi(\boldsymbol{u})] \right) \tag{5.42}$$

where weight matrix $\boldsymbol{W}$ is often chosen as the inverse of measurement $\boldsymbol{d}$ covariance matrix. The final estimation of unknown parameter (position of target) is then

$$[\hat{\boldsymbol{u}}, \hat{\boldsymbol{b}_u}, \hat{\chi}]^T = ([\boldsymbol{A}, \boldsymbol{B}, \boldsymbol{C}]^T \boldsymbol{W} [\boldsymbol{A}, \boldsymbol{B}, \boldsymbol{C}])^{-1} [\boldsymbol{A}, \boldsymbol{B}, \boldsymbol{C}]^T \boldsymbol{W}\, \boldsymbol{d} \quad . \tag{5.43}$$

The described approach is applied in several methods, using various transformations producing different versions of multiplicative matrices $\boldsymbol{A}$, $\boldsymbol{B}$, $\boldsymbol{C}$ and function $\chi(\boldsymbol{u})$ [46], [85]–[87].

The recent methods often combine several approaches together to ease the position solution, for example combining TDoA, FdoA and differential Doppler rate measurements for moving target to produce overdetermined system of equations and then application of linear LS estimation [88]. Other example of advanced positioning algorithm is a near-closed form solution by construction of low rank ToA matrix from TDoA measurements. The created matrix is then able to be described by a set of polynomial equations that can be solved by eigenvectors of polynomial coefficients matrix producing joint target and stations estimates thus suppressing the need of apriori synchronization of measuring stations [89].

The common strength of direct methods is in obtaining the estimated position from algebraic solution of the set of linear equations or the combination of linear equations and single non-linear element. The drawback on that some of the methods face the threat of singular or close to singular of the matrix in (5.43) that is inverted during estimation expression that can lead to

numerical problems [90]. The other possible complication is the fact, that most of the methods in case of lower number of sensors (typically if dimensinon of measurements *m* and dimension of unknown parameters *n* are equal) produce more candidates for position estimate, therefore there is a need of overdetermination of the system of measuring stations. It can be easily demonstrated on the case of popular closed method based on linear LS solution described in [86] and in detail provided in Appendix A.

The set of simulated calculations, for simplicity reasons in 2D (x,y) space, was done for different specific receiver positions. The constellation of three stations placed at positions (−10,−10) (station 1), (−10,10) (station 2), and (15,0) (station 3) is marked at the figures by small black squares. The station 1 was chosen as a reference one. The source of signal placed at coordinates (1,6) was chosen for definition of range distances to serve as input values for the computation. Correct solutions of equations are marked by black circles and false solution candidates are marked by white circles to be distinguished from remaining hyperbolas intersections that are not solutions of hyperbolic equations. As we can see from Figure 5.9 (left), the computation provides two possible positions, the correct one at (1,6) and a false candidate at (0.59, −5.87). In this case, we cannot eliminate the false solution by an often used approach that correct solution is inside area surrounded by receivers (this criterion makes sense for evaluation of position at the aerodrome surrounded by MLAT stations). The choice of different station as a reference one does not produce desired results which is demonstrated by a third hyperbolic curve (the green one) corresponding to the choice of station 2 to be the reference station.

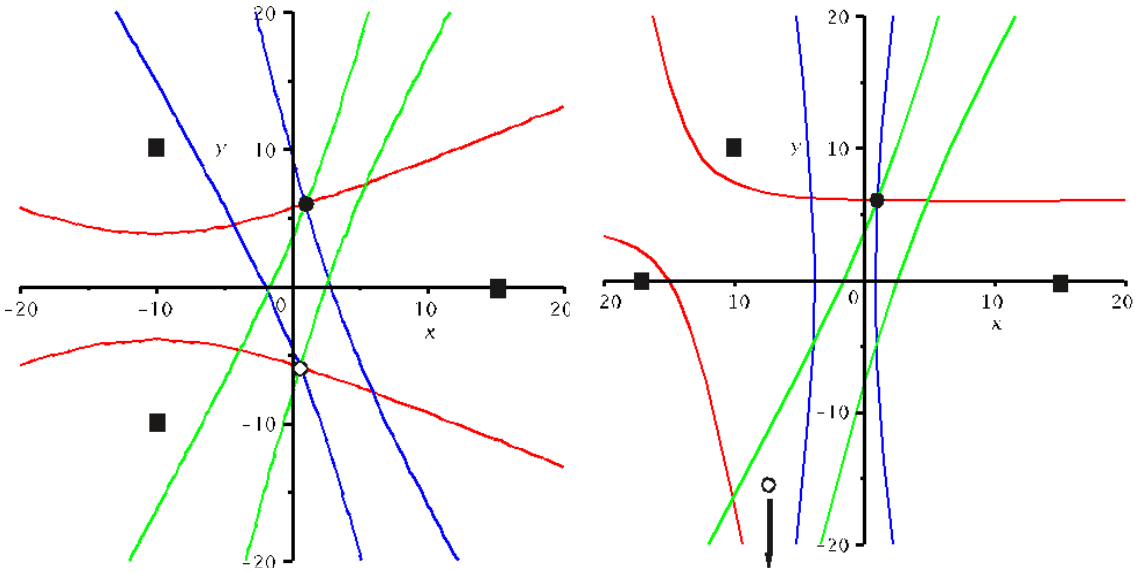

Figure 5.9: Solution of hyperbolic equations producing correct (black dot) and false (white dot) position. Left picture uses stations pairs 1–2(red), 3–2(blue), 1–3(green), right picture uses stations pairs 1–4(red),3–4(blue), 1–3(green).

This ambiguity can be resolved by either by using an additional station that increases measurement dimension by one, which will not only resolve the ambiguity in solution but it also will positively improve the CRLB of TDoA estimation. However it will lead to increase of number of equations in TDoA solution. The other simple approach is to use this fourth station to form new constellation of three receivers and jointly evaluate this TDoA solution with previous one. The computational load is not increased and with parallel processing possibilities it will bring no substantial delay in computations. This is demonstrated by right part of Figure 5.9, where station 1 from previous case was substituted by station 4 with coordinates (−18,0) which was chosen as a reference station. The computation provides again two solutions: (1,6) and (−8.3, −34.46). If we compare these two pair of solutions we can easily state the correct position.

6 Radio signal channel modeling

The propagation of radio signal is affected by various phenomena changing with the frequency, signal transmission rate, distance, time or propagation environment. To be able to describe the relationship between transmitted and received signal it is necessary to have some tool to express at least the approximation of such relationship. This is the reason, why various radio channel models are developed and evaluated.

The general relationship between transmitted signal $x(t)$ and received signal $y(t)$ can be described by the convolution operation

$$y(t) = h(t) * x(t) = \int_{-\infty}^{\infty} h(t-\tau)x(\tau)\ d\tau \tag{6.1}$$

where $h(t)$ is an impulse response of the channel. The expression describing the impulse response vary according to phenomena affecting signal propagation. The relation term is often complemented with a random addition additional component, representing additive noise, but for purposes of propagation channel description is usually omitted.

The main components of radio propagation are propagation path loss, shadowing effects described by large scale propagation models that predict the signal level for given distance between transmitter and receiver, and multipath propagation described by small scale propagation models that describe the signal fluctuations over short travel distance, equivalent to wavelength, or short time duration.

6.1 Path Loss

The free space path loss is a large scale general model to predict the received signal power loss over distance from transmitter. Its pure form is expressed by the Friis free space propagation equation [91]

$$P_r(d) = P_t \frac{G_t G_r}{\left(\frac{4\pi d}{\lambda}\right)^2} \tag{6.2}$$

where P_r is received power, P_t transmitted power, G_r and G_t are antenna gains of receiver and transmitter, respectively, λ is signal wavelength, and d is a distance between transmitter and receiver. The squared term represents the free space loss, related to the spherical spread of the electromagnetic wave from transmitter. The additional loses can be present in the equation,

representing attenuation caused by receiver antenna and hardware imperfection, impact of wave polarization etc.

Since the real environment is too complex to be analytically described, very often are applied empirical path loss models based on the statistical parameters derived from measurements in typical kinds of environment. Very popular for the wireless mobile communication is the Okumura-Hata model [92] that approximated the path loss for distance d in urban environment for frequencies 150–1500 MHz by term

$$L_{urban}(d)_{dB} = 69.55 + 26.16\log_{10}(f_c) - 13.82\log_{10}(h_t) - a(h_r) + \\ + (44.9 - 6.55\log_{10}(h_t))\log 10(d) \tag{6.3}$$

where f_c is a carrier wave frequency, h_t and h_r antenna heights of transmitter and receiver, respectively. The term $a(h_r)$ represents a correction factor for effective mobile antenna height depending on the type of environment (large city, small city, suburban area or open rural area). More complex models separate further the line-of-sight (LOS) and non-line-of-sight (NLOS) propagation e.g. a COST 231-Walfish-Ikegami model [93].

6.2 Shadowing

The situation when along the travel path of the radio signal exist any objects (such as buildings, trees, hills), some part of the transmitted signal is lost through absorption, reflection, scattering, and diffraction. This effect is called shadowing.

The most common model for such attenuation of the received signal is log–normal shadowing. The variations of the signal strength according to this model were empirically confirmed in both outdoor and indoor radio propagation environments [94].

In the definition of the log-normal shadowing, the transmitted P_t and received P_r power ratio ψ is assumed to be random variable with a log–normal distribution given by [91]

$$P(\psi) = \frac{\ln 10}{10\sqrt{2\pi}\sigma_{\psi dB}\psi}\exp\left[-\frac{(10\log_{10}\psi - \mu_{\psi dB})^2}{\sigma^2_{\psi dB}}\right] \tag{6.4}$$

where $\mu_{\psi dB}$ is the mean of $\psi_{dB} = 10\log_{10}(\psi)$ in decibels, and $\sigma_{\psi dB}$ is the standard deviation of ψ_{dB}. The mean $\mu_{\psi dB}$ includes both the path loss (i.e. free space loss component) and average of shadowing impact and often is obtained empirically for the particular environment.

There exist empirical models, that include both path loss and log–normal loss due to shadowing that state both mean values and variance of log–normal process, e.g. [94]–[96].

In practical use there is often implemented the combined term for relative power ratio in decibels in the form [91]

$$L_{dB}(d) = 10\log_{10}(K) + 10\,\gamma \log_{10}\left(\frac{d}{d_0}\right) + \psi_{sB} \tag{6.5}$$

where K is a unitless constant that depends on the antenna characteristics and the average channel attenuation, either obtained by measurement or approximated by $K_{dB} = 20\log_{10}(\lambda/(4\pi d_0))$, d_0 is a reference distance for the antenna far field, γ is the path-loss exponent with values varying from 1.5–6 depending on the propagation environment, and ψ_{dB} is a Gauss-distributed random variable with mean zero and variance $(\sigma_{\psi\mathrm{dB}})^2$ in range 4–10 dB according to the environment.

6.3 Multipath propagation

The signals emitted by transmitter can travel by not only the direct line-of-sight propagation path but they can be reflected or diffracted from near by objects and reach the receiver by other longer paths. The result of such multipath propagation then can be described as sum of incoming delayed copies of transmitted signal affected by multipath channel parameters

$$y(t) = \sum_{n=0}^{N_M(t)} \alpha_n(t) \exp(-j\,2\pi f_c\,\tau_n(t) - j\,\phi_{Dn})\, x(t - \tau_n(t)) \tag{6.6}$$

where the n index equal to zero represents direct path component, $N_M(t)$ is the number of multipath components, $\alpha_n(t)$, Φ_{Dn}, and $\tau_n(t)$ is a complex scaling factor, Doppler shift, and delay, respectively , of the n-th multipath component.

The impulse response of time–varying channel can be then described [91] as

$$h(t, \tau) = \sum_{n=0}^{N_M(t)} \alpha_n(t) \exp(-j\,\phi_n(t))\, \delta(\tau - \tau_n(t)) \tag{6.7}$$

where $\delta(\tau)$ is a Dirac delta and $\phi_n(t) = 2\pi f_c\,\tau_n(t) - \phi_{Dn}$. In case of time–invariant channel we will have $c(t, \tau) = c(t + T, \tau) = c(\tau)$, so the impulse response does not vary with time of application. If the time delay of the n-th multipath component is applied in combination with the frequency of the carrier wave f_c ,the combination of the resulting term $\exp(2\pi f_c \tau_n(t))$ will cause changes of the phase of the multipath component with respect to direct path component. In case that $f_c\tau_n(t) \gg 1$, a small change in the path delay can lead to a large phase change in the nth multipath component,which leads to additive (constructive or destructive)

impact to the levels of received signal causing rapid changes of the signal strength, a process that is called the fading.

The two parameters, a delay spread and a coherence bandwidth are used to describe the channel behavior in relationship with the delays of multipath components. The delay spread corresponds to a variance of delays of the multipath components which helps to classify the fading as a narrow–band fading (flat fading) case when the delay spread is lower than the duration of the symbol period and the wide–band fading (frequency selective), when the delay spread is greater than the symbol period and multipath components are separable in terms of symbol sampling. Since the delay spread covers all multipath components, including those, that are in real channel bellow the noise background level and therefore does not practically contribute to the signal dispersion, the delay spread is usually defined with respect to the channel power delay profile [97], which represents the average power associated with a given multipath delay. To better describe the delay spread, the additional parameters are usually defined:

- *Maximum excess delay* (*x* dB) is defined as the time delay during which power delay profile falls to *x* dB below given reference level (it can be level of the first registered component or the maximal level of excess delay)
- *Mean excess delay* is the first moment (mean) of the power delay profile
- *RMS delay spread* is the square root of the second central moment (variance) of the power delay profile

The typical values od RMS delay spread are in the order of fractions of microseconds to multiples of microseconds for outdoor channels and in the order of nanoseconds for indoor channels [98].

The coherence bandwidth B_c is a measure of channel independence in frequency, it defines the minimum frequency separation for which the channel impulse response is independent. In the relationship to the type of fading, it can be said, that the channel with coherence bandwidth greater than bandwidth of the signal can be considered as frequency flat and the channel with coherence bandwidth lower than bandwidth of the signal is considered as frequency selective.

6.3.1 Flat fading

In case of the flat fading, the multipath structure of the channel is such that the spectral characteristics of the transmitted signal are preserved at the receiver. For the received signal we can observe variations of the power level with time, which is mainly caused by fluctuations in the gain of the channel caused by multipath. The envelope of the multipath components r_n of the flat fading channel [91] can be described by Rayleigh distribution

$$p(r_n)=\begin{cases} \dfrac{r_n}{\sigma_n^{\,2}}\exp\left(-\dfrac{r_n^2}{2\,\sigma_n^{\,2}}\right) & ,r_n\geq 0 \\ 0 & otherwise \end{cases} , \tag{6.8}$$

where term $2(\sigma_n)^2$ represents average power of the received signal component. So the probability that envelope of *n*-th component does not exceed a given value A is given by a cumulative distribution function (CDF)

$$Pr(r_n\leq A)=\int_0^A p(r_n)\,d\,r_n=1-\exp\left(-\frac{A^2}{2\,\sigma_n^2}\right) . \tag{6.9}$$

If the multipath components of the complex envelope have the Rayleigh distribution, we can assume that the inphase and quadrature parts of the complex envelope have jointly Gaussian distributions. Then their autocorrelation functions depend only on difference of time intervals and the channel can be considered as wide-sense stationary (WSS).

In case that the signal has a dominant non fading component, e.g. the component related to the direct line-of-sight propagation, the fading envelope respects the Rice distribution

$$p(r)=\begin{cases} \dfrac{r}{\sigma^2}\exp\left(-\dfrac{r^2-\alpha_0^2}{2\,\sigma_n^{\,2}}\right)I_0\left(\dfrac{r\,\alpha_0}{\sigma^2}\right) & ,r_n\geq 0 \\ 0 & otherwise \end{cases} , \tag{6.10}$$

where $2\sigma^2$ is the average power in the non-LOS multipath components and α_0^2 is the power in the LOS component and I_0 is a modified Bessel function of zeroth order.

Although the description of the fading by Rayleigh and Rice distributions usually suffices for signal model, there exist some cases where it does not completely fit. Therefore, another distribution was developed for these cases with the parameters that can be adjusted to fit empirical measurements. It is called the Nakagami distribution or m-distribution [99] and is defined as

$$p(r)=\begin{cases} \dfrac{2m^m r^{2m-1}}{\Gamma(m)P_r^{\,m}}\exp\left(-\dfrac{m\,r^2}{P_r}\right) & ,r\geq 0, m\geq 0.5 \\ 0 & otherwise \end{cases} \tag{6.11}$$

Where P_r is signal average power and Γ(.) is a Gamma function. The Nakagami distribution can for m = 1 transform to Rayleigh fading and for m = (K + 1) 2 /(2K + 1) the distribution is approximately Rician fading with parameter K.

Since the detailed mathematical description of the flat fading is often too complex, some simplified or empirical models are often applied. An example can be a finite state Markov channel (FSMC) [91] which uses the discrete-time Markov process with time discretized to a given interval T (typically the symbol period). It can model all above described distributions for various applications and purposes [100].

6.3.2 Frequency selective fading

The case when coherence bandwidth of the channel is lower than bandwidth of the transmitted signal causes a constant-gain and linear phase response over only a small part of signal bandwidth, so certain frequency components in the received signal spectrum have greater gains than others. The received signal the includes multiple versions of the transmitted waveform which are attenuated and delayed in time with the delays equivalent or greater than symbol period and so induce inter-symbol interference. Such kind of fading is called frequency selective fading.

In case of the wideband signal the signal symbols do not any more represent combination of random multipath components within the time approximately equal to symbol period, so producing the random variation s of amplitude according to the particular distribution, on the contrary the delay of the multipath components cause combination of significantly shifted “copies” of the symbol pulse producing strong inter-symbol interference.

In case that the number of the multipath components is sufficiently large, the impulse response can be considered according to the central limit theorem to be Gaussian distributed and thus only the statistical parameters of mean, variance and autocorrelation function can describe the channel. If we can assume for in- phase and quadrature components of the complex envelope of the signal to be Gaussian distributed, we can then use again the distributions of multipath components with Rayleigh distribution [91].

The statistical description of many parameters of the frequency selective fading channel can be derived from the autocorrelation function of the channel impulse response

$$A_c(\tau_1, \tau_2; t, t+\Delta t) = \mathbf{E}[h^*(\tau_1; t) h(\tau_2; t+\Delta t)] \quad , \tag{6.12}$$

where **E**[.] is expectation. In case of a very common WSS channel, the autocorrelation function depends only on time difference, hence $A_c(\tau_1, \tau_2; t, t+\Delta t) = A_c(\tau_1, \tau_2; \Delta t)$. Moreover, in the real environment we can also often assume that different multipath components are produced by independent scatterers and thus are independent. Such channel

with autocorrelation function dependent only on the value of multipath delay and time difference $A_c(\tau; \Delta t)$ is called WSS channel with uncorrelated scattering (WSSUS).

The parameter Power delay profile (PDP) that describes distribution of the average power with multipath delay is equal to the autocorrelation function for zero time difference, i.e. $A_c(\tau; \Delta t = 0)$. The mean excess delay and RMS delay spread can be then defined with the help of $A_c(\tau)$ as

$$\mu_{Tm} = \frac{\int_0^\infty \tau A_c(\tau) d\tau}{\int_0^\infty A_c(\tau) d\tau} \quad , \quad \sigma_{Tm} = \sqrt{\frac{\int_0^\infty (\tau - \mu_{Tm})^2 A_c(\tau) d\tau}{\int_0^\infty A_c(\tau) d\tau}} \quad . \tag{6.13}$$

The delay spread $T_{\max}$ of the channel is usually taken as the value of delay, when $A_c(\tau)$ is approximately zero for any $\tau > T_{\max}$. The relationship between symbol period T_S and RMS delay spread can provide considerations about ISI in the channel, the ISI can occur significantly for $T_S \gg \sigma_{Tm}$.

The frequency selective fading channels are usually modeled as a sum of several flat fading channels with different delays and Rayleigh distributions of multipath components.

The empirical models also exist for modeling the simplified versions of mathematical model, an example can be a model from ITU recommendation .[101]

6.3.3 Fast and slow fading

Because the delay spread does not provide information about the time varying nature of the channel caused by either relative motion between the transmitter and the receiver, or by movement of objects in the channel, another parameters are introduced, a Doppler spread and a coherence time of the channel.

Doppler spread is a parameter describing the spectrum widening caused by the time rate of change of the mobile radio channel and is defined as the range of frequencies over which the received Doppler spectrum is essentially non-zero.

Coherence time is the time domain dual of Doppler spread and is used to characterize the time varying nature of the frequency dispersiveness of the channel in the time domain. Coherence time is a statistical measure of the time duration over which the channel impulse response is essentially invariant. and over which two received signals have a strong potential for amplitude correlation.

According to the Doppler spread and coherence time we can distinguish a channel with fast or slow fading.

In the channel with fast fading, the Doppler spread is high and coherence time is lower than the symbol period. The channel impulse response changes rapidly within the symbol duration and signal distortion due to fast fading increases with increasing Doppler spread relative to the bandwidth of the transmitted signal. In practice, fast fading only occurs for very low data rates or very fast motion speed.

On the other hand, in case of slow fading, the Doppler spread of the channel is much less than the bandwidth of the signal and the channel impulse response changes at a rate much slower than the transmitted signal. The channel then may be assumed to be static over one or several reciprocal bandwidth intervals.

6.3.4 Multipath modeling in the discrete time domain

To be able to realize modeling for signal processing and simulations, the models described in previous chapters are transformed to the discrete time domain.

The first possibility is to use clustering of the isolated point scatterers producing similar delay as introduced in [91]. In this model, the multipath components are assumed to form subpath clusters, the components from the same cluster with close delays are then described by a common delay, and incoming paths on different subpath clusters with delays τ_n and τ_m , where the delay difference is bigger than inverse value of the signal bandwidth, can be resolved.

Other approach, which will be used in this thesis models the impulse response as an linear transversal FIR filter represented as a tapped delay line (TDL) model [97].

The general time–variant model has variable tap gains a_k, variable tap delays τ_k, and variable number of taps K. The lowpass-equivalent impulse response of such discrete multipath channel is given

$$\widetilde{h}[\tau,n]=\sum_{k=1}^{K[n]}\widetilde{a}_k(\tau_k[n],n)\,\delta(\tau-\tau_k[n]) \tag{6.14}$$

where $\delta(.)$ is unit pulse and symbol ~ denotes lowpass-equivalent form of related parameter. For such outdoor multipath channel evaluated in time limited interval, we can assume approximation based on considered constant number of discrete components and negligible variation of delay values. The model then simplifies to

$$\widetilde{h}[\tau,n]=\sum_{k=1}^{K}\widetilde{a}_k[n]\,\delta(\tau-\tau_k) \tag{6.15}$$

and corresponding lowpass-equivalent output is

$$\tilde{y}[n]=\sum_{k=1}^{K}\tilde{a}_k[n]\tilde{s}[n-\tau_k] \tag{6.16}$$

where $\tilde{s}[n]$ is a lowpass-equivalent input signal to the radio channel.

Such band limited channel then can be described by output of the tapped delay line (TDL) system with corresponding structure shown at Figure 6.1. The output is given

$$\tilde{y}[n]=\sum_{m=0}^{M-1}\tilde{s}[n-mT]\tilde{g}_m[n] \tag{6.17}$$

where $\tilde{g}_m[n]$ are TDL tap gains in its lowpass-equivalent form

$$\tilde{g}_m[n]=\sum_{k=1}^{K}\tilde{a}_k[n]\alpha[k,m] \tag{6.18}$$

for total number of *N* taps from interval *m= 0,…,M-1* , where

$$\alpha[k,m]=sinc\left[\frac{\tau_k}{T}-m\right] \tag{6.19}$$

and $T=1/B$ is a sampling period.

For WSSUS channel we can further consider both tap gains $a_k(t)$ and related TDL tap gains $g_n(t)$ to be substituted by time invariant values a_k, g_n, respectively.

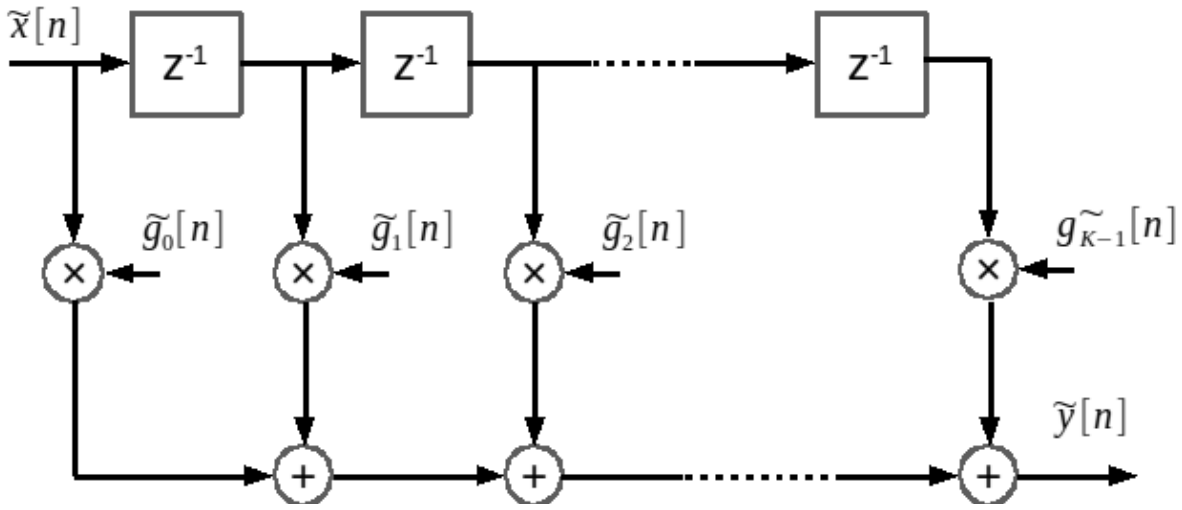

Figure 6.1: Uniformly spaced TDL model for band limited discrete multipath channel

7 ADS–B signal detection and decoding

7.1 General approach to signal detection

The common concept of radar signal receiver employs an envelope detector block followed by threshold evaluation and decision block (Figure 7.1). The detector block usually works either in terms of signal complex envelope or its in-phase and quadrature components.

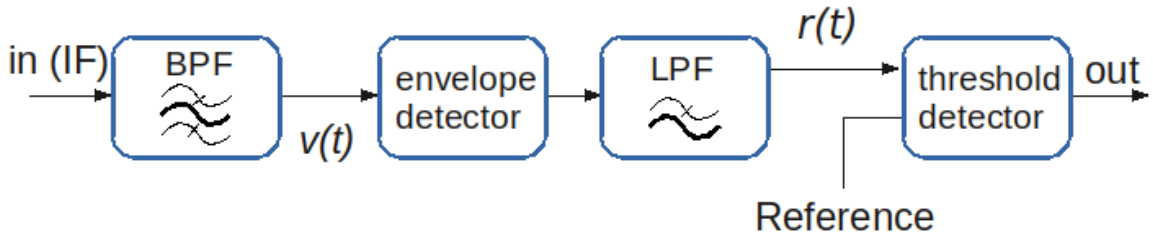

Figure 7.1: General block scheme of receiver with envelope detector and threshold based detection

The detection mechanism for radar signals is generally based on binary evaluation of hypothesis testing problem, where H_0 means the hypothesis that no signal from the target is present and H_1 is the hypothesis that the signal from target is present [16].

For most simple case, the signal coming to receiver consists of a target signal *s(t)* and additive zero mean white Gaussian noise *n(t)* with variance σ^2, uncorrelated with target signal. The bandpass signal *v(t)* (obtained from received combination of *s(t)* and *n(t)*) that is processed has a general form

$$\begin{aligned} v(t) &= v_I(t)\cos(\omega_{IF}t)+v_Q(t)\sin(\omega_{IF}t) = \\ &= r(t)\cos(\phi(t))\cos(\omega_{IF}t)+r(t)\sin(\phi(t))\sin(\omega_{IF}t) \end{aligned} \tag{7.1}$$

where ω_{IF} is the bandpass carrier frequency, *r(t)* is the envelope of *v(t)* and the phase $\phi(t)=\arctan(v_Q(t)/v_I(t))$.

The most simple and conservative approach is a threshold comparison of the processed signal to evaluate a presence of target produced signal in the received signal. The presence of the target is in the received signal detected when received envelope *r(t)* exceeds the defined threshold V_T in a form of standard binary hypothesis testing approach

$$\begin{array}{ll} \boldsymbol{H}_1: & s(t)+n(t)>V_T \quad \textit{Detection} \\ \boldsymbol{H}_0: & n(t)>V_T \quad \textit{False alarm} \end{array} . \tag{7.2}$$

The goal is then maximize the probability of detection for given probability of false alarm or minimize probability of false alarm for given probability of detection.

7.1.1 Probability of detection and probability of false alarm

The single trial probability of detection P_d and the single trial probability of false alarm P_{fa} can be determined by following formulas

$$\begin{array}{l} P_d = \int_{V_T}^{\infty} p_s(z)\,dz \\ P_{fa} = \int_{V_T}^{\infty} p_n(z)\,dz \end{array} , \tag{7.3}$$

where $p_s(z)$ is the PDF of the envelope $r(t)$ for the case of the signal presence, $p_n(z)$ is the PDF of the envelope $r(t)$ for the case of the absent signal.

Assuming the most common case [97], that I and Q parts of combination of signal and additive noise have a Gaussian distribution, the envelope *r(t)* can be expressed as $\sqrt{I^2+Q^2}$ and $p_s(z)$ has a Ricean distribution

$$p_s(z) = \begin{cases} \frac{z}{\sigma_n^2}\exp\left(-\frac{z^2+A^2}{2\sigma_n^2}\right) I_0\left(\frac{zA}{\sigma_n^2}\right) & \text{for } z \geq 0 \\ 0 & \text{otherwise} \end{cases} , \tag{7.4}$$

Where σ_n^2 is a root mean square (RMS) noise power, A is a RMS signal amplitude, and I_0 is a modified Bessel function of zeroth order that can be approximated as

$$I_0(x) \approx \frac{e^x}{\sqrt{2\pi x}} \quad \text{for } x \gg 1 . \tag{7.5}$$

In a case that no signal is present, the (7.4) evaluated for $A=0$ yields in $p_n(z)$ with Rayleigh distribution described as

$$p_n(z) = \frac{z}{\sigma_n^2}\exp\left(-\frac{z^2}{2\sigma_n^2}\right) \tag{7.6}$$

Using (7.6) for evaluating P_{fa} with (7.3) we can derive the threshold level V_T for desired single trial probability of false alarm in terms of measured 1-sigma noise power as follows:

$$V_T = \sigma_n \sqrt{-2 \ln P_{fa}} \tag{7.7}$$

The single trial probability of detection P_d is the probability that sample of envelope *r(t)* will exceed the threshold level V_T for case H_1 (signal plus noise) and can be expressed using (7.3), (7.4) and (7.6)

$$P_d = \int_{\sigma_n \sqrt{-2 \ln P_{fa}}}^{\infty} \frac{z}{\sigma_n^{\,2}} \exp\left(-\frac{z^2 + A^2}{2\,\sigma_n^{\,2}} \right) I_0\left(\frac{zA}{\sigma_n^{\,2}} \right) dz \tag{7.8}$$

or

$$P_d = Q\left[\sqrt{\frac{A^2}{\sigma_n^{\,2}}}, \sqrt{2 \ln\left(\frac{1}{P_{fa}} \right)} \right] \quad , \tag{7.9}$$

where Q[.] is Marcum's Q–function [102]

$$Q[\alpha, \beta] = \int_{\beta}^{\infty} x\, I_0(\alpha x) \exp\left(-\frac{1}{2}(x^2 + \alpha^2) \right) dx \quad . \tag{7.10}$$

There are several approximations for calculation of Marcum's Q–function, e.g. [103], [104], the latter was used for calculations of the single trial probability of detection versus SNR for various values of probability of false alarm at Figure 7.2.

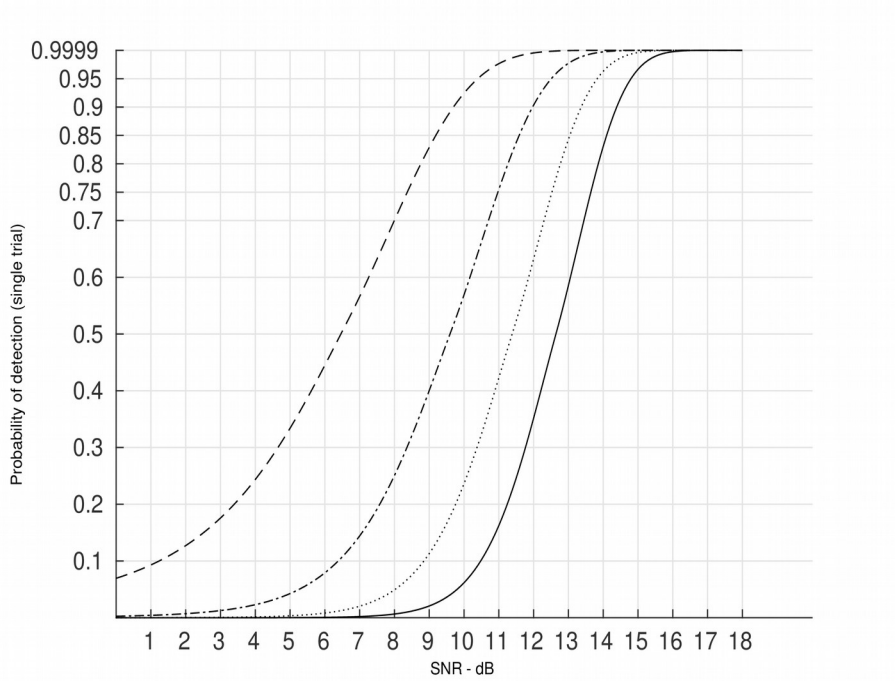

Figure 7.2: Probability of detection for single trial versus SNR for various values of Pfa (10^{-2} – dashed line, 10^{-4} – dash-dot line, 10^{-6} – dotted line, 10^{-8} – solid line).

Since modern radar signals, including ADS-B, consist of several pulses transmitted in one message, the single trial detection can be improved by an integration of several pulses and evaluation of this result. We can distinguish a coherent integration, preserving the phase relationship between the received pulses, and a non-coherent integration executed after the envelope detector, where the phase information is lost.

It can be shown that the coherent integration of of N_p consecutive pulses reduces the noise variance (power) by factor N_p [105]. Therefore, the required SNR of N_p coherently integrated pulses is N_p times lower than SNR for single pulse for same probability of detection. However, the precise estimation of exact phase of each transmitted pulse, especially in a difficult propagation environment, is a very complex task. Therefore, most of radar systems use for signal detection an approach of non-coherent integration usually from the reason of more simple implementation.

The criterion appropriate for ranging oriented signals (radar, navigation systems) is the Neyman-Pearson criterion [106] that maximizes the probability of detection P_d for a given probability of false alarm Pf_a by evaluation likelihood ratio with respect to given threshold for set of N consecutive signal samples in integration

$$L(v_1,\ldots,v_N)=\frac{p(v_1,\ldots,v_N;\boldsymbol{H}_1)}{p(v_1,\ldots,v_N;\boldsymbol{H}_0)}\geq V_T \tag{7.11}$$

where $p(v_1,\ldots,v_N;\boldsymbol{H}_1)$ and $p(v_1,\ldots,v_N;\boldsymbol{H}_0)$ are the joint probability density functions of N observations v_i under the conditions of signal source presence and absence, respectively.

The optimal detector with linear response and assumptions about signal stated by (7.4) and (7.6), the likelihood function transforms to

$$L(v_1,\ldots,v_N)=\prod_{i-1}^{N} I_0\left(\frac{A_i v_i}{\sigma_n^2}\right)\geq V_T \quad , \tag{7.12}$$

where I_0 is the modified Bessel function of zero order, σ_n^2 is the noise power, and A_i is the amplitude of the i–th pulse which for strong signals $(A_i \gg \sigma_n)$ becomes to a form of simple linear comparison $\sum_i A_i v_i > V_T$.

The other classical approach to detection of pulse presence is a Bayesian approach[107], minimizing probability of error of choice of opposite hypothesis as correct in contrary to the true one. If we assume again two hypotheses, $\boldsymbol{H}_0$, the received signal of pulse duration length contents noise only, and $\boldsymbol{H}_1$, the received signal of pulse duration contents signal with amplitude A and additive noise, the probability of error of detection can be written as

$$P_e = P(\boldsymbol{H}_0|\boldsymbol{H}_1)\,P(\boldsymbol{H}_1)+P(\boldsymbol{H}_1|\boldsymbol{H}_0)\,P(\boldsymbol{H}_0) \tag{7.13}$$

Then the criterion for the declaration of $\boldsymbol{H}_1$ as correct one in case of received signal $\boldsymbol{v}=\{v_1,\ldots,v_N\}$ is

$$\frac{P(\boldsymbol{v}|\boldsymbol{H}_1)}{P(\boldsymbol{v}|\boldsymbol{H}_0)} > \frac{P(\boldsymbol{H}_0)}{P(\boldsymbol{H}_1)} \tag{7.14}$$

If we consider same conditions of received signal as in previous derivations, i.e. a validity of (7.4) and (7.6), and assume equal probability of occurrence of $\boldsymbol{H}_0$ and $\boldsymbol{H}_1$, the criterion of choice of $\boldsymbol{H}_1$, so the declaration of presence of signal is

$$\frac{A}{\sigma_n^2}\sum_{n=1}^{N} v_n - NA^2 > 0 \tag{7.15}$$

The practical realization of the detectors can vary according to signal and application [16], but in present systems prevail several non-coherent integration detectors: a moving window, a

binary integrator (*M* of *N* detector), and a cumulative detection (1 of *N* detector) [108], [109]. Their principle is similar, they accumulate (integrate) *N* samples of received signal and compare result with declared threshold.

The common *M of N* search detector takes *N* pulses and compares them to the threshold for each consecutive pulse. If *M* or more of them are higher that threshold, the signal is declared present (Figure 7.3).

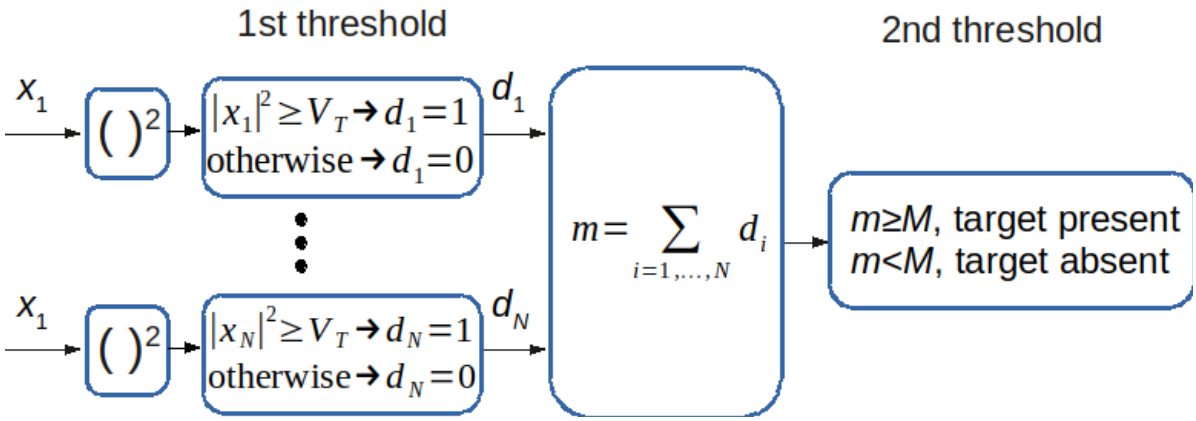

Figure 7.3: Block principle of binary non-coherent integration (M of N detection)

If not, the set is evaluated as without signal presence and the search continues in the next set. All these tests can then be described by Bernoulli trials and the binomial distribution characterizes both overall probability of false alarm

$$P_{FA} = \sum_{n=M}^{N} \binom{N}{n} (P_{fa})^n (1 - P_{fa})^{N-n} \tag{7.16}$$

and overall probability of detection

$$P_D = \sum_{n=M}^{N} \binom{N}{n} (P_d)^n (1 - P_d)^{N-n} \quad . \tag{7.17}$$

There can be said that integration over several pulses can improve probability of detection for given SNR in comparison to single trial detection, as can be seen at Figure 7.4 for various numbers of integrated pulses. The numbers respect possible number of evaluated pulses for selected parts of ADS–B signal.

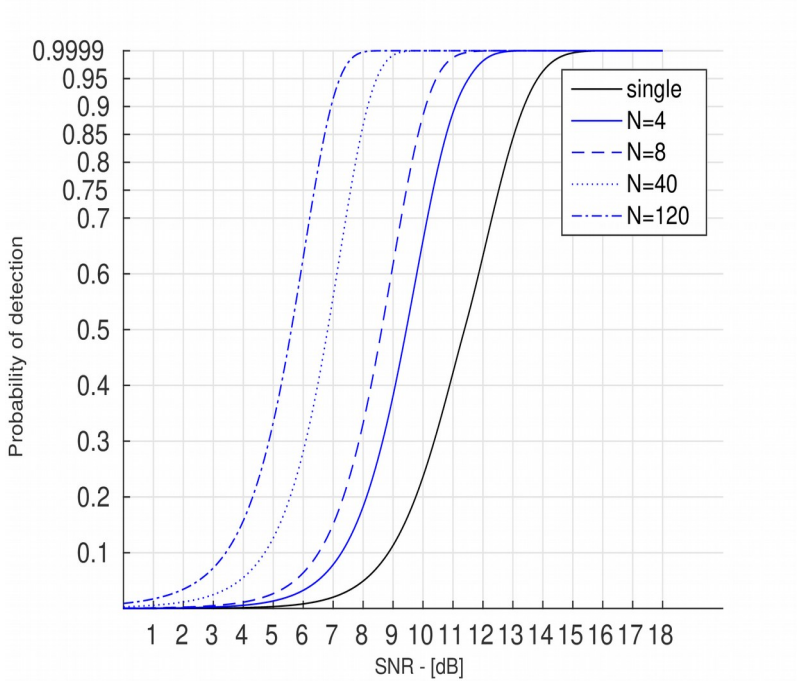

Figure 7.4: Comparison of probability of detection for various numbers of integrated pulses with single trial probability of detection for same probability of false alarm $P_{fa}=10^{-6}$.(black – single pulse trial, blue: solid – N=4, dashed – N=8, dotted – N=40, dash–dotted – N=120)

The possible detector approaches and realizations vary according to character of signal that has to be detected and processed. The case, common in present radars, when the signal is in the form of regular set of pulses, the spectral estimation for signal presence can be used as well[110]. The signal (without presence of noise) has a form of uniform pulse train

$$r(t)=\frac{1}{\sqrt{N T_p}}\sum_{n=0}^{N-1}\left(\eta(t-nT_r)-\eta(t-nT_r-T_p)\right) \tag{7.18}$$

or in case binary PPM modulation

$$r(t)=\frac{1}{\sqrt{N T_p}}\sum_{n=0}^{N-1}\left(\eta(t-nT_r-b_i\frac{T_r}{2})-\eta(t-nT_r-T_p-b_i\frac{T_r}{2})\right) \tag{7.19}$$

where N is a number of transmitted pulses, T_p is a pulse duration, T_r is a repetition interval for pulses (in case of ADS–B signal $T_r=2T_p$), b_i is a value of data bit {0,1}, and $\eta(t)$ is a Heaviside step function.

The spectrum of such rectangular uniform pulse sequence has for $T_r \ll 1$ a form of

$$S_r(f)=\sqrt{(NT_p)}\,sinc(\pi T_p f)\,sinc(\pi N T_r f)\exp(-j\pi f((N-1)T_r+T_p)) \tag{7.20}$$

with spectrum peaks separated according to time parameters (T_p, T_r) of pulse signal (Figure 7.5). The accumulation across several intervals then can be used to increase detection probability[110].

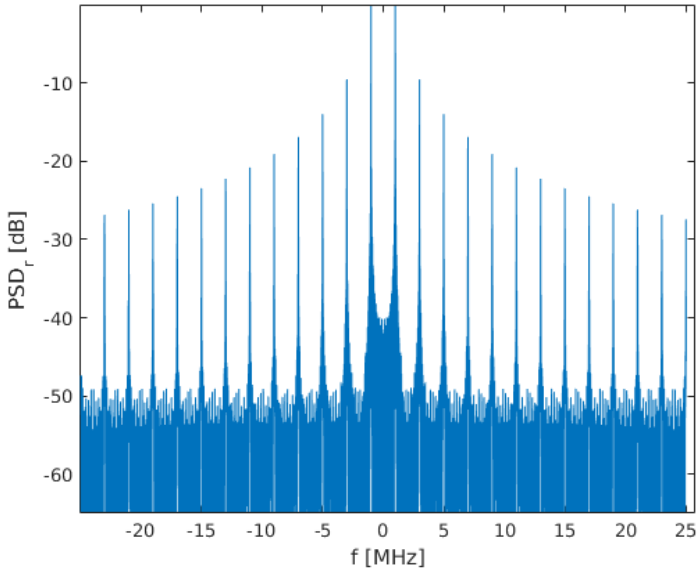

Figure 7.5: The PSD of pulse train (adequate to e.g. ADS–B signal with all zeros as data values)

7.2 Correlation detector or matched filter for signal detection

The power spectrum evaluation is suitable to detect presence of pulse sequence in case of moderate SNR values and for regular sequences of pulses, the same approach applied to the ADS–B signal with real non-uniform data is less appropriate due to character of real ADS–B signal spectrum (Figure 3.2) and other approaches produce more reliable results. There are also some proposed methods using evaluation of higher order spectrum characteristics,e.g. bispectrum or up to fourth-order moment spectrum [111], [112] but they produce practically usable results for very narrowband signals in the presence of Gaussian noise [111].

The approach described in previous chapters works well for uniform set pulses, where the benefits of integration can be used. However, for signals with pseudorandom character as in the case of ADS–B extended squitter signal, there is a more appropriate approach of matched filter or correlation reception that will be described in this chapter. This approach uses the benefit of knowledge of at least the original waveform of the signal and some statistical information about radio channel that was used for signal travel to construct optimal

detector [107]. The optimality of the detector depends on the accurateness of statistical description of the random parameters.

Assuming *N* samples of the received signal *x(t)* obtained at the integer multiples of sampling period T_s, i.e. $\boldsymbol{x}=x[n]=x(nT_s),\quad n=0,\ldots,N-1$. The hypotheses in the case of presence of signal in additive noise have the form

$$\begin{aligned}\boldsymbol{H}_0&: x[n]=w[n]\\ \boldsymbol{H}_1&: x[n]=s[n]+w[n]\end{aligned}\quad,\quad n=0,\ldots,N-1\quad. \tag{7.21}$$

The s[n] is the deterministic signal (in simple form the transmitted signal waveform, in the generalized form the signal waveform affected by known or estimated parameters of radio channel) and w[n] is a zero mean Gaussian noise process with variance σ_n^2 and autocorrelation function $\sigma_n^2\delta[n]$ where $\delta[n]$ is a discrete delta function.

Applying the condition used for Neyman–Pearson detection criterion, the likelihood function for positive detection of signal (i.e. hypothesis $\boldsymbol{H}_1$)

$$L(\boldsymbol{x})=\frac{P(\boldsymbol{x};\boldsymbol{H}_1)}{P(\boldsymbol{x};\boldsymbol{H}_0)}>\xi\quad, \tag{7.22}$$

where ξ is a stated threshold.

Since x[n] has a normal distribution, the joint probabilities have forms

$$\begin{aligned}P(\boldsymbol{x};\boldsymbol{H}_1)&=\frac{1}{\left(\sqrt{2\sigma_n^2}\right)^N}\exp\left(-\frac{1}{2\sigma_n^2}\sum_{n=0}^{N-1}(x[n]-s[n])^2\right)\\ P(\boldsymbol{x};\boldsymbol{H}_1)&=\frac{1}{\left(\sqrt{2\sigma_n^2}\right)^N}\exp\left(-\frac{1}{2\sigma_n^2}\sum_{n=0}^{N-1}(x[n])^2\right)\end{aligned}\quad. \tag{7.23}$$

Evaluation of log-likelihood function using (7.22) and (7.23) yields a criterion for presence of signal

$$\sum_{n=0}^{N-1}s[x]x[n]>\underbrace{\sigma_n^2\ln\xi+\frac{1}{2}\sum_{n=0}^{N-1}s[n]^2}_{\xi'} \tag{7.24}$$

The evaluated term on the left side then represents the cross-correlation function between deterministic version of signal *s[n]*, called a *replica*, and received from of signal *x[n]*. The

detector according this approach is then called correlation receiver and its principial block scheme is on the Figure 7.6.

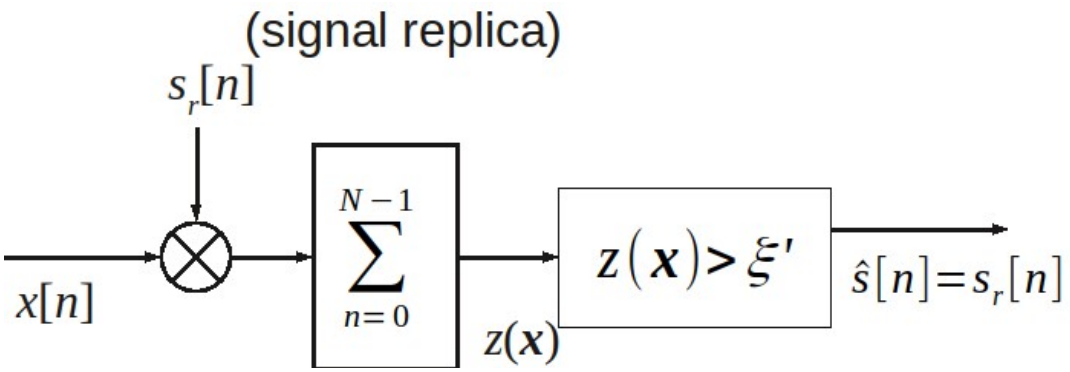

Figure 7.6: Basic scheme of correlation detector

The variant with matched filter uses the evaluation of output of an FIR filter that has impulse response equal to time mirrored and delayed waveform of replica

$$h[n] = s[N-1-n], \quad n = 0, \ldots, N-1 \tag{7.25}$$

The output of such filter would then be

$$y[n] = \sum_{k=0}^{n} s[N-1-(n-k)]\,x[k] \tag{7.26}$$

and in time $n = N-1$ it becomes

$$y[N-1] = \sum_{k=0}^{N-1} s[k]\,x[k] \tag{7.27}$$

which is equal to correlation term from (7.24).

The matched filter is an recommended approximation to maximize SNR even for noises that are only close to Gaussian so the further application will be based on this approach.

Our case of signal detection is even in simple case of no multipath propagation further affected by tolerance of carrier frequency and possible movement of target. So the detection problem can be described in first step more precisely as a detection of known signal with several unknown parameters in additive noise. The major unknown parameters are the time of signal arrival with respect to clock of receiver (further used for statement of TDoA task), the

frequency covering both the carrier frequency remainder due to the tolerance of ADS–B signal definition and the Doppler frequency, caused by possible movement of the transmitting target. The minor unknown parameters is the phase of the signal causing angular shift in OOK (on-off keying) constellation representing the PPM signal.

Since two major parameters can be considered as deterministic, the general likelihood ratio test (GLRT) [107] can be applied for the detection of the signal. The general detection problem statement is again in the form of two hypotheses

$$\begin{aligned} \boldsymbol{H}_0 &: x[n] = w[n], && n = 0,\ldots,N-1 \\ \boldsymbol{H}_1 &: \begin{cases} x[n] = w[n], & n = 0,\ldots,n_0-1, n_0+M,\ldots,M+N-1 \\ x[n] = A[n]e^{j2\pi f_o n+\phi} + w[n], & n = n_0,\ldots,n_0+M-1 \end{cases} \end{aligned} \tag{7.28}$$

where $w[n]$ is a zero mean Gaussian white noise process with variance σ_n^2 , $A[n]$ is a sequence of PPM pulses of ADS–B signal, f_o is and frequency offset of down–converted signal from carrier frequency (combining carrier frequency tolerance and Doppler shift), and ϕ is signal phase. The GLRT states signal presence if likelihood ratio

$$L_g(\boldsymbol{x}) = \frac{P(\boldsymbol{x}; \hat{f}_o, \hat{\phi}, \hat{n}_0, \boldsymbol{H}_1)}{P(\boldsymbol{x}; \boldsymbol{H}_0)} > \xi$$

$$L_g(\boldsymbol{x}) = \frac{\frac{1}{\left(\sqrt{2\sigma_n^2}\right)^N} \exp\left(-\frac{1}{2\sigma_n^2} \sum_{n=n_0}^{n_0+M-1} \left(x[n] - A[n]\exp\left(j2\pi \hat{f}_o + \hat{\phi}_0\right)\right)^2 \right)}{\frac{1}{\left(\sqrt{2\sigma_n^2}\right)^N} \exp\left(-\frac{1}{2\sigma_n^2} \sum_{n=0}^{N-1} \left(x[n]\right)^2 \right)} > \xi \quad . \tag{7.29}$$

Using again the logarithm evaluation we obtain

$$\ln L_g(\boldsymbol{x}) = \frac{1}{M\sigma_n^2} \left| \sum_{n=n_0}^{n_0+M-1} x[n]A[n]e^{-j2\pi \hat{f}_o n} \right|^2 > \xi' \tag{7.30}$$

Which is actually a short–time periodogram futher maximized across values of possible delays n_0 and frequencies f_o

$$\max_{n_0, f_o} \frac{1}{M\sigma_n^2} \left| \sum_{n=n_0}^{n_0+M-1} x[n]A[n]e^{-j2\pi \hat{f}_o n} \right|^2 > \xi' \quad . \tag{7.31}$$

So the practical realization is a search through space of delayed signal replicas and possible frequency offsets and looking for the maximum reaching over the threshold which corresponds with a detector on Figure 7.7.

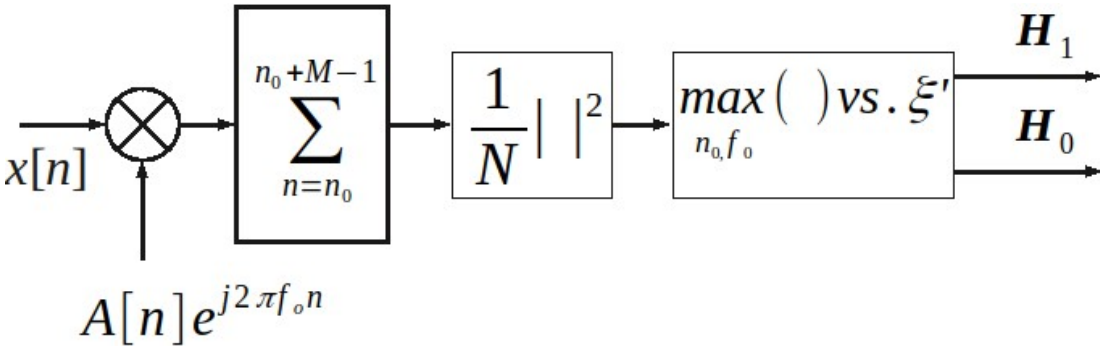

Figure 7.7: GLRT based detector of ADS–B signal

7.2.1 Proposal of correlator using higher order statistics

The criterion of threshold comparison can provide in some cases multiple positive detections across signal duration interval. Moreover, the width and slope of correlation peak is also affected by the width of signal used for correlation, respective by the width of known signal part, e.g. preamble, ans also it is affected by noise and interference. These phenomena bring a complication in use of such correlator for estimation of the signal delay.

This fact is even more significant in case of relatively short pseudorandom sequences. The Gold codes, pseudorandom sequences used for satellite navigation, provide ratio of maximum of autocorrelation function (ACF) and sidelobes as $1+1/N$ where N is a length of code [29]. Since the ADS–B signal is not the specially chosen pseudorandom sequence, its correlation properties are naturally weaker as can be sen on Figure 7.8. Moreover, the replica, used for correlation with the received signal, shall consist of known sequence of pulses. This is true only in special cases, in other cases we can count at least with the preamble or with combination of preamble and fixed message header (DF, CA, ICAO address). The ambiguity in correlation results can be suppressed by using higher order parameters [112], in our case with proposal of higher order correlation.

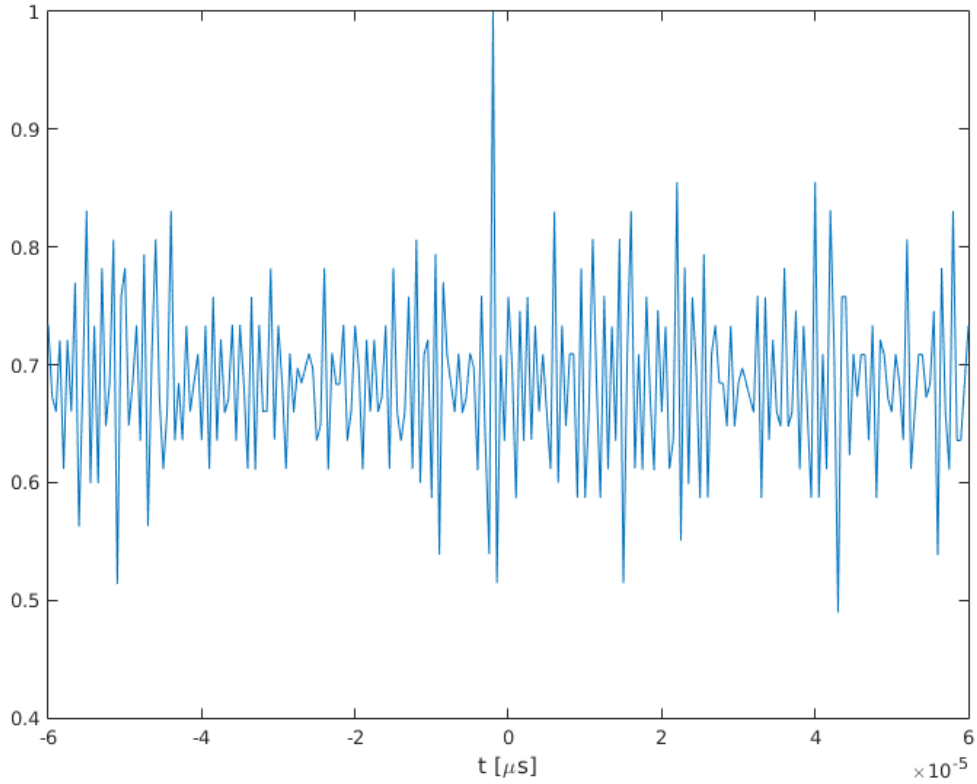

Figure 7.8: ACF of ADS–B signal (low pass equivalent)

Assume the signal $\boldsymbol{x}$ $x[n]=s[n]+w[n]$, $n=0,\ldots,N-1$ and the replica $\boldsymbol{p}_0$, formed from a part of signal, $p_0[n]=s[n]$, $n=0,\ldots,K-1$, where $K<2N$ .The correlation function will then be defined as

$$R1[\tau]=\sum_{n=0}^{N-1} s[n]p_0^{*}[n-\tau]+\sum_{n=0}^{N-1} w[n]p_0^{*}[n-\tau] \tag{7.32}$$

or in matrix form

$$\boldsymbol{R1}=\boldsymbol{P}\boldsymbol{x} \tag{7.33}$$

where $\boldsymbol{R1}=\{R1[0],\ldots,R1[N-K-1]\}^T$ are $N-K$ results of correlation function, $\boldsymbol{x}=\{x[0],x[1],\ldots,x[N-1]\}^T$ is input signal and $\boldsymbol{P}$ is $(N-K)\times N$ matrix with form

$$P=\begin{bmatrix} s[0] & s[1] & \cdots & s[K-1] & 0 & 0 & 0 & \cdots & 0 \\ 0 & s[0] & s[1] & \cdots & s[K-1] & 0 & 0 & \cdots & 0 \\ \vdots & & & & & & & & \vdots \\ 0 & 0 & 0 & \cdots & s[0] & s[1] & \cdots & s[K-1] & 0 \\ 0 & 0 & 0 & \cdots & 0 & s[0] & s[1] & \cdots & s[K-1] \end{bmatrix} \tag{7.34}$$

The auto correlation function of the replica can be expressed as

$$P2[k]=\sum_{n=0}^{K-1} p_0[n]\, p_0^{*}[k-n] \tag{7.35}$$

or in matrix form

$$\boldsymbol{P2}=\boldsymbol{P1}\left[\mathbf{I}_K\, \mathbf{0}_K\right]^T \boldsymbol{p_0} \tag{7.36}$$

Where ***P1*** is a $K\times 2K$ matrix in the same format as ***P***, i.e. populated with shifted vectors of $\boldsymbol{p_0}$. The partial replica we propose for the second order correlation detector for ADS–B signal is the preamble with the remaining gap between preamble and data, so with the total length of 8 μs. Its autocorrelation function is on Figure 7.9.

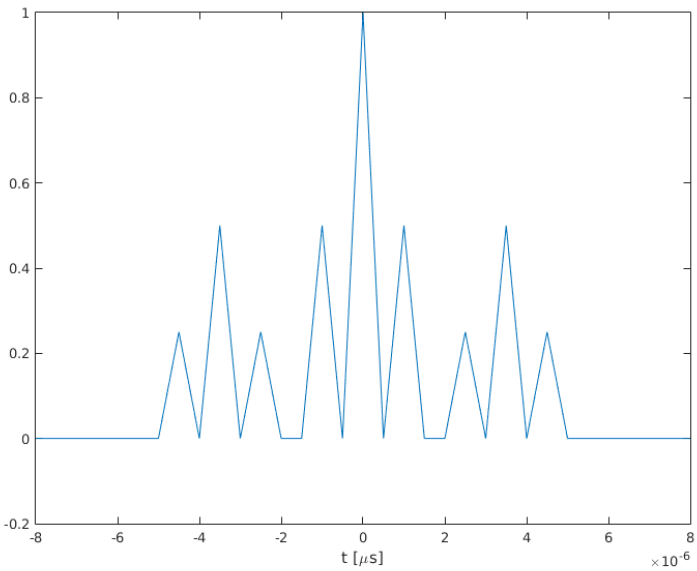

Figure 7.9: ACF of ADS–B preamble

The second order correlation is then obtained using ***R1*** and ***P2*** as

$$\boldsymbol{R2}=\boldsymbol{U}\,\boldsymbol{R1}=\begin{bmatrix} \boldsymbol{P2}^{\boldsymbol{T}} & 0 & \cdots & 0 & 0 \\ 0 & \boldsymbol{P2}^{\boldsymbol{T}} & \cdots & 0 & 0 \\ \vdots & & & & \vdots \\ 0 & 0 & \cdots & \boldsymbol{P2}^{\boldsymbol{T}} & 0 \\ 0 & 0 & \cdots & 0 & \boldsymbol{P2}^{\boldsymbol{T}} \end{bmatrix} \begin{bmatrix} R1[0] \\ R1[1] \\ \vdots \\ R1[N-K-1] \end{bmatrix} \tag{7.37}$$

The criterion is then the search of maximum of second order correlation result over $N-2K$ values of ***R2***.

It has to be clarified that the proposed detector was tailored for the specific format of signal, related to ADS–B. The correlator uses the benefit of the gap between the preamble and the data part of ADS–B signal forming the specific pattern of correlation function as can be seen from Figure XXX. The similar sequence of PPM pulses occurring in the message with lower probability, moreover, it will be surrounded by other data pulses thus distorting the correlation function pattern. The performance of the detector is compared to the other realizations further in Chapter 7.2.4.

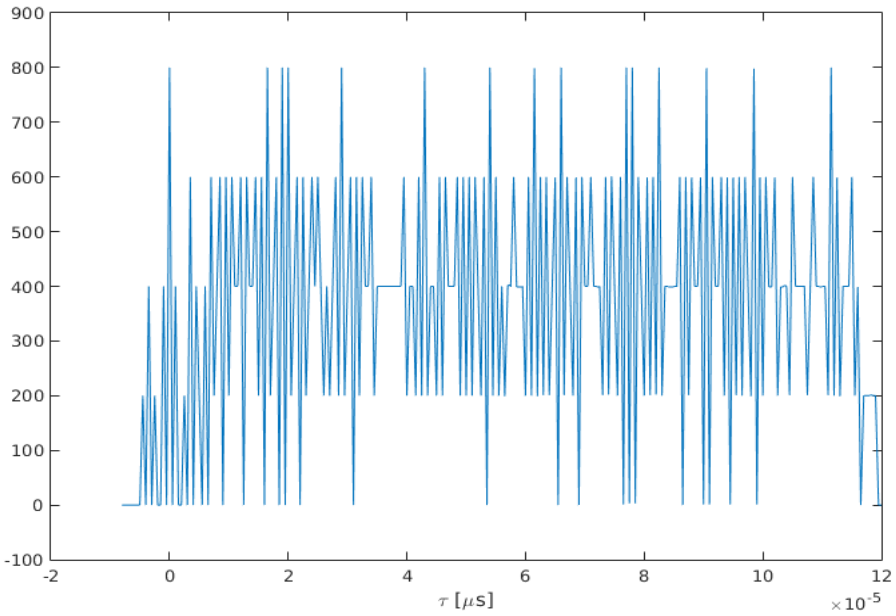

Figure 7.10: Cross–correlation between ADS–B signal and preamble

7.2.2 The multipath propagation impact on signal detection

The described detector can be used also for estimation of time of arrival of the particular ADS–B signal, because the maximum of correlation function over generated replica delays determines the relative shift of the signal in time with respect to receiver clocks. This information then can be used in the TDoA solution. The position of maximum of correlation function will be corrupted by noise and mainly by the impact of multipath propagation (Figure 7.11)

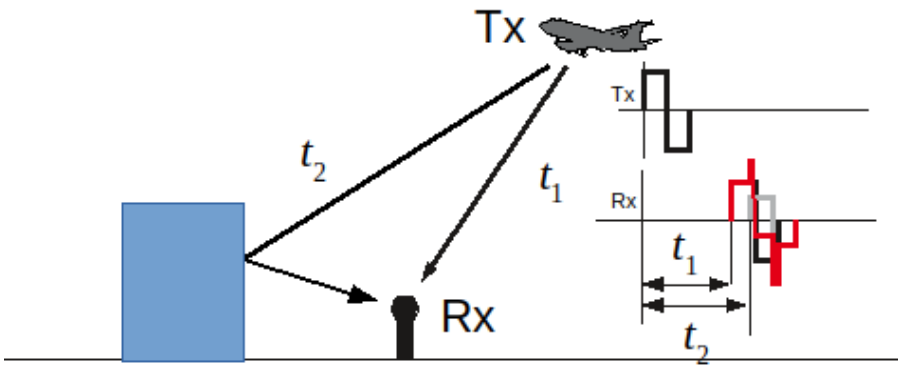

Figure 7.11: Multipath propagation principle

The received signal at the antenna is accomplished by its attenuated and delayed copy. This causes a distortion of received pulses and makes the detection and decoding of signal much more complicated. The multipath propagation present in band-limited channels (virtually all practically used systems are band limited) causes then intersymbol interference. In case of multilateration, where the measurement of ToA of the incoming signal is closely related to resulting precision of position determination it can induce an additional position error.

The correlation detector modified for estimation delay is modified using usually two branches that use replicas shifted mutually by pulse duration T_p and producing the difference of correlator outputs. Since one branch comes sooner that the position of the pulse and the other one comes later, such correlator configuration is called early–late correlator. The results of correlations

$$R_E[\tau]=\sum_{n=0}^{N-1} x[n]s\left[n-\tau+\frac{T_p}{2}\right]$$
$$R_L[\tau]=\sum_{n=0}^{N-1} x[n]s\left[n-\tau-\frac{T_p}{2}\right] \quad (7.38)$$

are then combined in various manner (a most simple one is $R_E[\tau]-R_L[\tau]$) usually in the terms of inphase and quadrature parts of complex envelope and the process itself is known as a delay discriminator. This circuit with proper feedback blocks providing adjustment of variable delay τ forms circuit dominantly used in positioning systems and is known as a delay locked loop (DLL) [113]. The typical shape of such delay discriminator of early and late branches equal to width of signal pulse is shown at Figure 7.12.

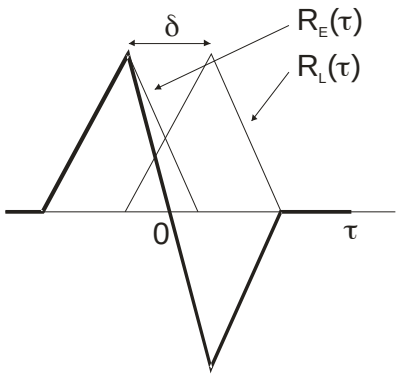

Figure 7.12: Delay discriminator response example for distance $\delta=T_p$

The multipath propagation then causes distortion of discriminator curve and thus inducing shift in the detection of delay (shift of zero value from zero delay position of delay discriminator) which is related to error of position determination. The impact of multipath propagation for ADS-B signal to ToA measurement and related error in distance determination can be expressed in a form of multipath induced correlator error envelope. We calculated multipath error envelope with respect to multipath delay based on ADS-B signal for one extended squitter message (length 120 microseconds), sampling rate 400MHz, width of discriminator of 500 ns, and channel with one multipath component with 6dB loss to line-of-sight path. The result of multipath induced error is at Figure 7.13 both for positive and negative value of reflection component. We can observe the induced error up to 38 meters with dominant impact for multipath component delay till 0.6 μs.

It can be seen that multipath error is also affected by chosen bandwidth (it becomes bigger for smaller bandwidth, i.e. lower sampling ratios) [114] therefore the design of receiver has to be

taken into account during the signal processing. We can see the result for sampling 40 MHz on the Figure 7.14.

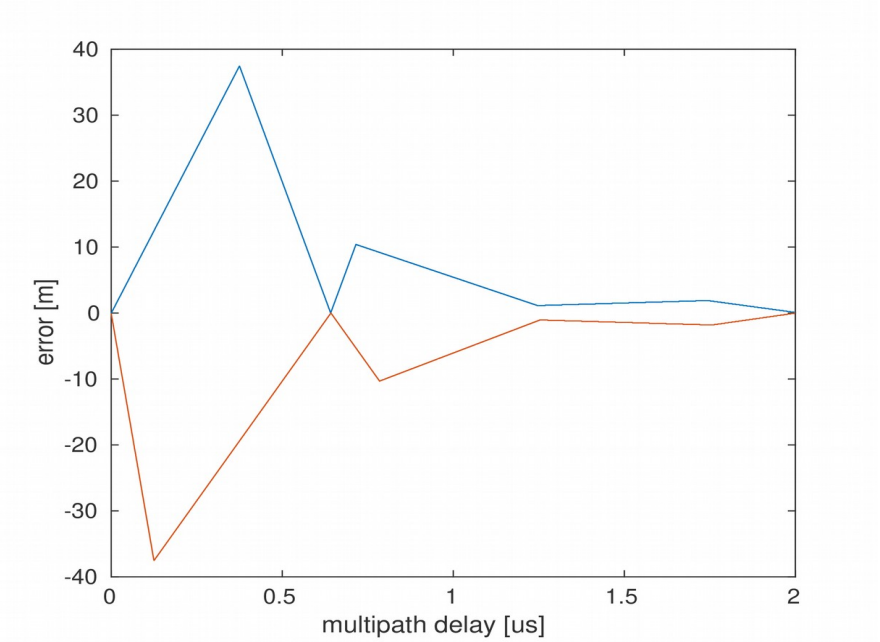

Figure 7.13: Multipath error envelope for ADS–B single message correlation for sampling frequency 400 MHz

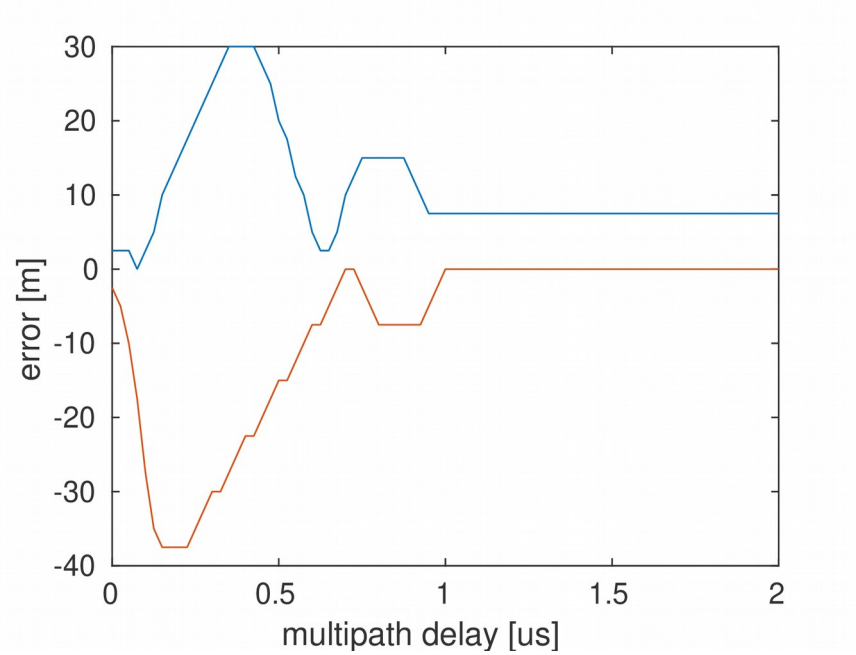

Figure 7.14: Multipath error envelope for ADS–B single message correlation for sampling frequency 40 MHz

Since the ADS–B signal is in general principle with unknown content (although we are able to predict some of the messages content) we also investigated the impact of choice of only portion of the signal as a replica to provide correlation operation. The significant parts are the preamble (8 μs), the preamble together with fixed part of ADS–B DF 17 message, including the 24 bits of ICAO address (40 μs). The multipath induced error for these replicas applied to the ADS–B signal are together with full length of replica at the Figure 7.15.

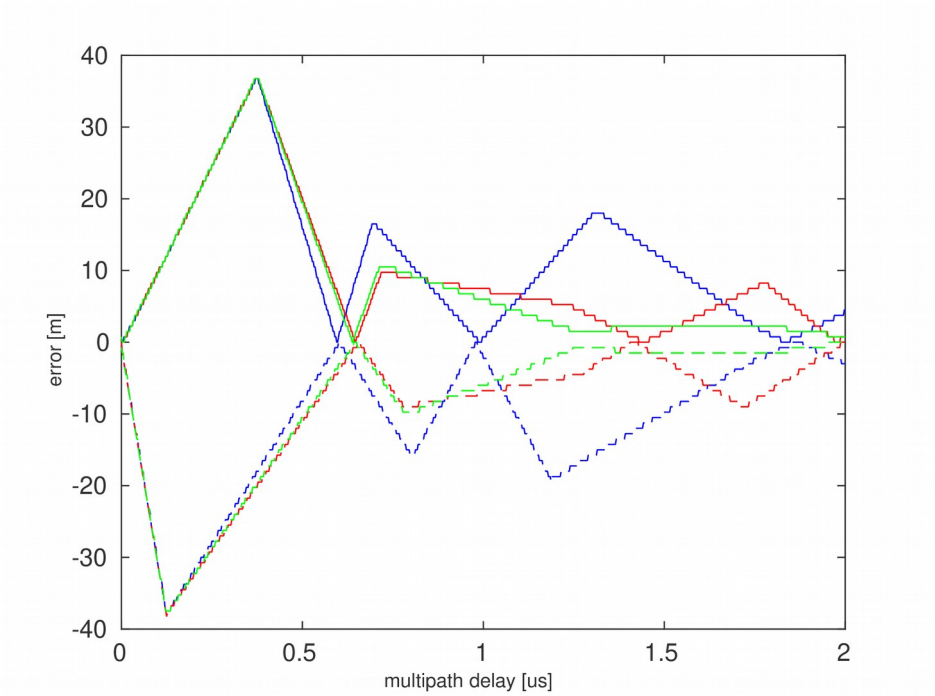

Figure 7.15: Multipath induced error for ADS–B signal using different replica lengths (120 μs – green, 40 μs – red, 8 μs – blue)

As we expected, the shorter replicas perform worse resistance to multipath induced error, but the common region remains same at the beginning of the message, i.e. till first of the pulse of the preamble.

The correlation properties are dependent on the signal waveform, therefore the design of navigation system signals is oriented to produce pseudo-random sequences (e.g. Gold codes for GPS). The ADS–B signal can be considered as pseudo-random to some extent, strongly dependent on data message content. For comparison as an extreme case, the Figure 7.16 presents multipath induced error for ADS–B signal containing message with zero content, which means regular sequence of uniform pulses. We can see that the maximal value of error remains the same but it occurs also beyond first pulse interval due to periodical nature of the signal waveform. The possible improvement is in a “randomization” of the ADS–B signal which is possible only to some extent because the parameters of the standard does not allow too big extension of bandwidth or modification of the shape pulses or PPM modulation. The

possible approach was used in [115] introducing the pseudorandom BPSK modulation into PPM pulses with improvement of correlation peak to sidelobes ratio by about 6 dB but it assumes the a priori knowledge of signal content.

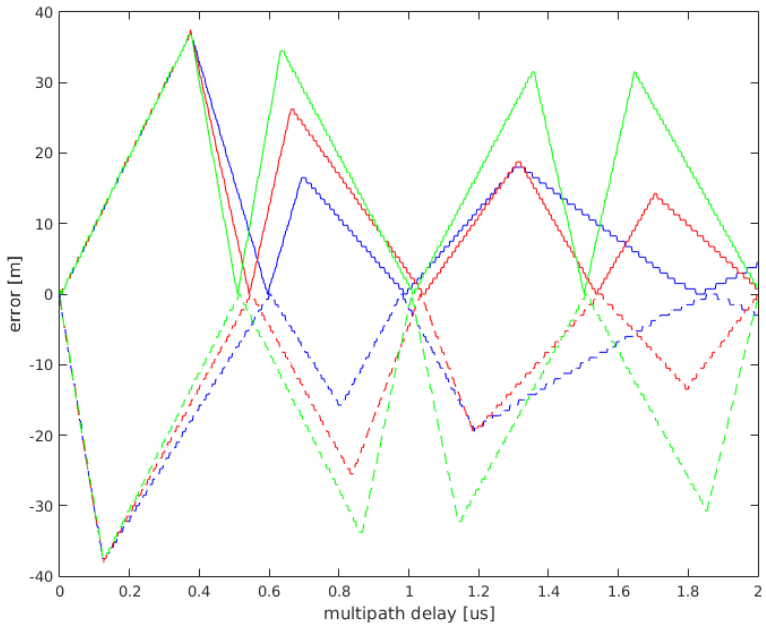

Figure 7.16: Multipath induced envelope for ADS–B signal with data bins equal to zero

It can be concluded, that the multipath propagation is a significant contributor to the error of the delay estimation for the purpose of TDoA and further we will propose mechanism to deal and potentially suppress its impact.

7.2.3 Signal detection in presence of multipath

The use of detection can be further extended to general case of correlated noise samples and random signal [107], which is more often in the case of reception in difficult environment. In case that signal $\boldsymbol{s}$ is a random process with normal distribution, mean μ_s and covariance matrix $\mathbf{C}_s$ and additive noise $\boldsymbol{w}$ is zero mean white Gaussian with covariance matrix $\mathbf{C}_w$, the Neyman–Pearson likelihood function for hypotheses $\boldsymbol{x}=\boldsymbol{w}$ and $\boldsymbol{x}=\boldsymbol{s}+\boldsymbol{w}$ has a form of

$$L(x)=\frac{\frac{1}{\sqrt{(2\pi)^N|(\boldsymbol{C}_s+\boldsymbol{C}_w)|}}\exp\left(-\frac{1}{2}(\boldsymbol{x}-\boldsymbol{\mu}_s)^T(\boldsymbol{C}_s+\boldsymbol{C}_w)^{-1}(\boldsymbol{x}-\boldsymbol{\mu}_s)\right)}{\frac{1}{\sqrt{(2\pi)^N|(\boldsymbol{C}_w)|}}\exp\left(-\frac{1}{2}\boldsymbol{x}^T\boldsymbol{C}_w^{-1}\boldsymbol{x}\right)}>\xi \tag{7.39}$$

which after simplification of using log-likelihood variant and inclusion of non-random parameters independent on received signal to the comparison level results in

$$\boldsymbol{x}^T(\boldsymbol{C}_s+\boldsymbol{C}_w)^{-1}\boldsymbol{\mu}_s+\boldsymbol{x}^T\boldsymbol{C}_w^{-1}\boldsymbol{C}_s(\boldsymbol{C}_s+\boldsymbol{C}_w)^{-1}\boldsymbol{x}>\xi' \tag{7.40}$$

where first part is equivalent to matched filter with noise correlation suppression (prewhitening) and second part is an estimator–correlator in the form of $\boldsymbol{x}^T\boldsymbol{C}_w^{-1}\boldsymbol{C}_s(\boldsymbol{C}_s+\boldsymbol{C}_w)^{-1}\boldsymbol{x}=\boldsymbol{x}^T\boldsymbol{C}_w^{-1}\hat{\boldsymbol{s}}$, where $\hat{\boldsymbol{s}}=\boldsymbol{C}_s(\boldsymbol{C}_s+\boldsymbol{C}_w)^{-1}\boldsymbol{x}$ is a MMSE (minimum mean square error) estimate of $\boldsymbol{s}$ from current realization of $\boldsymbol{x}$, de facto application of Wiener filter [65].

In case of multipath channel propagation, the received signal can be modeled according to multipath channel model in Chapter 6. So the detection hypotheses will have a form of

$$\begin{aligned}\boldsymbol{H}_0&: x[n]=w[n], && n=0,\ldots,N-1\\ \boldsymbol{H}_1&: x[n]=\sum_{k=0}^{K-1}h[k]s[n-k]+w[n], && n=0,\ldots,N-1\end{aligned}, \tag{7.41}$$

where $N=S+K-1$ and S is a length of signal $s[n]$. The signal model can be described in matrix form as

$$\boldsymbol{x}=\boldsymbol{H}\,\boldsymbol{\theta}+\boldsymbol{w} \tag{7.42}$$

where $\boldsymbol{w}=\sigma_n^2\boldsymbol{I}$ is Gaussian zero mean uncorrelated normal distributed noise, $\boldsymbol{\theta}$ are channel tap weights $\boldsymbol{\theta}=[h[0],\ldots,h[K-1]]^T$, and $\boldsymbol{H}$ with dimensions $N\times K$

$$\boldsymbol{H}=\begin{bmatrix} s[0] & 0 & \cdots & 0 & 0\\ s[1] & s[0] & & 0 & \vdots\\ \vdots & s[1] & & s[0] & 0\\ s[K-1] & \vdots & & s[1] & s[0]\\ 0 & s[K-1] & & \vdots & s[1]\\ \vdots & \vdots & & s[K-1] & \vdots\\ 0 & 0 & \cdots & 0 & s[K-1]\end{bmatrix} \tag{7.43}$$

For a common case of random time invariant channel (as we can consider for small time intervals), the $\boldsymbol{\theta}$ has a normal zero mean distribution with covariance matrix independent on w with form $\boldsymbol{C_h} = \mathrm{diag}(\sigma_{h,0}^2, \sigma_{h,1}^2, \ldots, \sigma_{h,K-1}^2)$, these values represent a multipath delay profile [97]. The metrics $L(\boldsymbol{x})$ from (7.40) then becomes

$$L(\boldsymbol{x}) = \boldsymbol{x}^T \boldsymbol{H} \boldsymbol{C_h} \boldsymbol{H}^T \left(\boldsymbol{H} \boldsymbol{C_h} \boldsymbol{H}^T + \sigma_n^2 \boldsymbol{I} \right)^{-1} \boldsymbol{x} > \xi' \quad . \tag{7.44}$$

Using the Woodbury matrix identity for term inside the brackets we obtain

$$L(\boldsymbol{x}) = \boldsymbol{x}^T \boldsymbol{H} \boldsymbol{C_h} \left(\frac{\boldsymbol{H}^T}{\sigma_n^2} - \frac{\boldsymbol{H}^T \boldsymbol{H}}{\sigma_n^4} \left(\frac{\boldsymbol{H}^T \boldsymbol{H}}{\sigma_n^2} + \boldsymbol{C_h}^{-1} \right)^{-1} \boldsymbol{H}^T \right) \boldsymbol{x} > \xi' \tag{7.45}$$

Since the columns of H are a shifted version of each other, for the pseudorandom nature of the signal ,as ADS–B signal is, they can be considered as approximately orthogonal and therefore $\boldsymbol{H}^T \boldsymbol{H} = \epsilon_s \boldsymbol{I}$ where $\epsilon_s = \sum_{k=0}^{K-1} s[k]^2$. The previous term for metrics then can be expressed as

$$L(\boldsymbol{x}) = \boldsymbol{x}^T \boldsymbol{H} \left(\frac{\boldsymbol{C_h}}{\sigma_n^2} - \frac{\epsilon_s \boldsymbol{C_h}}{\sigma_n^4} \left(\frac{\epsilon_s}{\sigma_n^2} \boldsymbol{I} + \boldsymbol{C_h}^{-1} \right)^{-1} \right) \boldsymbol{H}^T \boldsymbol{x} > \xi' \quad . \tag{7.46}$$

The term inside the brackets is a diagonal matrix consisting of energy of signal and variances of the channel and noise with elements *ii* equal to $\sigma_{h,i}^2 / (\epsilon_s \sigma_{h,i}^2 + \sigma_n^2)$. So the detector of signal in case of multipath propagation will have the form of

$$L'(\boldsymbol{x}) = \sum_{k=0}^{K-1} \frac{\sigma_h^2, k}{\epsilon_s \sigma_h^2, k + \sigma_n^2} \left(\sum_{n=k}^{S-1+k} x[k] s[n-k] \right)^2 \quad , \tag{7.47}$$

and the scheme of detector on Figure 7.17. This format of detector is then further used for signal detection evaluation in case of channel equalization tests.

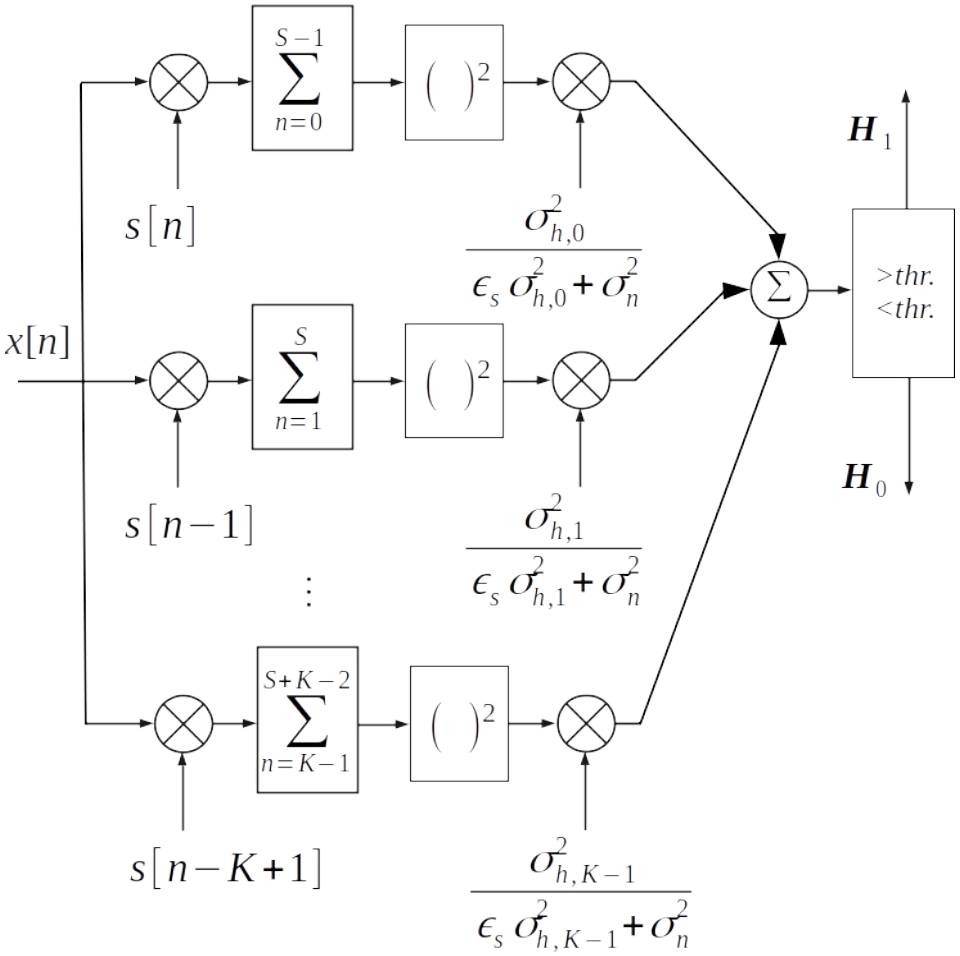

Figure 7.17: Combiner detector for TDL modeled multipath channel

7.2.4 Performance tests of signal detectors

The set of tests was executed to evaluate the performance of ADS–B signal detection for several scenarios. The three kinds of detectors were used, the detector based on classical MofN integration approach, the detector with matched filter (correlation) and the proposed detector using the second order correlation. There was made an evaluation of Probability of error in detection of beginning of ADS–B signal, i.e. the position of the first of pulses from preamble. The scenarios were set as follows:

- Scenario 1 – plain ADS–B signal in AWGN
- Scenario 2 – ADS–B signal in multipath channel

During each of scenarios, the Monte Carlo method was used for evaluation of detector performance. For each configuration, there was executed a set of 10 000 simulations in

Matlab with random generated data and with variable SNR of AWGN. Both the signal and the noise were generated in terms of low pass equivalent, i.e. as a complex envelope of ADS–B signal. The sampling frequency for all simulations was 40 MHz.

Scenario 1 – ADS–B signal in AWGN channel

Although all detectors work successfully in sufficient SNR above 1 dB, the both matched filter and second order correlator outperformed plain integrator in terms of sufficient SNR for producing same value of precision in determination of message start. The Figure 7.18 shown comparison of all detectors in dependence of RMS of error on SNR, the Figures 7.19–7.21 show each detector dependence of mean of error in samples together with standard deviation of the error. There can be seen a consistency of standard deviation of error throughout variable SNR in comparison with decrease of error spread in case of second order correlator with increasing SNR.

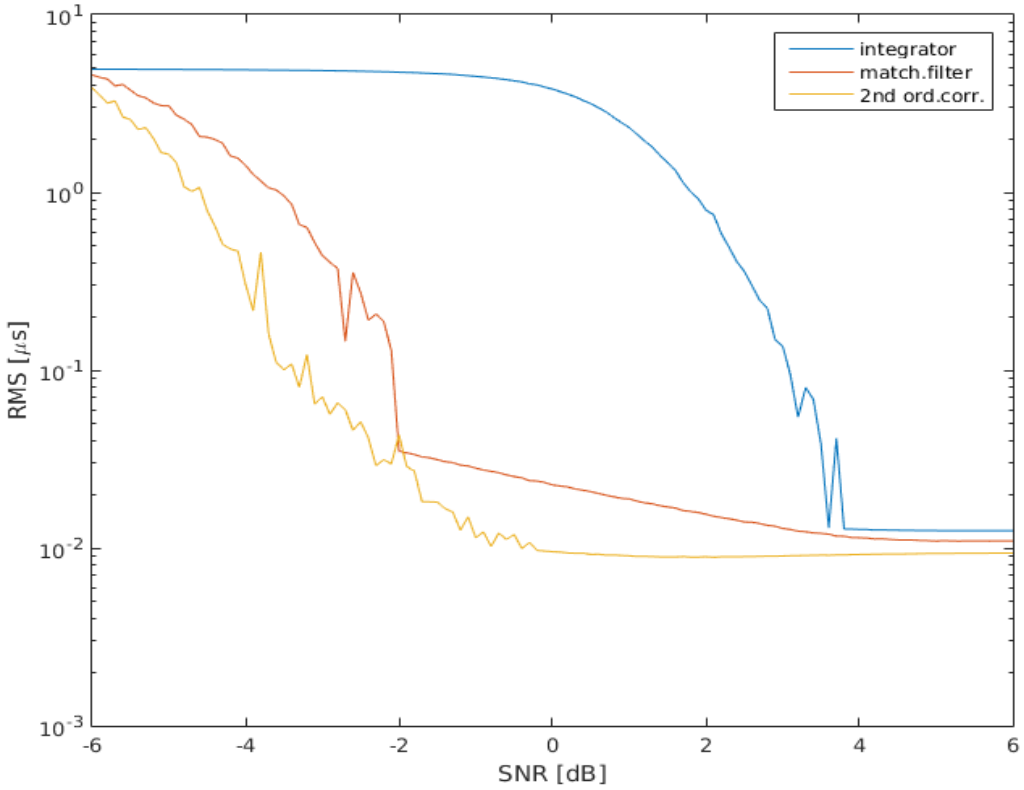

Figure 7.18: RMS error of detectors in case of channel with AWGN and variable SNR

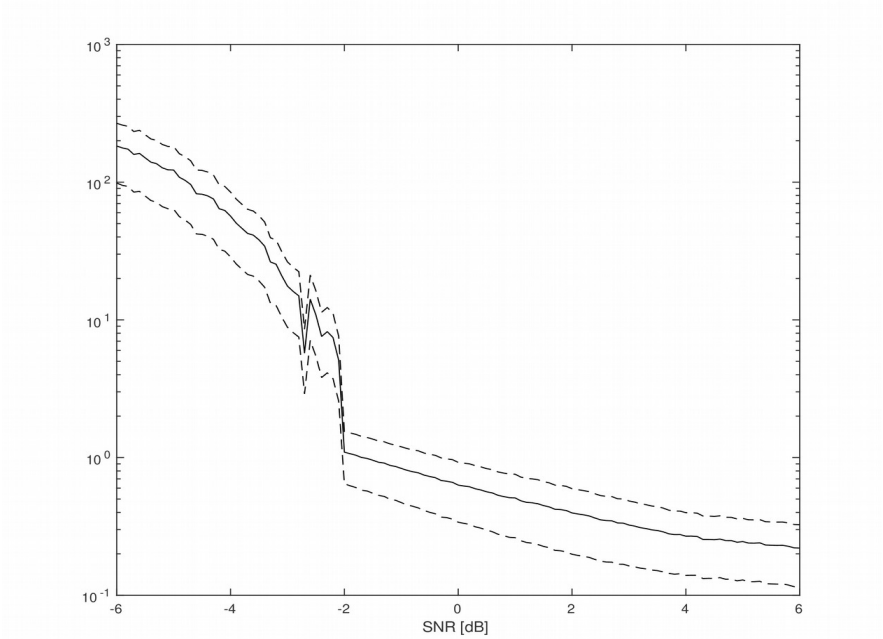

Figure 7.19: Mean (solid) and standard deviation (dashed) of error in samples for message start detection dependence on SNR for matched filter detector in scenario 1

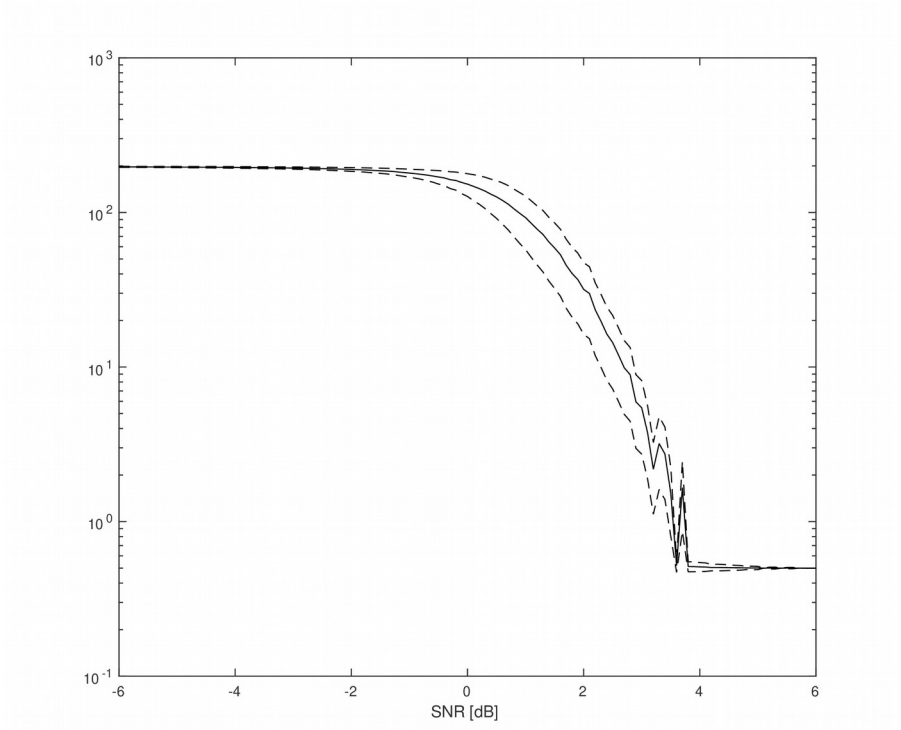

Figure 7.20: Mean (solid) and standard deviation (dashed) of error in samples for message start detection dependence on SNR for integrator detector in scenario 1

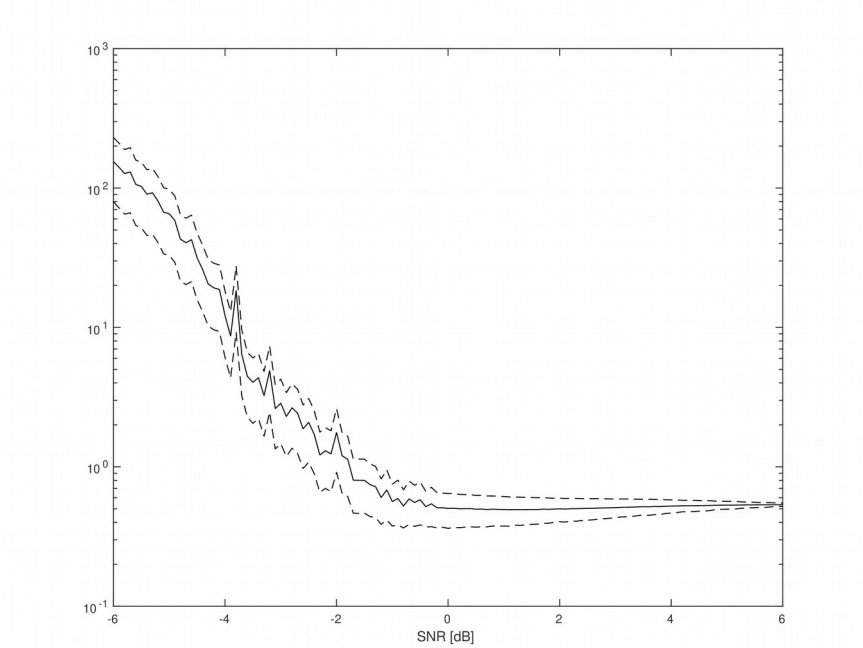

Figure 7.21: Mean (solid) and standard deviation (dashed) of error in samples for message start detection dependence on SNR for second order correlator in scenario 1

Scenario 2 – ADS–B signal in multipath channel

Since it would be extremely time consuming (or almost impossible) to test all possible multipath cases, there were chosen the significant cases that can bring potential complications. The first case (A) is a case of single multipath component with delay 125 ns, phase shift π, and relative amplitude 0.5 (with respect to direct component equal to 1), causing the negative cut of the preamble pulses, the second case (B) has two multipath components, first with delay 475 ns, phase 0, and relative amplitude 0.5, second with delay 600ns, phase 0, and relative amplitude 0.25. The second case produces attenuated copy of the pulse before and thus filling the spaces between preamble pulses. The third case (C) has a single mutipath component with delay 150 ns, phase shift 0 and relative amplitude 0.5. This case virtually "amplifies" the direct signal with a change of the raising part of pulses. The RMS errors for all cases are in Figure 7.22, the values of means and standard deviations are in Appendix B.

(A)

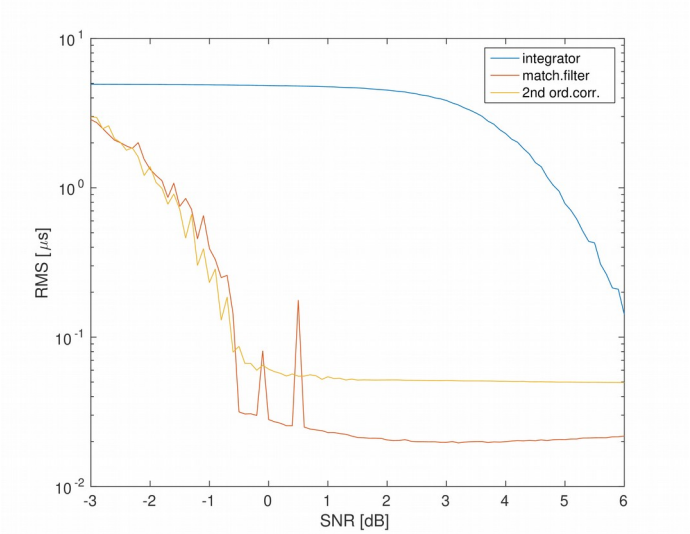

(B)

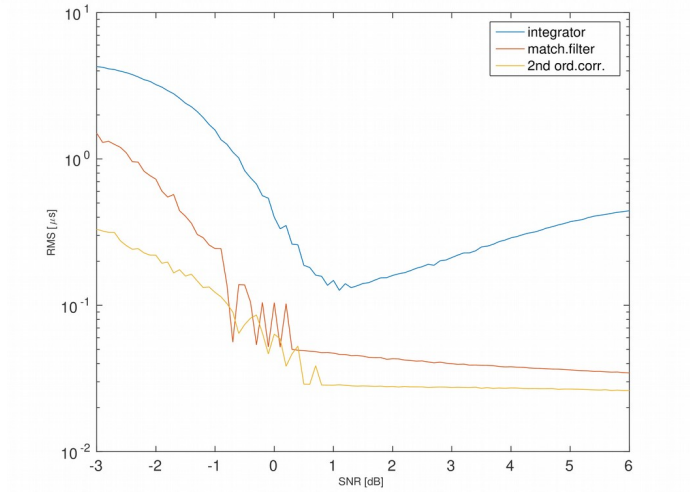

(C)

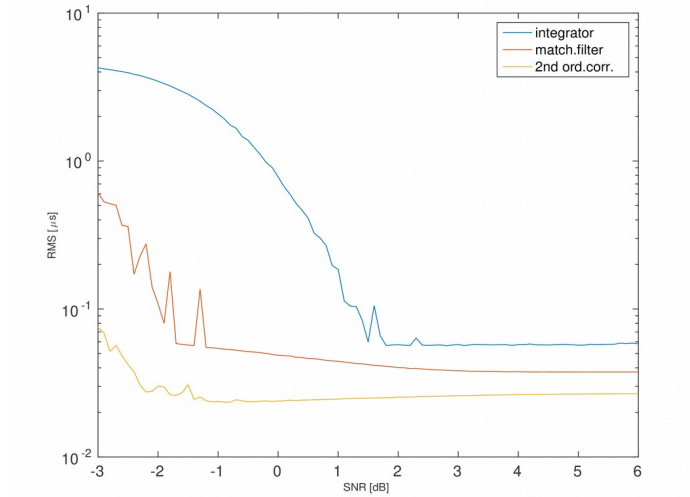

Figure 7.22: RMS error for detectors in Scenario 2: cases (A) - top, (B) - middle, (C) - bottom

As can be seen, the multipath propagation affect mainly the integration detector, but the impact can be observable on two remaining detectors as well, the case C speeds up the convergence to the correct delay of signal because of de facto providing a approximate sum of the same signal with uncorrelated noise and thus virtually improving the SNR. However neither in this case nor in other two cases the detection error did not drop below the values of 250 ns, which is the duration of one symbol, so the multipath induced error can even for high SNR bring additional worsening of position determination, where 250 ns is equivalent of 7.5 m of pseudorange error. Therefore the proposed intent of application of channel equalization can bring suppression of this error.

7.3 ADS–B data symbol estimation

The estimation of data bin can be executed after positive evaluation of signal presence. The estimation of the value of each consecutive PPM pulse can be evaluated using either Neyman–Pearson approach or the Bayesian approach in the same manner as was described in Chapter 7.1.1. Since the data bit is specified by the PPM pulse, the hypotheses can be stated as follows:

$$\begin{aligned} \boldsymbol{H}_1&: \; x[n]=s_1[n]+w[n] \\ \boldsymbol{H}_0&: \; x[n]=s_0[n]+w[n] \end{aligned}, \qquad n=0,\ldots,N_p-1 \tag{7.48}$$

Where $s_1[n]$ and $s_0[n]$ is a PPM signal related to bit “1” and “0”, respectively (Figure 2.2), and N_p is a duration of one symbol in ADS–B message in samples. The here more natural Bayesian approach then yields in a minimal probability of error receiver[107]

$$\frac{P(\boldsymbol{x}|\boldsymbol{H}_1)}{P(\boldsymbol{x}|\boldsymbol{H}_0)} > \frac{P(\boldsymbol{H}_0)}{P(\boldsymbol{H}_1)} = 1 \qquad \rightarrow \qquad \boldsymbol{H}_1, \qquad otherw.\boldsymbol{H}_0 \tag{7.49}$$

So in practical realization it is comparison of correlation results between signal $\boldsymbol{x}$ and replicas $\boldsymbol{s}_1$ and $\boldsymbol{s}_0$ as described on the scheme at Figure 7.23.

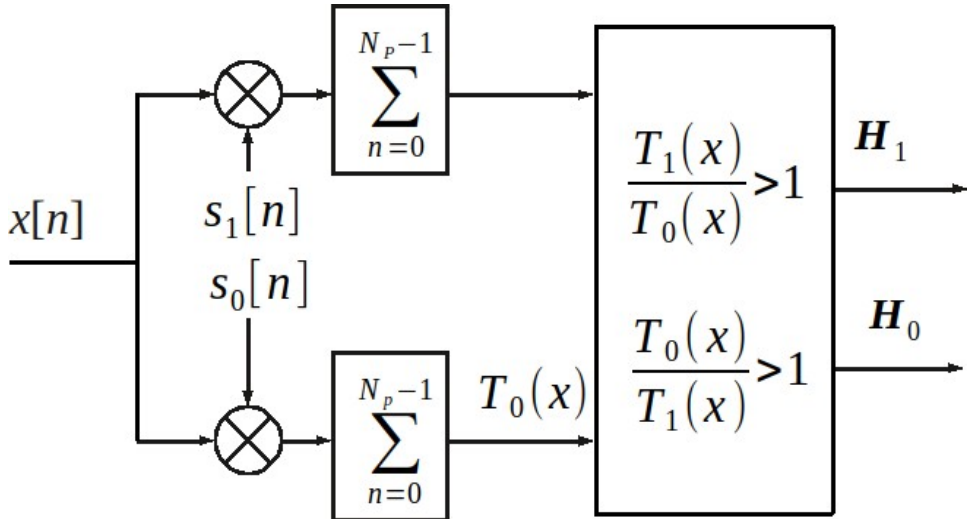

Figure 7.23: Minimum probability of error based receiver for ADS–B symbol detection and decoding

It is evident that probability of error for data symbols will be proportionally dependent on precision of the determination of the beginning of the ADS–B signal therefore the mechanisms in chapters dedicated to signal detection error will apply here too. The above defined approach for symbol determination is further used in evaluation of impact of equalization of radio channel during simulated and practical tests.

7.4 Probability of single ADS–B message reception

The ADS–B full message reception and decoding is affected not only by the radio channel characteristics performed on signal itself but also by the co-channel interference. Since the ADS−B service does not use any message traffic management, the most common source of interference are other ADS–B messages.

At first, we can express the probability of messages collision and then use it to formulate the probability of correct reception of an ADS–B message. If we assume that a message generated by ADS–B transponder is a random variable with Poisson distribution (common distribution to express probability of occurrence of some event in a fixed interval[116]), the probability of arrival of *k* messages in time *t* is

$$P(k,t)=\frac{(\lambda t)^k}{k!}e^{-\lambda t} \tag{7.50}$$

where $\lambda = N \cdot r_{gen}$ is a messages generation rate for *N* visible aircrafts and r_{gen} is a message generation rate of a single ADS–B transponder.

If we assume the duration of a single ADS–B message as τ, the number of messages received by a ADS–B receiver is

$$M_r = \lambda \tau = N r_{gen} \tau \tag{7.51}$$

If the single message arrives to the receiver at particular time t_0, to prevent a messages conflict, another message cannot come during an time interval of length 2τ symmetrically placed around t_0. The probability of no conflict is then equal of probability of zero occurrence of message in interval 2τ

$$P_{nc} = P(0,2\tau) = e^{-\lambda 2\tau} = e^{-2M_r} \tag{7.52}$$

Using the 7.52, the probability of message collision during reception is then expressed as

$$P_{col} = 1 - P_{nc} = 1 - e^{-2M_r} \tag{7.53}$$

The probability is then dependent on number of reachable aircrafts as seen in Figure for airborne and ground cases of generation of ADS–B messages.

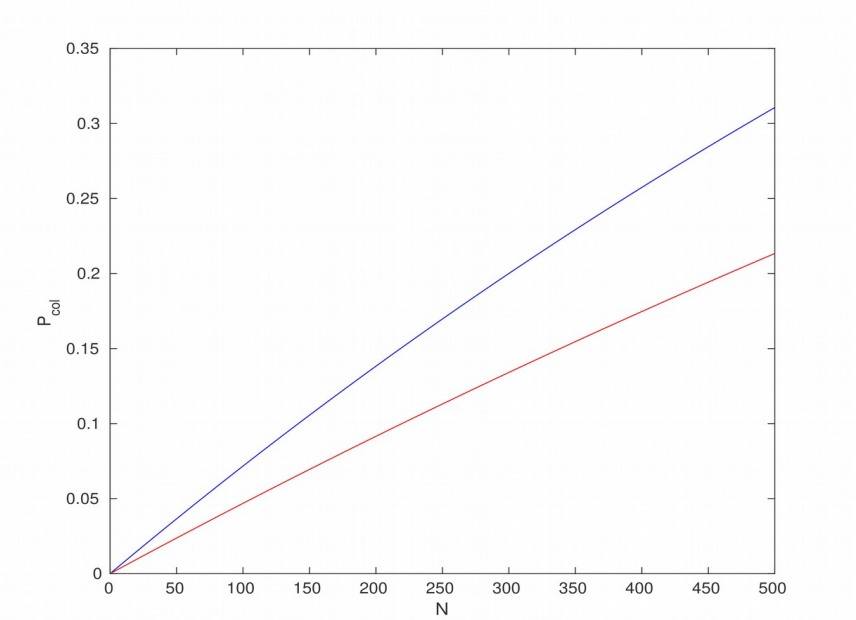

Figure 7.24: Probability of collision of ADS–B messages dependent on number of aircrafts for airborne message rate (blue) and ground message rate (red)

Since the ADS–B system was preliminary designed for airborne use with low obstructions in the travel path of the radio signal, the use of the system in ground operation has to address also the impact of signal blockage, in-band interference caused by multipath propagation, and

out-of-band interference by transmission in the vicinity of the 1090 MHZ band. These phenomena can be considered as an decrease of signal to noise ratio and therefore increase of the probability of error detection of the data symbols. Another impact to the mentioned probability has an above described case of collisions with other ADS–B signals. Let's take a closer look to a case of reception of message without collisions.

If we assume the probability of the error of channel symbol P_{se} and the number of symbols of ADS–B message n, the probability of a correct reception of the ADS–B message is

$$P_d = (1 - P_{se})^n \approx 1 - nP_{se} \tag{7.54}$$

where approximation for small values of P_{se} is made using a binomial expansion

$$(1 - P_{se})^n = \sum_{k=0}^{n} \binom{n}{k} 1^{n-k} (-P_{se})^k = 1 - nP_{se} + \frac{n(n-1)}{2!} P_{se}^2 - \frac{n(n-1)(n-2)}{3!} P_{se}^3 + \dots \tag{7.55}$$

If we consider the event of no collision of ADS–B messages as A and an event of correct reception of message as B, the probability P_r of correctly received ADS–B message without collision is

$$P_r = P(B, A) = P(B \cap A) = P(B/A) P(A) \tag{7.56}$$

where *P(A)* is a probability of no conflict of messages and *P(B/A)* is a probability of correct reception of ADS–B message in case of no conflict during transmission interval.

Finally, substituting 7.52 and 7.54 to 7.56, we obtain the probability of correctly received ADS–B message without conflict as

$$P_r = P_d \cdot P_{nc} = (1 - P_{se})^n \cdot e^{-\lambda 2\tau} \approx (1 - nP_{se}) \cdot e^{-N r_{gen} 2\tau} \tag{7.57}$$

The probability of ADS–B message reception for various symbol error probabilities, airborne or ground message generation rate, and various number of visible aircrafts is depicted at Figure 7.25.

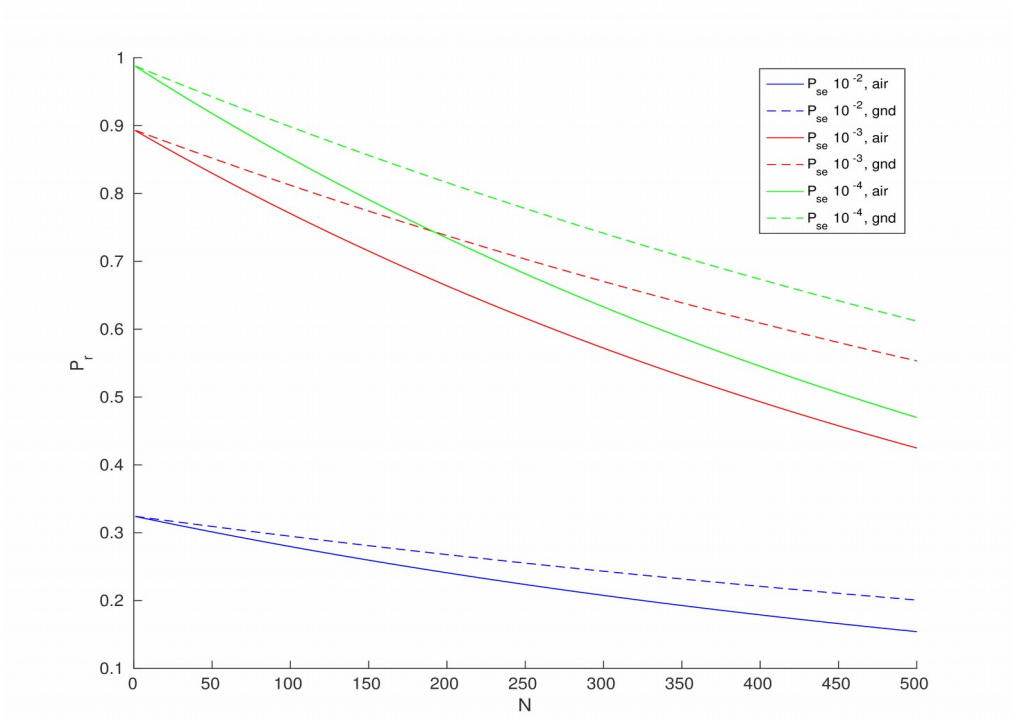

Figure 7.25: Probability of ADS–B message reception in dependence to number of visible aircrafts for various channel symbol probabilities (10^{-2} — blue, 10^{-3} — red, 10^{-4} — green) and airborne (solid) or ground (dashed) message generation rate

As can be seen, the symbol decoding probability has bigger influence to the message reception and decoding success than absolute number of visible aircrafts, so occurrence of messages collision for reasonable amount of signal sources plays minor role to the message decoding.

8 The ADS–B signal reception based on estimation and equalization

The radio channel for transmission of ADS–B signal can have several significantly different forms, the air–air radio channel during transmission between two airborne aircrafts, air–ground channel for reception of signals broadcast by airborne aircraft to an observer on the ground or land–mobile channel for airport facilities and taxiing or standing aircrafts and airport infrastructure equipped ADS–B transmitters (cars,etc.). Our focus is the land–mobile channel that brings the most difficult propagation environment from three mentioned and can complicate successful ATC operations at the airport and in its close vicinity. The typical situations that occur at the airport are signal attenuation, signal blockage, and signal travel through multipath propagation (Figure 8.1).

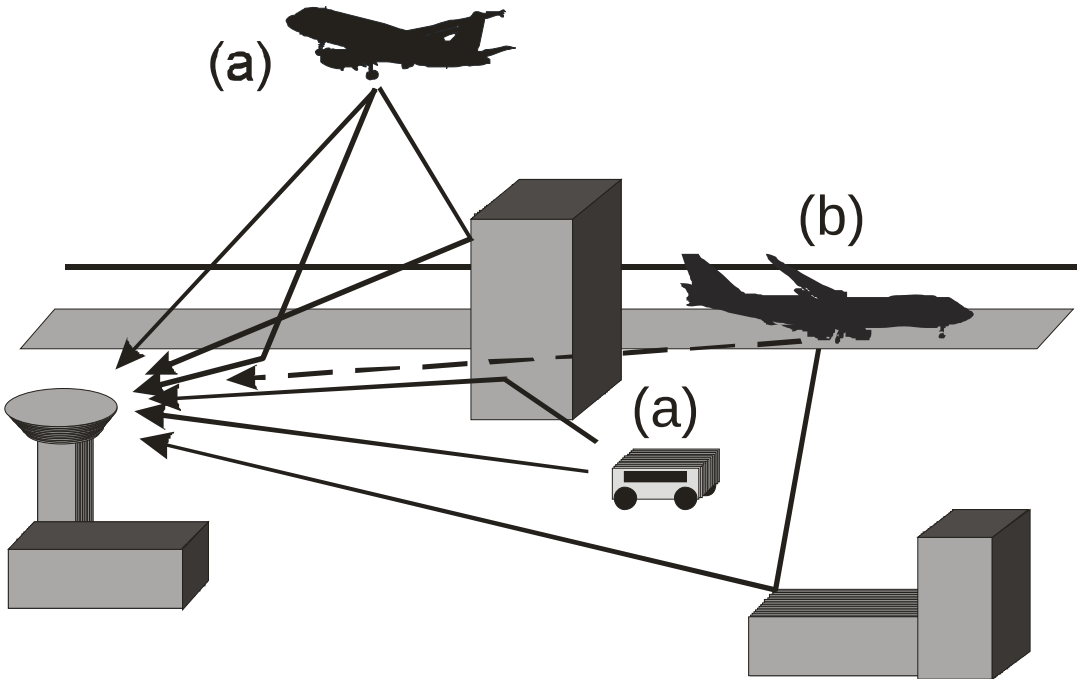

Figure 8.1: Typical airport airside area propagation environment with examples of LOS – line-of-sight signal propagation (a) and NLOS – non-line-of-sight signal propagation with a shadowing of direct signal (b)

The ideal radio channel would be defined by its impulse response as an single Dirac delta function (or unit impulse in sampled representation of the channel) with amplitude related to attenuation of signal during its travel path and time shift representing the delay caused by signal travel. The frequency band limitation of radio channel brings possible threat of inter-symbol interference by shaping the transmitted signal pulse symbol pulses. This fact can be suppressed or completely prevented by careful design of the signal waveform.

In case of corruption by the multipath propagation the impulse response is formed by several non-zero impulses representing the related multipath components. Their value can be generally complex to respect both attenuation and phase change and their delay represents the length of particular multipath component travel path.

The estimation of channel symbols by optimal MLSE method leads to exponential increase of signal space metrics computation and thus is in practical use not the meaningful way of received signal processing in channels with multipath propagation [97]. The more reasonable from the point of realization is an sub-optimal equalization using a linear transversal filtering applied to the received signal to produce estimates of message symbols.

The equalization process is generally a mechanism counteracting to phenomena causing a signal distortion during its way through radio channel. The aim is to minimize their impact to symbol decoding and timing synchronization. The equalizer actually tries to construct a reverse system to the channel impulse response to correct the multipath distortion while simultaneously reject or not emphasize the additional uncorrelated interference (narrowband interference, noise). In case of unstructured interference, e.g. AWGN, the possibilities of equalizer are very poor, however, in case of structured interference (other artificial signal), the equalizer can often reduce its impact.

The simple approach of equalizers, that use the taps of transversal filter delayed equivalent to symbol rate fails in performance for channels, that does not in the spectral characteristics exhibit spectral nulls, which is not the case of radio propagation. Therefore the approach to equalization was directed towards decision feedback equalizers. If the parameters of radio channel are known or estimated, the linear or non-linear approaches can be used, using either peak-distortion criterion or mean square error (MSE) criterion.

However, when the knowledge about the radio channel is not known or can change in time, the classical transversal filter based algorithm works with problems. Therefore the approach of adaptive equalizers, both linear and non linear, is introduced.

8.1 Trained least squares (LS) equalization

This approach is quite suitable for ADS–B signal because of the known structure of the transmitted signal. The preamble or even the beginning of the signal data part can work as an training sequence to adjust the coefficients of equalizer impulse response. The basic concept is depicted on Figure 8.2.

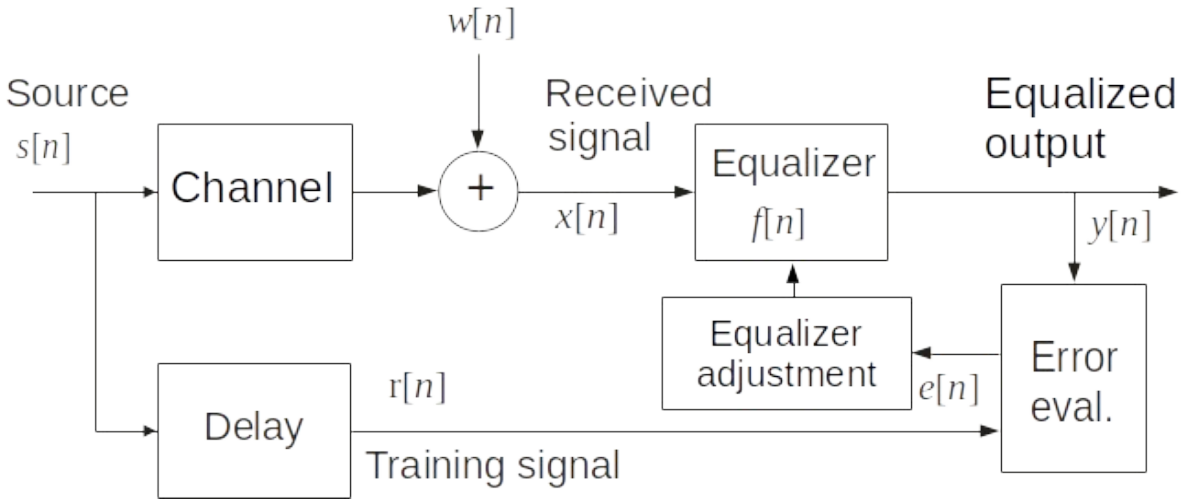

Figure 8.2: Trained equalizer block scheme

The relationship between received signal and the equalizer output can be described by simple FIR filter convolution operation

$$y[n]=\sum_{k=0}^{K-1} f_k\, x[n-k] \tag{8.1}$$

or depicted as a tapped delay line (Figure 8.3).

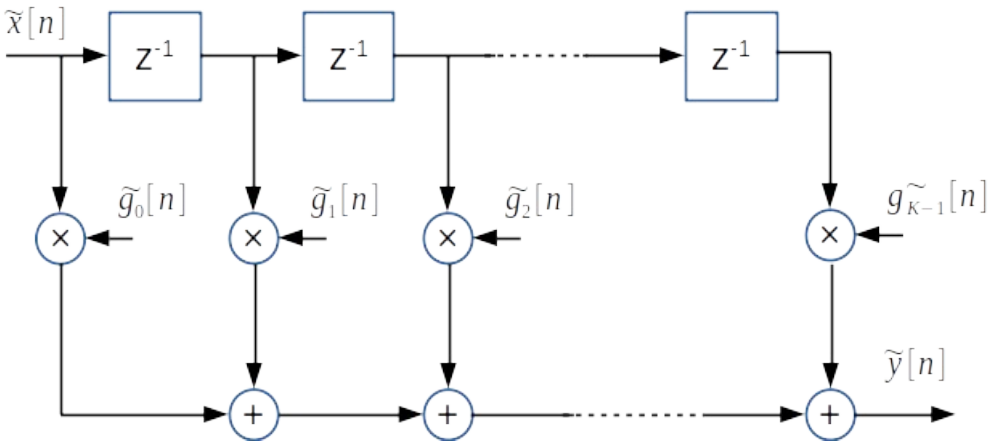

Figure 8.3: Tapped delay line form of FIR filter, where z^{-1} block represents delay by one sample

So the N output samples of $y[n]$ can be obtained by

$$\begin{bmatrix} y[n] \\ y[n+1] \\ \vdots \\ y[n+N-2] \\ y[n+N-1] \end{bmatrix} = \begin{bmatrix} x[n] & x[n-1] & \cdots & x[n-K+1] \\ x[n+1] & x[n] & & x[n-K+2] \\ \vdots & & & \vdots \\ x[n+N-2] & x[n+N-3] & & x[n+N-K-1] \\ x[n+N-1] & x[n+N-2] & \cdots & x[n+N-K] \end{bmatrix} \begin{bmatrix} f_0 \\ f_1 \\ \vdots \\ f_{K-2} \\ f_{K-1} \end{bmatrix} \tag{8.2}$$

or

$$\boldsymbol{y} = \boldsymbol{T}_X \boldsymbol{f}$$

where $\boldsymbol{T}_X$ is a Toeplitz matrix consisting of values of received signal.

The least squares equalization process is then based on expression of error metrics between transmitted signal (or its delayed version used as training signal) and received and equalized signal with the help of parameters of equalization FIR filter. The minimization of this metric across values of filter coefficients provides the best design for equalization solution [117].

The vector of errors $\boldsymbol{\epsilon} = \{e[n], e[n+1], \ldots, e[n+N-1]\}$ is produced by differences of delayed training signal sequence $\boldsymbol{s} = \{s[n-\delta], s[n+1-\delta], \ldots, s[n+N-1-\delta]\}$ and equalized sequence $\boldsymbol{y} = \{y[n], y[n+1], \ldots, y[n+N-1]\}$ and the equalization metric is a sum of squares of errors

$$J_{LS}(\boldsymbol{f}, \delta) = \|\boldsymbol{s} - \boldsymbol{y}\|^2 = \|\boldsymbol{s} - \boldsymbol{T}_X \boldsymbol{f}\|^2 = \boldsymbol{\epsilon}^H \boldsymbol{\epsilon} = \sum_{i=n}^{n+N-1} |e[i]|^2 \tag{8.3}$$

and after substitution

$$J_{LS}(\boldsymbol{f}, \delta) = (\boldsymbol{s} - \boldsymbol{T}_x \boldsymbol{f})^H (\boldsymbol{s} - \boldsymbol{T}_x \boldsymbol{f}) = \boldsymbol{s}^H \boldsymbol{s} - 2\boldsymbol{s}^H \boldsymbol{T}_x \boldsymbol{f} + (\boldsymbol{T}_x \boldsymbol{f})^H \boldsymbol{T}_x \boldsymbol{f} \tag{8.4}$$

Since $\boldsymbol{s}^H \boldsymbol{s}$ is not function of $\boldsymbol{f}$, the minimal value of metric depends of the second and the third terms of (8.4). The minimum of J_{LS} occurs for given δ in case of

$$\boldsymbol{f}_{LS} = (\boldsymbol{T}_x{}^H \boldsymbol{T}_x)^{-1} \boldsymbol{T}_x{}^H \boldsymbol{s} \tag{8.5}$$

The minimal value of metric is then

$$J_{LS}^{min}(\boldsymbol{f}_{LS}, \delta) = \boldsymbol{s}^H [\boldsymbol{I} - \boldsymbol{T}_x (\boldsymbol{T}_x{}^H \boldsymbol{T}_x)^{-1} \boldsymbol{T}_x{}^H] \boldsymbol{s} \tag{8.6}$$

The algorithm to achieve the best possible solution is then for set length of equalizer (i.e. number of taps of FIR filter) calculate minimal metric for every delta and then choose the best one and the related filter coefficients.

The search can be implemented as investigation of result of a matrix construction using possible delays for chosen length of equalizer. The signal with possible delays $\delta = 0, \ldots, D-1$

$$\boldsymbol{S} = \begin{bmatrix} s[n+D-1] & s[n+D-2] & \cdots & s[n+1] & s[n] \\ s[n+D] & & & & s[n+1] \\ \vdots & & \cdots & & \vdots \\ s[n+D+N-2] & s[n+D+N-3] & \cdots & s[n+N] & s[n+N-1] \end{bmatrix} \tag{8.7}$$

is compared with equalized result

$$\boldsymbol{XF} = \begin{bmatrix} x[D] & x[D-1] & \cdots & x[D-K+1] \\ x[D+1] & x[D] & & \\ \vdots & & \vdots & \\ x[D+N-1] & & \cdots & x[D+N-K] \end{bmatrix} \begin{bmatrix} f_{0,0} & f_{0,1} & \cdots & f_{0,D-1} \\ f_{1,0} & f_{1,1} & \cdots & f_{1,D-1} \\ \vdots & & & \vdots \\ f_{K-1,0} & f_{K-1,1} & \cdots & f_{K-1,D-1} \end{bmatrix} \tag{8.8}$$

The *j*th column of $\boldsymbol{F}$ corresponding to delay of *j*-1 producing with $\boldsymbol{X}$ result approximating the *j*th column of $\boldsymbol{S}$. The LS solution of $\boldsymbol{F}$ is according to (8.5)

$$\boldsymbol{F_{LS}} = (\boldsymbol{X}^H \boldsymbol{X})^{-1} \boldsymbol{X}^H \boldsymbol{S} \tag{8.9}$$

In order to the existing term of $(\boldsymbol{X}^H \boldsymbol{X})^{-1}$ the $N > K + D - 1$ must be satisfied. Then the minimum of metric, for jth column of F is according to (8.6)

$$J_{LS}^{min}(\boldsymbol{F_j}) = \boldsymbol{S}_j^H [\boldsymbol{I} - \boldsymbol{X}(\boldsymbol{X}^H \boldsymbol{X})^{-1} \boldsymbol{X}^H] \boldsymbol{S}_j \tag{8.10}$$

approximating the *j*th column of $\boldsymbol{S}$. Then set of these minimal values are along the diagonal of J_{LS}^{min} matrix and the desired minimal value is an *j*,*j* element of

$$\boldsymbol{S}^H [\boldsymbol{I} - \boldsymbol{X}(\boldsymbol{X}^H \boldsymbol{X})^{-1} \boldsymbol{X}^H] \boldsymbol{S} \tag{8.11}$$

The described method was then the object of the simulations described further in this work to verify its feasibility in case of ADS–B signal.

The other known approach using the knowledge of transmitted signal as training sequence described in [118] uses the two way communication where the receiver a predetermined pilot part to the transmitter and using the assumption of symmetrical communication channel the transmitter modifies the next transmission of data to compensate the channel distortion. The concept assumes slow fading channel with changes of channel response to be negligible for coherence time which shall be bigger than duration of pilot and data. The principle of training sequence is the same as in case of proposed solution for ADS–B, the benefit can be seen in lower complexity of receiver signal processing because the signal is inverted to channel

distortion in transmitter. It is however paid by a necessity of two way communication, which is hardly feasible in ADS–B systems.

The whole class of equalizers works without a priori knowledge of training sequence, generally is such kind of process called as a blind equalization. Their methods to obtain an information about channel vary according to system of transmission[119]–[121] or modulation used [122]. These methods are usually more computationally demanding than equalizers with training sequence so in our case we can avoid them.

8.2 The simulations for evaluation of equalization algorithm for ADS–B signal

The set of simulations in Matlab was executed for evaluation of performance of the equalization algorithm described in previous chapter. The several different channels described by their impulse response were generated and the algorithm was applied to the data produced by these channels. The evaluation was made for sampling frequency of 20 MHz, which corresponds with parameters of the receiver, that was used for testing the ADS–B reception and processing on the real data. The test were made for additional AWGN with SNR in range of -6 dB to 4 dB with step 0.1 dB for 10 000 repetitions with each SNR value. As a reference result, the no equalization case for particular response was evaluated as well.

The first set of figures (Figure 8.4–8.6) corresponds to the channel response (A) from Scenario 2 in chapter with simulations of impact of multipath propagation on message detection precision (Chapter 7.2.4). The three selected equalizer lengths were chosen, the length 7 that is shorter than some of impulse responses, the length 14, that is on par with the impulse responses and the length 20, which is longer than all of evaluated responses.

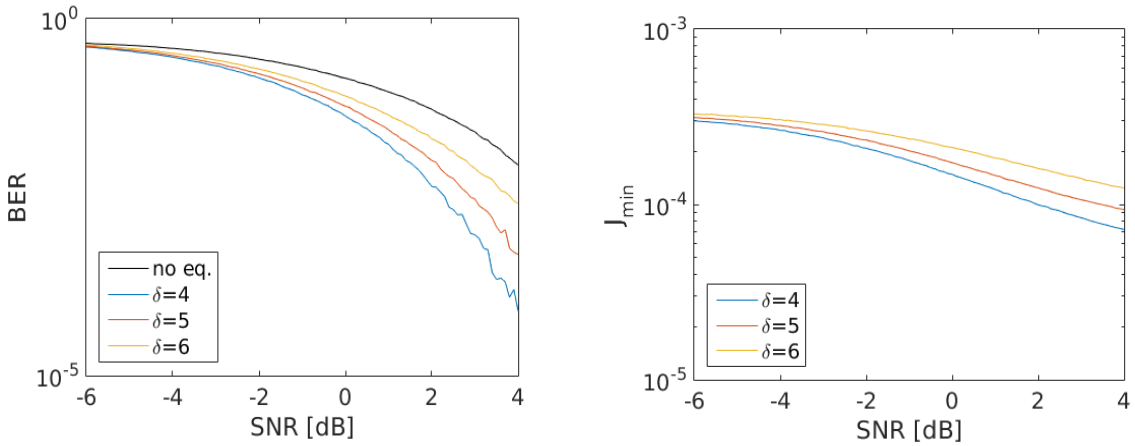

Figure 8.4: The results for channel response (A), equalizer length 7 and various delays δ. BER (left) and J_{min} (right) dependence on SNR

The equalization algorithm improves the BER for all values of delta with best result for shortest delay. The longer delay performance decrease is caused by inclusion of more samples without multipath interference but with AWGN. The best performance of delay 4 is also shown by lowest value of J_{min} across all values of SNR.

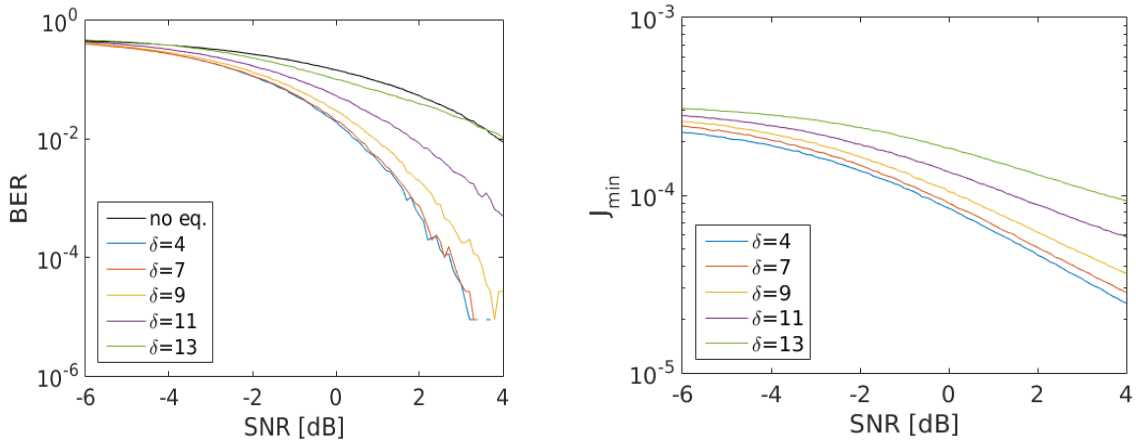

Figure 8.5: The results for channel response (A), equalizer length 14 and various delays δ. BER (left) and J_{min} (right) dependence on SNR

The situation for equalizer of length 14 remains consistent with the previous one, again the lowest delay approximates the signal model with the best results.

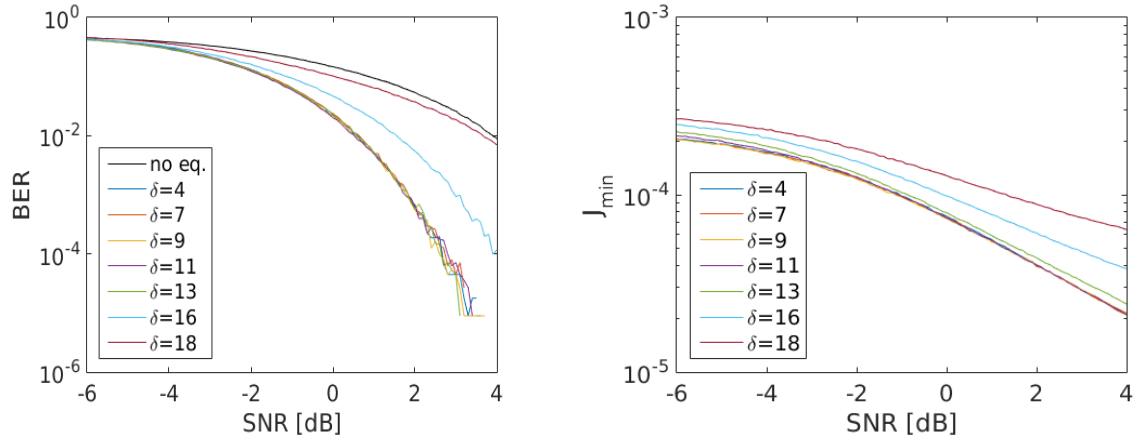

Figure 8.6: The results for channel response (A), equalizer length 20 and various delays δ. BER (left) and J_{min} (right) dependence on SNR

The longest evaluated equalizer produces same results as in the previous two cases with the best performance for shortest delay. The reason is, that the delay of the multipath component (125 ns) is a fraction with respect to length of ADS–B pulse 500 ns so the interference has similar impact as band limitation of the channel causing distortion of pulse slopes.

The second set of tests was done for impulse response (B) from scenario 2 with results on Figures 8.7–8.9. The other conditions (equalizer lengths, delays, SNR range) remained the same.

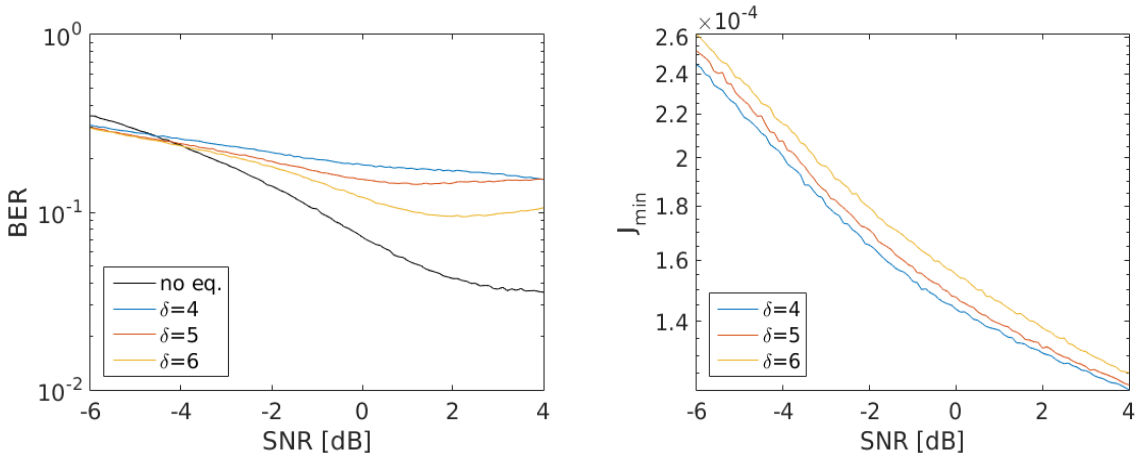

Figure 8.7: The results for channel response (B), equalizer length 7 and various delays δ. BER (left) and J_{min} (right) dependence on SNR

Here can be seen a significant property of the equalization algorithm that the J_{min} as an optimization criterion fails in the case that the equalizer length is shorter than the channel delay profile. The equalizer then provides faulty results.

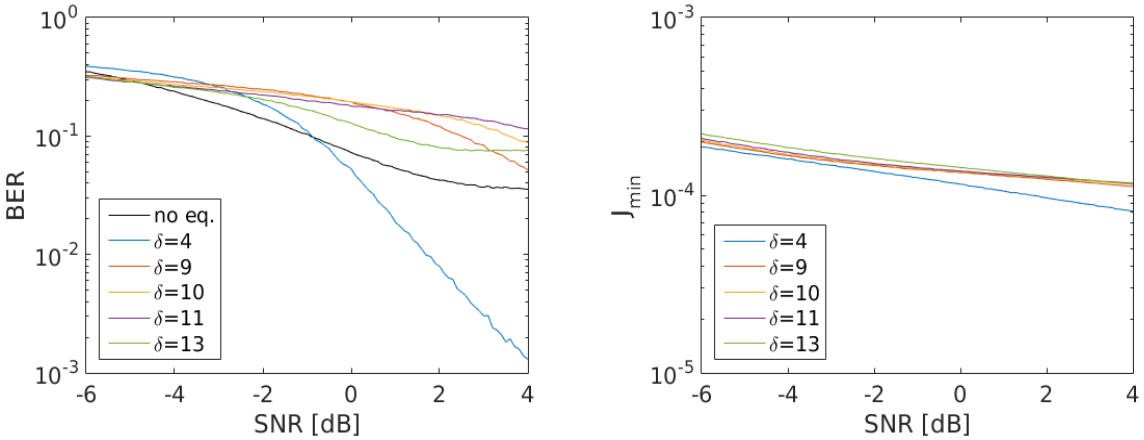

Figure 8.8: The results for channel response (B), equalizer length 14 and various delays δ. BER (left) and J_{min} (right) dependence on SNR

The equalizer length 14 already produces an improvement of BER for some δ value (δ = 4) and the criterion of is already valid for moderate SNR values although it does not provide unambiguous information about the choice of proper δ.

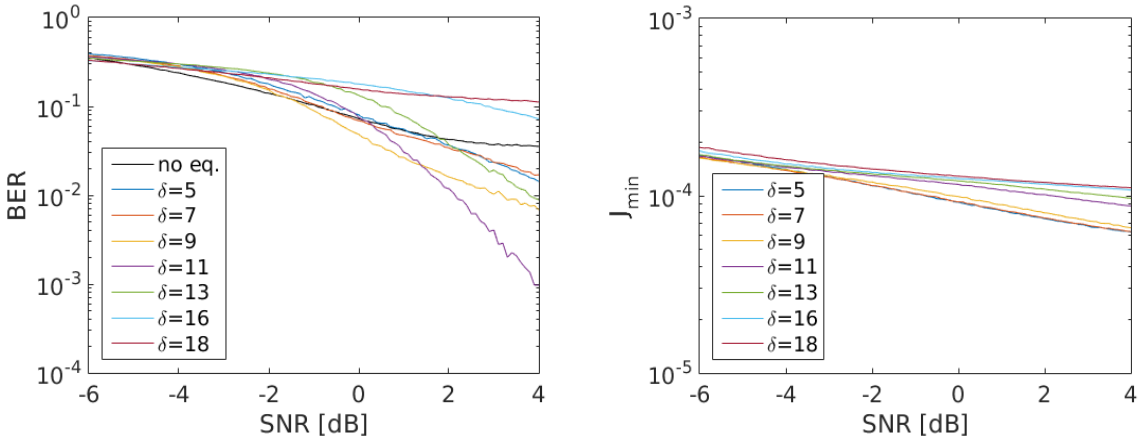

Figure 8.9: The results for channel response (B), equalizer length 20 and various delays δ. BER (left) and J_{min} (right) dependence on SNR

The increase of the length of the equalizer did not bring a substantial improvement in BER. The break border in the improvement with respect to non equalized case remains about 0 dB of SNR but the optimal choice of δ = 11 is now not any of the margin values as in the previous cases. It can be said, that this case represents the one of the more complicated scenarios for equalizer.

To consider the possible impact of equalizer and delay choice in case of such problematic response the simulations for combination of lengths and delays were executed. The combinations of equalizer length *Eq_lenght* = 2,…, 20 and delays δ = 1,…,*Eq_length*−1 in the range of SNR −2 dB,,…,2 dB was evaluated by Monte Carlo method with 1000 iterations. The equalizer used replica constructed from 8 μs of ADS–B signal (equal to preamble up to data part). The results are shown for selected values of SNR in Figures 8.10–8.12.

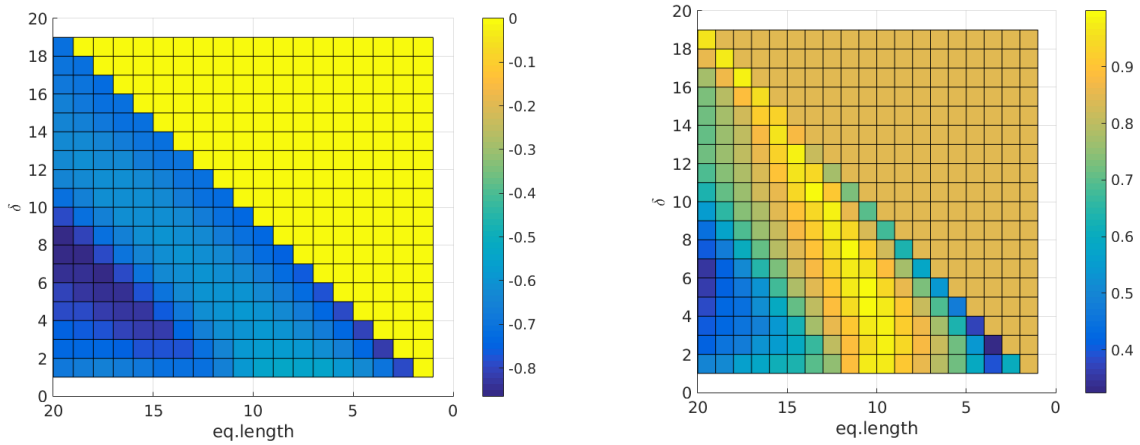

Figure 8.10: The BER (left, in form of log10(.)) and J_{min} (right, normalized to maximum) values across equalizer length (eq.length) and δ for SNR=−1.8 dB

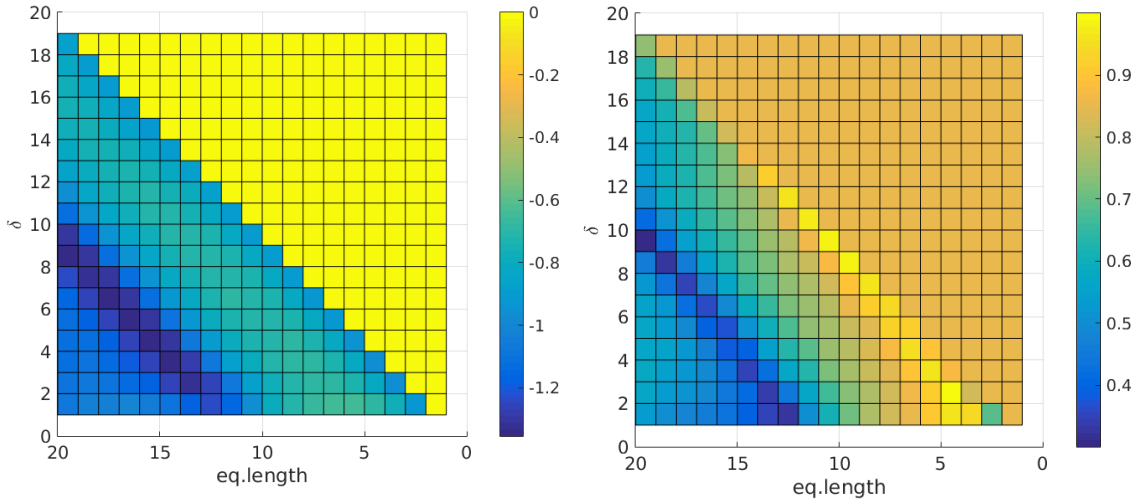

Figure 8.11: The BER (left, in form of log10(.)) and J_{min} (right, normalized to maximum) values across equalizer length (eq.length) and δ for SNR=0 dB

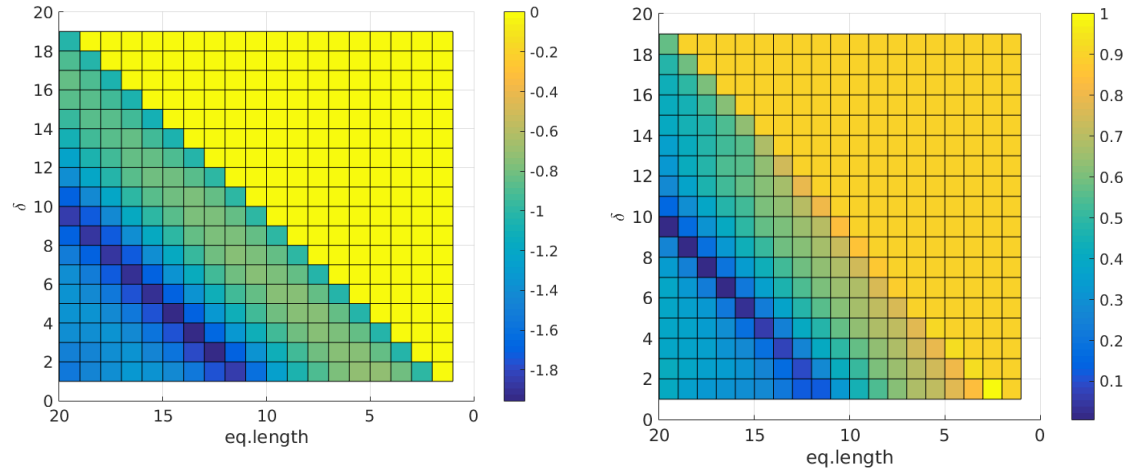

Figure 8.12: The BER (left, in form of log10(.)) and J_{min} (right, normalized to maximum) values across equalizer length (eq.length) and δ for SNR=1.9 dB

The uper right triangles of all figures represent the unrealizable combination of equalizer length and δ, so they are not relevant for evaluation. The criterion of $J_{\min}$ works well for moderte and better SNR (SNR > 0 dB) since the differences between values of $J_{\min}$ are bigger as can be seen from colorbar ranges. The optimal combinations for SNR above 0 dB are equalizer length between 11–17 and delta 2–6 (the complete table in Appendix C).

The third described set of simulations (Figures 8.13–8.15) uses channel response representing the NLOS case, the direct component with the relative amplitude 0.2 and the complex multipath component with delay 0.5 μs and relative amplitude $0.707e^{0.142j}$.

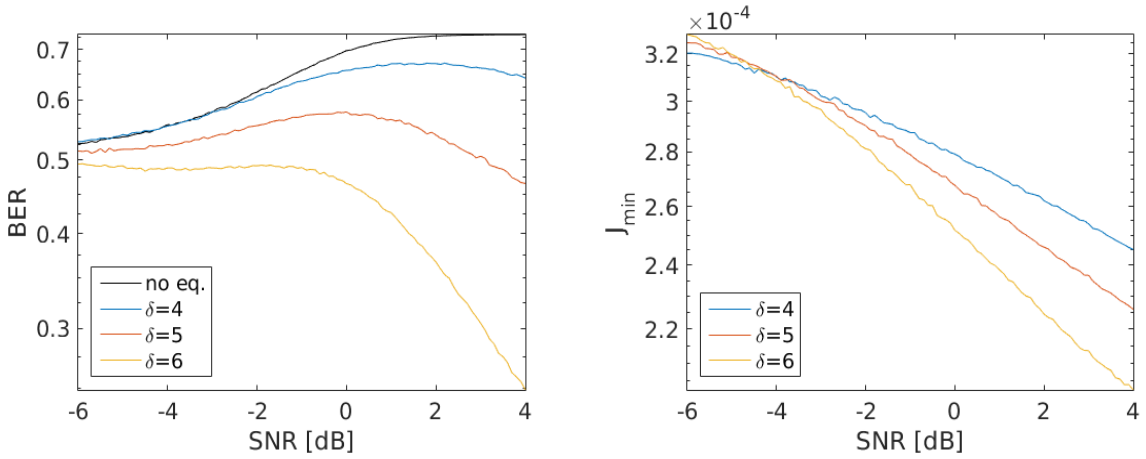

Figure 8.13: The results for simulation of NLOS channel, equalizer length 7 and various delays δ. BER (left) and J_{min} (right) dependence on SNR

In case that the direct component provides at least minimal level for the detection of the signal, the mechanism of equalizer can improve the BER also for the NLOS case, as can be seen even in case of shortest variant of evaluated equalizer. The remaining lengths of equalizers continue then in consistency of BER improvement with J_{min} as an unambiguous criterion.

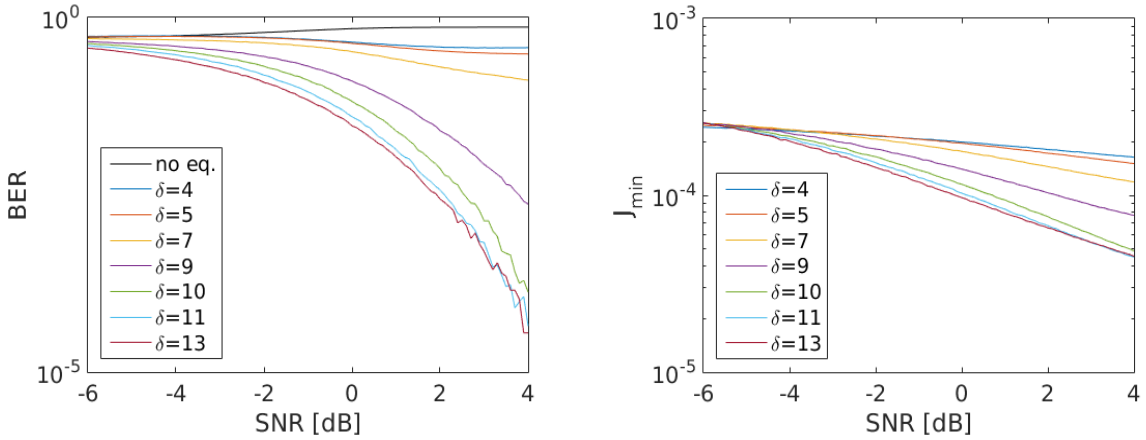

Figure 8.14: The results for simulation of NLOS channel, equalizer length 14 and various delays δ. BER (left) and J_{min} (right) dependence on SNR

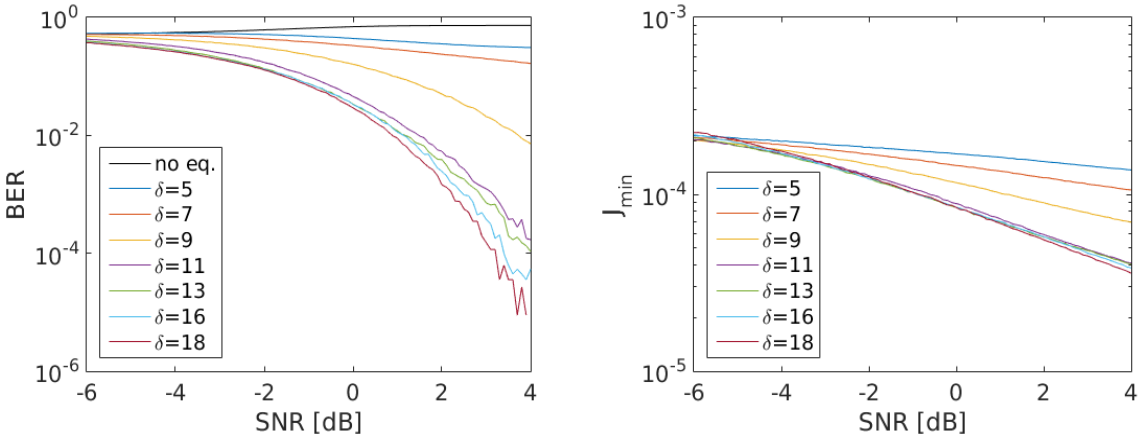

Figure 8.15: The results for simulation of NLOS channel, equalizer length 20 and various delays δ. BER (left) and J_{min} (right) dependence on SNR

As the results of simulations had shown, the critical parameter for equalizer performance is the relation between its length and delay profile of the radio channel. This is the reason, why it is necessary to make at least an estimation of impulse response of the radio channel for particular application.

Since the aim of the work is the airport area and ADS–B service, the natural case is to make a set of measurements at the particular airport. Thanks to the Civil Aviation Authority of the Czech Republic (Úřad pro civilní letectví ČR) we could make a set of measurements at the Prague Vaclav Havel airport to obtain the data for the estimation of the average impulse response (mainly the number of substantial taps of the impulse response) [123].

The measurement in the first phase used existing set of MLAT (multilateration) transponders that were installed at the Vaclav Havel Airport Prague to provide stable source of known signal. The measured locations were chosen to cover all typical cases of combinations of source, receiver, and obstacles to be able to evaluate both LOS (line of sight) and NLOS (non line of sight) cases of reception. Moreover, the effect of distance of possible obstacles for producing multipath components of the received signal was taken into account during choice of measurement points. The map of airport that shows measurement points and evaluated sources is at Figure 8.16.

Figure 8.16: Situation plan of the Vaclav Havel Airport Prague with view to positions of transmitters (TXAxx) and measured points (00x) (shown on map layer of OSM maps)

These transponders periodically broadcast ADS-B extended squitter signals at the frequency 1090 MHz. The incoming signal was received by specially designed WNav receiver [124] equipped by suitable ADS-B antenna and selective preamplifier installed in laptop via PCI-E interface. The position of the measurement points was obtained from GPS receiver with antenna placed together with ADS-B antenna on the roof of the measuring vehicle. Each measurement consisted of several records, each of them with one second duration. The received signal was sampled with sampling frequency of 20 MHz in the form of complex envelope. Appropriate signal samples for both in-phase and quadrature part of complex envelope (lowpass-equivalent signal) were then stored in laptop and external drive for further post processing.

The focus was aimed to search ADS-B extended squitter data, thus responses in modes A/C and S without extended data had to be excluded from processing. This was done by the search for a pattern equal to Mode S. Then the length was checked to exclude “short” responses without extended squitter data. The result was then processed for obtaining the impulse response estimate. Since we could test the algorithm on known data provided by MLAT transponders, we could generate proper replicas.

The recorded signal in therms of complex envelope was subject to several phenomena, related to radio channel and signal definition as described in previous chapters. The residual carrier wave offset induced distortion caused by allowed variance of transmitter’s carrier wave frequency as specified in was resolved using the GLRT based detector expressed in (7.31).

The remaining phase shift does not produce a problem in envelope based decoding of symbols.

The received signal and the replica generated according to the knowledge of the MLAT transmitter data were used for least squares (LS) based estimation of impulse response to form a power delay profile of the radio channel, mainly to provide information about the length of impulse response that limits the minimal length of equalizer as was demonstrated in simulation part.

For the LS estimation, we assume that the discrete channel output can be expressed by general discrete convolution of input signal and impulse response. For real situation we can assume that the impulse response is finite in time i.e. it can be considered zero or negligible outside time interval <0,m_{max}>. Then the convolution will run through finite interval and can be expressed as

$$\tilde{y}[k]=\sum_{m=0}^{m_{max}} \tilde{x}[k-m]h[m] \tag{8.12}$$

where $\tilde{x}[k]$ are samples of input (transmitted) signal, $\tilde{y}[k]$ are samples of output (received) signal, and $h[m]$ is a channel impulse response. The symbol ~ denotes low-pass-equivalent form (complex envelope) of affected signals.

The K samples of output signal can be obtained using matrix operation of $K+m_{max}+1$ samples of input signal, $m_{max}+1$ samples of impulse response and noise

$$\boldsymbol{y}=\boldsymbol{M}\boldsymbol{h}+\boldsymbol{w} \tag{8.13}$$

in a form

$$\begin{bmatrix} \tilde{y}[0] \\ \tilde{y}[1] \\ \vdots \\ \tilde{y}[K-1] \end{bmatrix} = \begin{bmatrix} \tilde{x}[0] & \tilde{x}[-1] & \cdots & \tilde{x}[-m_{max}] \\ \tilde{x}[1] & \tilde{x}[0] & & \tilde{x}[1-m_{max}] \\ \vdots & & & \vdots \\ \tilde{x}[K-1] & \tilde{x}[K-2] & \cdots & \tilde{x}[K-1-m_{max}] \end{bmatrix} \begin{bmatrix} h[0] \\ h[1] \\ \vdots \\ h[m_{max}] \end{bmatrix} + \begin{bmatrix} w[0] \\ w[1] \\ \vdots \\ w[m_{max}] \end{bmatrix} \tag{8.14}$$

From this term we can obtain LS (least squares) estimate of the desired channel impulse response [97]

$$\mathbf{h}_{est} = \left(\mathbf{M}^T\mathbf{M}\right)^{-1}\mathbf{M}^T y \tag{8.15}$$

The average values of impulse for LOS a NLOS cases had shown, that channel taps over 350 ns can be considered negligible [5]. The examples of normalized power delay profiles (to the highest component) are shown at Figure 8.17.

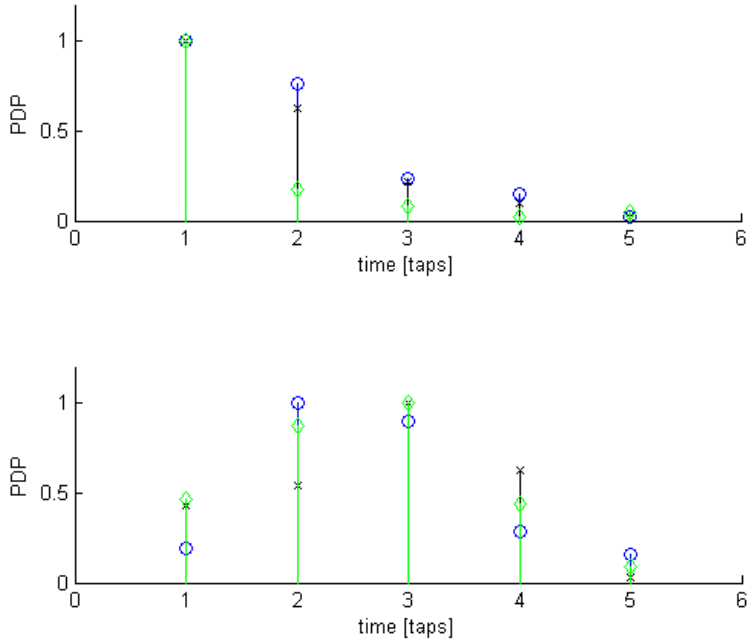

Figure 8.17: Example of PDPs for LOS case (upper) and NLOS case (lower), with various distance of obstacles relative to line of sight – less (diamonds,green), equal (circle, blue, and cross, black).

The separation of delays of the rays $\Delta\tau = \tau_{i+1}-\tau_i$ obtained from estimated power delay profiles is much lower than ADS-B data symbol duration T_S, here $\Delta\tau/T_S = 0.05$ for T_S equal to 1 microsecond. According to [125] we can then consider the channel to be frequency non–selective and the equalizer approach can be fully applied. From the channel values variation point of view, ADS-B response received from landing or taxiing airplane can be affected also by Doppler shift of the transmitted signal. The caused shift for typical speed of 160 knots is for the 1090 MHz signal in the order of kHz and therefore several orders bellow allowed variance of the carrier wave of the transmitter (1000 ppm) [12]. The other objects at the airport ground (support, guidance and airport authority vehicles), they move with even lower speed. Thus, for current set of signal sources the Doppler spread and its impact to channel coherence time caused by movement could be considered negligible and to be included into estimation of frequency offset of carrier wave realized in the above described processing of measured data.

8.3 The processing of real measured data

The last step that remains in evaluation of suitability of proposed equalization approach on ADS–B signal processing is the application on real measured data. The location of data

capture was chosen in the area of university campus to assure the enviroment prone to the multipath propagation. The several sets of measurement were executed using a software receiver (SDR) as a recording device. The SDR that was used for cata capture was the nuand® bladeRF x40 receiver [126] connected to laptop through USB 3.0 interface. The SDR receiver is capable of collect complex envelope samples in range of carrier frequencies 300MHz to 3.8GHz with 12 bit sample resolution and sampling frequency up to 40 Msps. The sampling frequency, used during recording, was chosen 20 MHz to prevent USB bus data transfer issues.

The receiver was equipped with suitable ADS–B antenna and bandpass filter Teroz 519 (parameters in Appendix D) to suppress possible interference. The recorded data were captured by open source software package gqrx [127], that stores complex samples in the interleaved float32 format. The records were captured with duration of about 10 seconds producing approximately 2 GB of datafile each. To relax the memory demand related to processing of such data, the file was split to 105 MB chunks representing 0.6554 seconds and 13107200 complex samples.

The processing itself was realized in Matlab in two stages, first stage covered algorith for ADS–B signal detection as described in Chapter 7.2.4, using for comparison all three types of detectors that participated in simulations. The detected presence of ADS–B signal was then evaluated by tim eframing to distinguish, whether it is an A/C reply, short Mode S reply or long Mode S reply, including ADS–B. The related time tags were then collected and passed to the second stage, where the equalization algorithm and decoding were realized. In the end the resulting product were decoded hexadecimal values of ADS–B message which was checked by CRC according to [13] for correctness. The results were then compared with third party software (Dump1090 [128]) capable to process raw samples of complex envelope applied on the same signal.

Since the used SDR is based on concept of direct conversion receiver (i.e. direct conversion to baseband without intermediate frequency stage), the recorded signal samples were corrupted by imperfections of SDR, namely the DC component offset and inphase and quadrature unbalance [129]. The problem with DC offset can be solved by compensation feedback circuits for the penalty of the distortion of the central frequency on which oscillates a local oscillator. The one possible solution to this problem for spectral analysis is to use a higher frequency resolution of the signal when distorted frequency bin is ignored and replaced by the interpolated value. In our case the DC component was reduced by using a tuning of the central frequency by 1.5 MHz below the ADS–B system 1090 MHz center frequency, the signal was averaged to obtain the mean value related to DC component and this value was subtracted form the original signal. The result was then in the signal processing shifted by 1.5 MHz down to get the low-pass frequency component corresponding to 1090 MHz back to zero frequency. The efficient bandwidth of the receiver was by this operation reduced by 3 MHZ which still covers sufficient bandwidth of ADS–B signal [9]. The inphase and quadrature

unbalance is a problem that can completely destroy the measurement or can bring new effects that are caused by the receiver imperfection. The sufficient suppression of 40 dB was achieved by the receiver prior calibration according to the instructions provided by manufacturer.

The Figure 8.18 shows a spectrogram of down–converted signal in base band in terms of power spectral density for one 0.6554 s chunk of record. There can be seen the ADS–B signal at zero frequency and the in-band interference at 2 MHz from center. This interference was usually caused by other radio systems in urban areas, although the signal was for the processing filtered by digital low-pass filter of bandwidth 4 MHz, some in-band interference was still present.

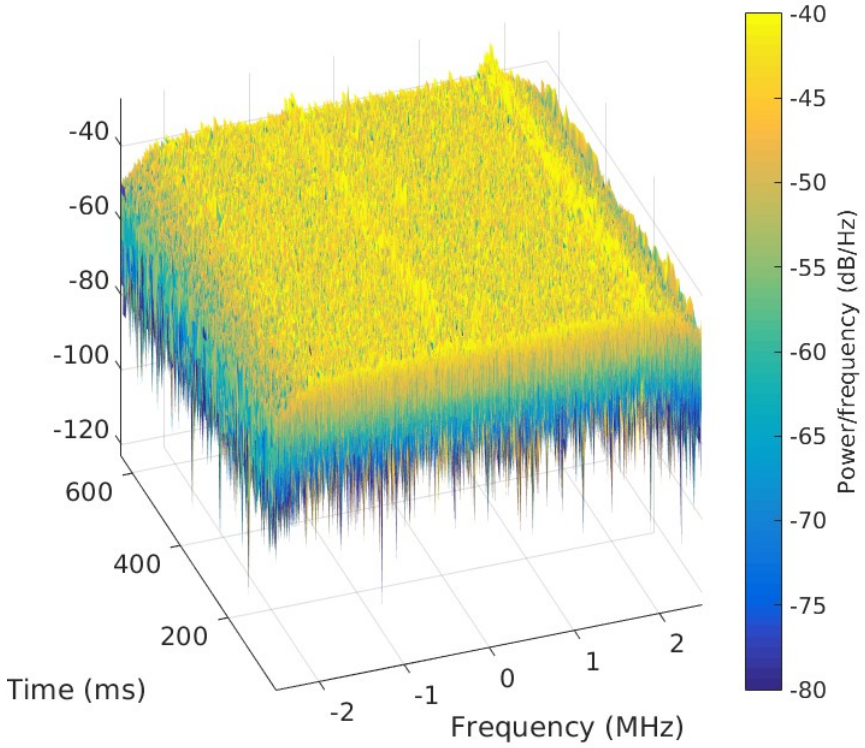

Figure 8.18: Spectrogram of single chunk of ADS–B recorded measurement with duration 0.6554 s

The next image (Figure 8.19) shows the application of detectors on the complex envelope of the signal. The colored spikes present the message starts as determined by detectors output. It can be clearly seen, that classical integrator detector (upper graph) provides many false positives. Therefore, the last two detectors (matched filter – middle graph, second order correlator – lower graph) were used for further processing.

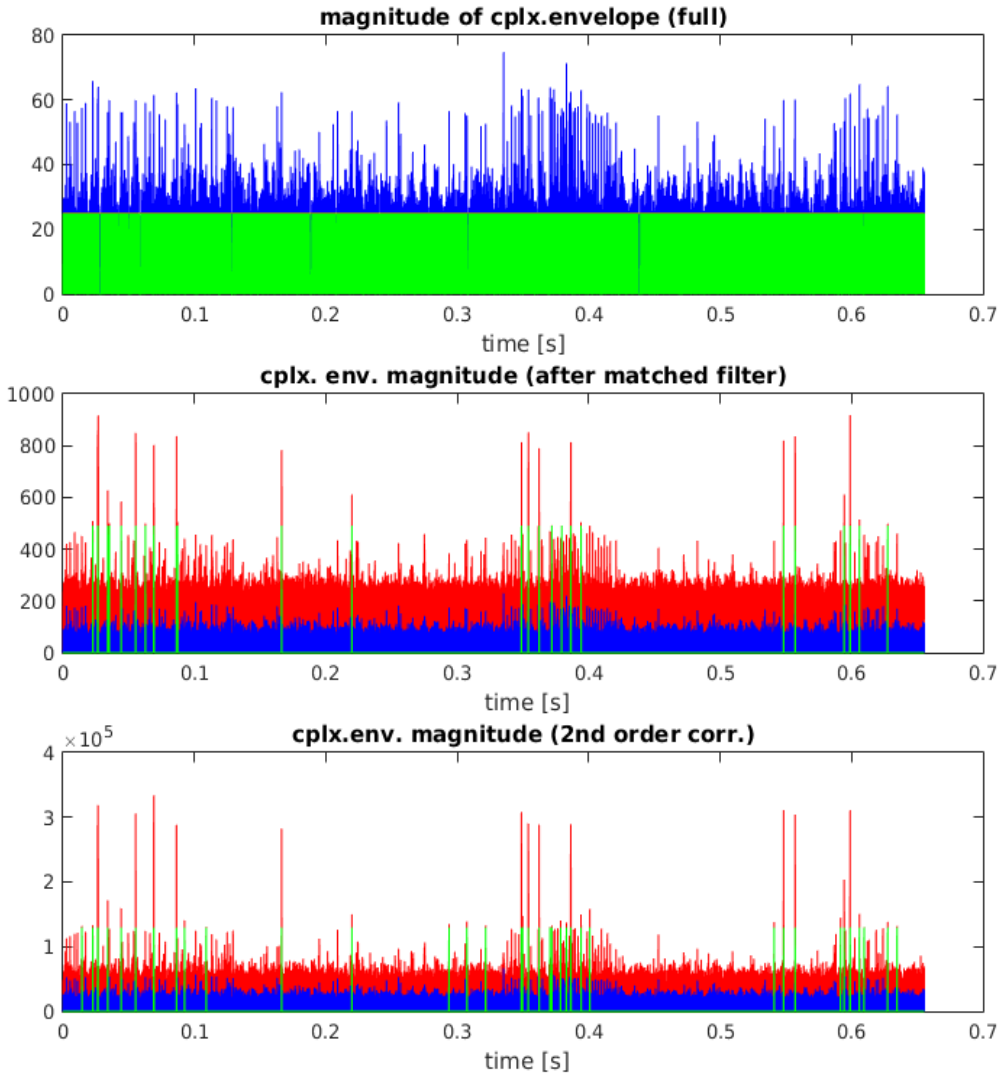

Figure 8.19: The complex envelope magnitude in time of the recorded signal with outputs of detectors (integrator – upper, matched filter – middle, second order correlator – lower). The blue signal represents original signal before detectors, the red shows detector outputs (i.e. correlation results) , the green suggested detections

The detected signal was then fine tuned to suppress the remaining frequency offset due to ADS–B carrier frequency tolerance by estimation of such frequency offset producing the lowest error variance in On-Off keying (OOK) modulated PPM signal. Moreover, the unknown phase shift of the symbols in the constellation was estimated and compensated to produce best possible OOK constellation for symbols decoding. This process is shown at Figure 8.20.

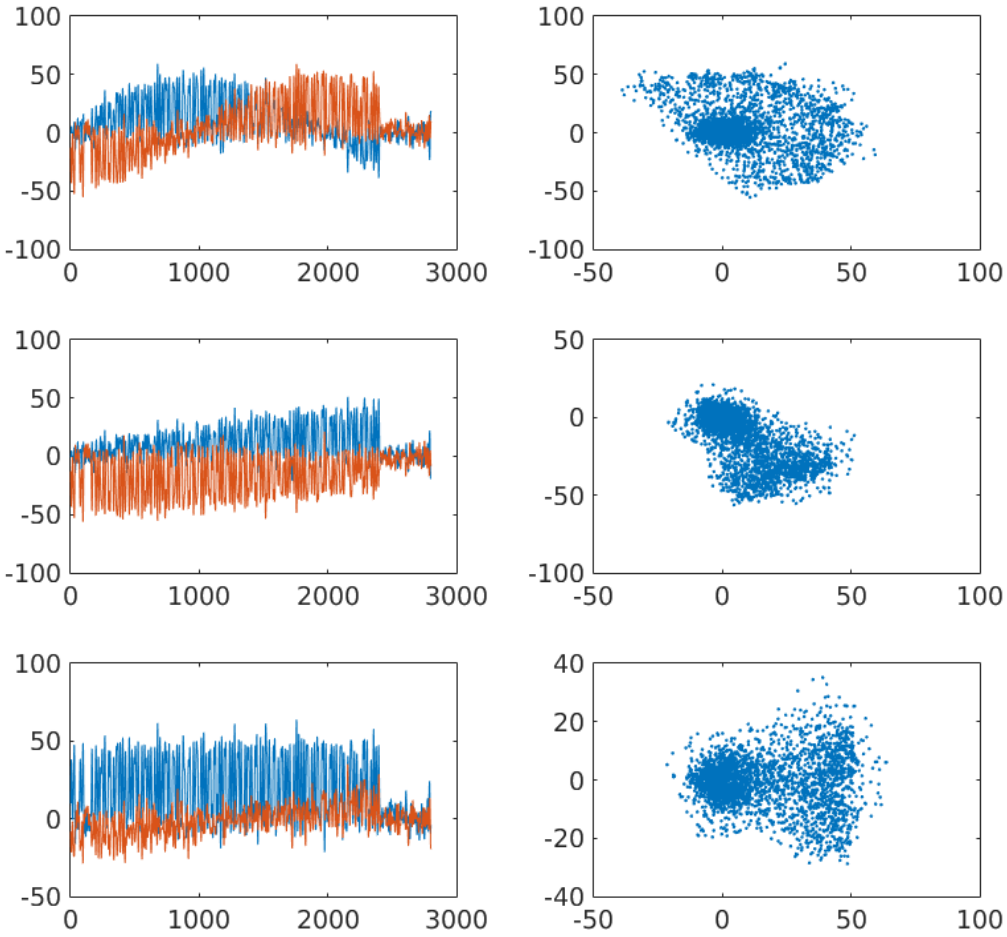

Figure 8.20: The removal of remaining carrier frequency offset and "focusing and steering" the OOK constellation

Then there is executed the process of symbols decoding together with equalization of the complex envelope samples based on replica constructed from 8 μs of ADS–B preamble. The equalizer was set according to result obtained by simulations to lengths 14 to 16 and parameter δ to range 4 to 7, the result was optimized according to simultaneously computed $J_{\min}$ value. The signal before and after equalization is shown at Figure 8.21. The last Figure 8.22 shows the complex envelope and decoded pulses relevant to PPM modulation scheme. The decoded PPM symbols are then converted to HEX value of ADS–B message , which corresponds to message $\texttt{8D3C6706EA4288668D3C08B76730}_{\text{HEX}}$, ICAO address 3C6706, DF14, TC 29, related to aircraft with registration D-AIXF, Airbus A350-941 (the registration and type of aircraft obtained from public database [130]).

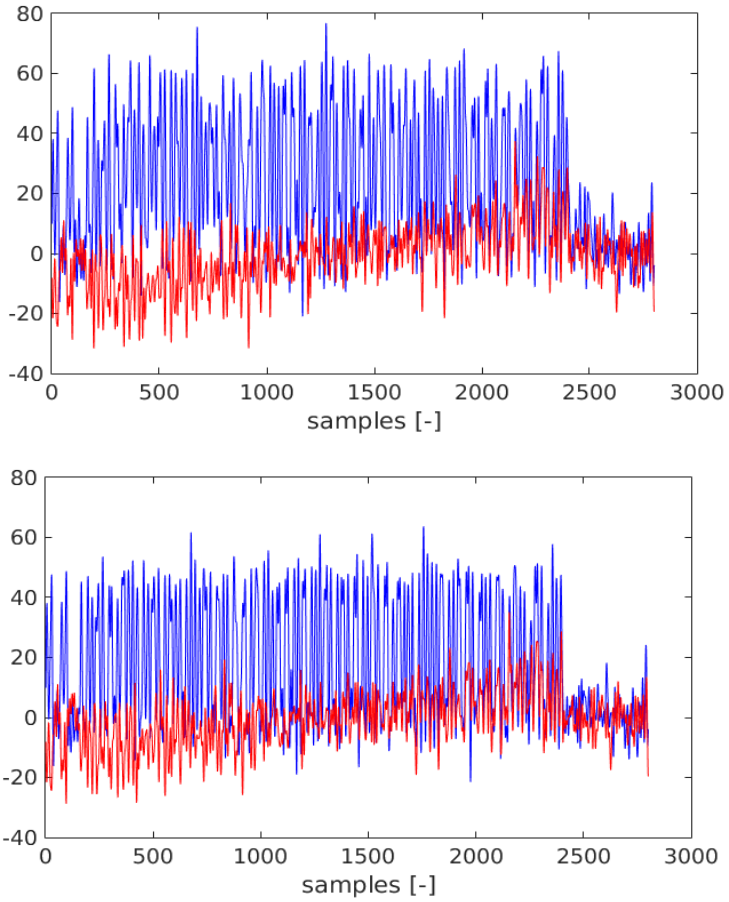

Figure 8.21: The real (blue) and imaginary (red) part of complex envelope of ADS–B signal before (upper picture) and after equalization (lower picture)

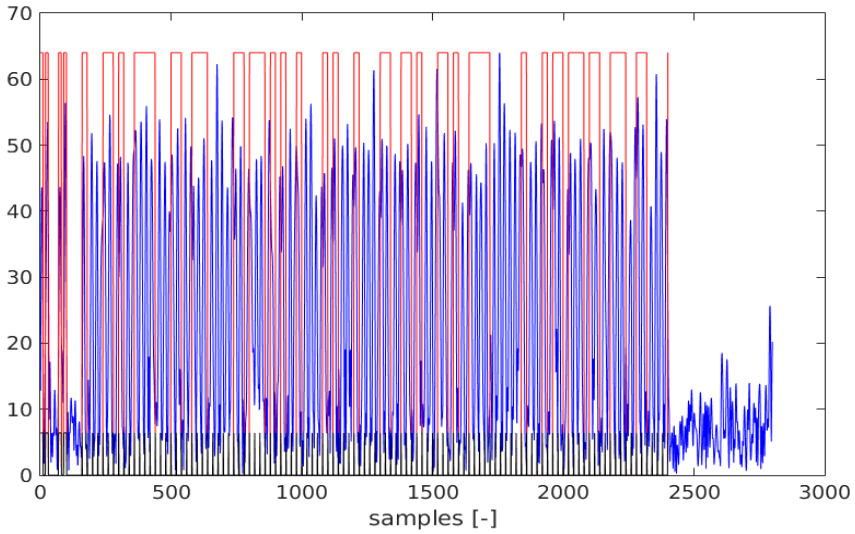

Figure 8.22: Complex envelope of ADS–B message with decoded PPM pulses

Since the processing was made on real signal, there is actually no possibility to precisely evaluate the performance that is usually made of artificial simulated data. However, It was compared the number of detections and decoded messages with the output of the third party software performed on the same data record. The five records with average duration of 10 seconds each were evaluated. There was evaluated number of detections, number of detections corresponding to Mode S messages (i.e. correct detection based on preamble, covering both short and long Mode S messages) and number of Mode S messages with correct CRC (i.e. decoded without error). The results are summarized in the Table .

Table 8.1: Statistics of records of ADS–B signal experimental measurement and processing

No. of detections	**No. of Mode S messages**	**Mode S messages with correct CRC**	**Mode S messages detected by third party SW**
1825	249	117	102
1905	294	126	113
1499	204	110	115
1890	226	111	79
1834	298	102	104

The most of the false positives in the detections were replies in mode A/C producing the approximately similar pattern as preamble used for correlation. These detections were further in processing removed based on the complex envelope energy framing set for duration of short and long Mode S reply (comparison of relative levels in frames with length corresponding to duration of A/C, short Mode S or long Mode S replies). Since the number of real signal sources naturally vary throughout the records, the precise statistics is an object of long term evaluation which was not due to time available for measurement campaign yet realized and is planned to continue also in the future. However, from the available results can be stated, that combination of proposed detector and equalization produces about 10% more of correctly decoded ADS–B messages in comparison to the conventional approach which brings a promise for further work in optimization of the solution described in conclusion and outlook chapter.

9 Conclusions and Outlook

The described thesis presents a closer view to the area of surveillance of air traffic based on the ADS–B signal for difficult environment, typical by various signal influences, e.g. shadowing or multipath propagation. I tried to cover main aspects of the ADS–B signal characteristics and the possible application not only as source of information that carries but also as a ranging signal for multilateration purposes.

The benefit of the knowledge of the substantial part of the ADS–B signal, either from the previous reception with better conditions or by different communication channels (e.g. the aircraft ICAO code can be stated from the information obtained during communication), brings the use of such signal on par with radar self generated signals or signals of navigation systems with predefined format (e.g. GPS). I tried in the thesis to exploit these features for ADS–B signal processing improvement. Of course not everything was resolved with the complete success so I would like here to summarize the achievements and also provide a view to things that from my point of view deserve a further investigation or research.

The main intent was to investigate possible methods how to improve the performance of ADS–B signal detection and decoding which brought a proposal of the detection based on not commonly used second order correlation which provided good performance here strongly benefits from the structure of the ADS–B signal. The use of such method for general communication or ranging signal can however bring different results. The possibility of an improvement of the correlation function is limited due to the strict format of the message and signal in space definition by aviation standards, however the possible ways were to further investigate the idea of pseudorandom phase modulation of PPM signals as suggested in reviewed literature [115]. The realization of the higher order correlation detector by a set of matched filters could potentially improve computation demands and this is one the not yet investigated tasks that remained.

The achieved detection within one sample interval brings optimistic view to the use of such obtained relative time of arrival for multilateration task. The comparison of here calculated Cramer-Rao lower bound for TDoA position computation with practical values obtained with mechanisms described in this thesis is another path to walk in. The lack of properly synchronized system of the stations at present prevented to practically investigate the achievable performance, however, it is in the focus of research activities in nearby future.

The idea of radio channel equalization is naturally not new, it was introduced for the communications and came to popular with the evolution of the mobile communication networks operating with higher frequencies, where multipath propagation plays significant role of the interference. In the area of air traffic communication and surveillance it was not such often applied since the methods for resolution and separation of multipath components

were oriented towards use of spatial diversity and array processing techniques, e.g. [131]. The here provided simulations and results applied on the real signal have shown that this approch can also bring an improvement on signal decoding performance. The future way can be the combination of channel equalization and array processing in MIMO systems that can further enhance the performance of these systems, so the results in this thesis could provide the supplementary background for further activities. Although the approximation of the channel by the simple time invariant model, or more precisely, with assumption of time invariance for duration of the single ADS–B message, since the equalization algorithm is executed for each detected message separately, successfully worked according to the realized measurements, I feel that there is still a broad area of extension of such approach to the more complex types of the radio channels that could more precisely fit to the airport environment.

The next practically oriented step is the implementation in the hardware that is not dependent on custom software packages (Matlab), so the coding to the binary executable and implementation to the experimental software receiver similar to our solution in adjacent projects [6].

References

[1] EUROCONTROL, “Challenges of Growth 2013. Task 4: European Air Traffic in 2035,” 2013. [Online]. Available: https://www.eurocontrol.int/sites/default/files/article/content/documents/official-documents/reports/201306-challenges-of-growth-2013-task-4.pdf. [Accessed: 14-Jun-2019].

[2] IATA, “New IATA Passenger Forecast Reveals Fast-Growing Markets of the Future,” 14-Jul-2019. [Online]. Available: https://www.iata.org/pressroom/pr/pages/2014-10-16-01.aspx. [Accessed: 14-Jul-2019].

[3] “Code of Federal Regulations. Title 14: Aeronautics and Space. Volume2.” [Online]. Available: https://www.govinfo.gov/content/pkg/CFR-2019-title14-vol2/pdf/CFR-2019-title14-vol2-chapI.pdf. [Accessed: 25-Aug-2019].

[4] “Commission Implementing Regulation (EU) 2017/ 386 - of 6 March 2017 - amending Implementing Regulation (EU) No 1207 / 2011 laying down requirements for the performance and the interoperability of surveillance for the single European sky,” *Official Journal of the European Union*, no. L 59, p. 3.

[5] P. Puricer and P. Kovar, “Měření a stanovení parametrů ADS-B kanálu na kmitočtu 1090 MHz (Mesurement and Determination of the ADS-B Channel Parameters at the Frequency 1090 MHz. Resarch Report for project TA01030722 ADS-B/TIS-B Integrated System,” CTU Prague, Prague, Research Report, 2013.

[6] P. Puricer, P. Kovar, and M. Barta, “Modernized Solar Radio Spectrograph in the L Band Based on Software Defined Radio,” *Electronics*, vol. 8, no. 8 (861), pp. 1–16, Aug. 2019.

[7] Lord Bowden, “The story of IFF (Identification Friend or Foe),” *IEE Proceedings A - Physical Science, Measurement and Instrumentation, Management and Education - Reviews*, vol. 132, no. 6, pp. 435–437, Oct. 1985.

[8] International Civil Aviation Organization, “Manual on the Secondary Surveillance Radar (SSR) Systems. Third Edition.” International Civil Aviation Organization, 2004.

[9] International Civil Aviation Organization, “Annex 10 - Aeronautical Telecommunications. Volume IV - Surveillance and Collision Avoidance Systems. Fifth Edition.” International Civil Aviation Organization, 2014.

[10] ICAO, “Circular 174-AN/110 Secondary Surveillance Radar Mode S Advisory Circular.” ICAO, 1983.

[11] International Civil Aviation Organization, “Annex 10 - Aeronautical Telecommunications. Volume III - Communication Systems. Second Edition.” International Civil Aviation Organization, 2007.

[12] RTCA, Inc., “RTCA/DO-260B, Minimum Operational Performance Standards for 1090 MHz extended Squitter Automatic Dependent Surveillance – Broadcast (ADS-B) and Traffic Information Services – Broadcast (TIS-B).” RTCA, Inc., 2009.

[13] J. L. Gertz, “Fundamentals of Mode S Parity Coding. DOT/FAA/PM-83/6 Project report.” Lincoln Laboratory, MIT, 1984.

[14] “Technical Provisions for Mode S Services and Extended Squitter, 2nd Edition.” Inter- national Civil Aviation Organization, 2012.

[15] *Radio Direction Finding. Field manual FM30-476*. United States. Department of the Army, 1977.
[16] M. I. Skolnik, *Radar Handbook*, 3rd edition. McGraw-Hill, 2008.
[17] H. You, X. Jianjuan, and G. Xin, *Radar Data Processing with Applications*, 1st edition. Singapore: John Wiley & Sons, Ltd, 2016.
[18] M. G. Stock *et al.*, "Continuous broadband digital interferometry of lightning using a generalized cross-correlation algorithm," *Journal of Geophysical Research: Atmospheres*, vol. 119, 2014.
[19] R. A. Thompson, J. M. Moran, and G. W. Swenson Jr., *Interferometry and Synthesis in Radio Astronomy*, 3rd edition. Cham, Switzerland: Springer, Cham, 2017.
[20] I. Jami, M. Ali, and R. F. Ormondroyd, "Comparison of methods of locating and tracking cellular mobiles," in *IEE Colloquium on Novel Methods of Location and Tracking of Cellular Mobiles and Their System Applications (Ref. No. 1999/046)*, 1999, pp. 1/1-1/6.
[21] A. Drosopoulos and S. Haykin, "Angle-of-Arrival Estimation in the Presence of Multipath," in *Adaptive Radar Signal Processing*, vol. 2007, John Wiley & Sons, Inc., 2007.
[22] H. Lee, K. Lee, and K. You, "AOA Measurement based Localization Using RLS Algorithm under NLOS Environment," *Journal of Physics: Conference Series*, vol. 1060, no. 1, pp. 1–6, 2018.
[23] J. Latvala, J. Syrjärinne, H. Ikonen, and J. Niittylahti, "Evaluation of RSSI-based human tracking," in *2000 10th European Signal Processing Conference*, 2000, pp. 1–4.
[24] S. Shukri *et al.*, "RSSI-based Device Free Localization for Elderly Care Application," in *2nd International Conference on Internet of Things, Big Data and Security - Volume 1: IoTBDS*, Porto, Portugal, 2017, pp. 125–135.
[25] M. Vossiek, L. Wiebking, P. Gulden, J. Wieghardt, C. Hoffmann, and P. Heide, "Wireless local positioning," *IEEE Microwave Magazine*, vol. 4, no. 4, pp. 77–86, Dec. 2003.
[26] J. Yin, Q. Yang, and L. M. Ni, "Learning Adaptive Temporal Radio Maps for Signal-Strength-Based Location Estimation," *IEEE Transactions on Mobile Computing*, vol. 7, no. 7, pp. 869–883, Jul. 2008.
[27] J. Ying and K. Pahlavan, "Precision of RSS-Based Localization in the IoT," *International Journal of Wireless Information Networks*, vol. 26, no. 2, pp. 10–23, 2019.
[28] S. B. Wibowo and M. Klepal, "Rao-Blackwellized particle filter for pattern matching indoor localisation," in *2010 Ubiquitous Positioning Indoor Navigation and Location Based Service*, 2010, pp. 1–6.
[29] E. D. Kaplan and C. Hegarty, *Understanding GPS: Principles And Applications*, 2nd edition. Artech House, 2005.
[30] D. Doberstein, *Fundamentals of GPS Receivers: A Hardware Approach*. Springer Science & Business Media, 2011.
[31] B. Hofmann-Wellenhof, H. Lichtenegger, and E. Wasle, *GNSS – Global Navigation Satellite Systems: GPS, GLONASS, Galileo, and more*. Springer Science & Business Media, 2008.
[32] J. B.-Y. Tsui, *Fundamentals of Global Positioning System Receivers: A Software Approach*. John Wiley & Sons, 2005.

[33] E. Shytermeja, “Robust GNSS Positioning in Urban Environment,” in *Accuracy of GNSS Methods*, Dogan Ugur Sanli, Ed. IntechOpen, 2018, pp. 29–46.
[34] H. Liu, H. Darabi, P. Banerjee, and J. Liu, “Survey of Wireless Indoor Positioning Techniques and Systems,” *IEEE Transactions on Systems, Man, and Cybernetics, Part C (Applications and Reviews)*, vol. 37, no. 6, pp. 1067–1080, Nov. 2007.
[35] K. Pahlavan, X. Li, M. Ylianttila, R. Chana, and M. Latva-aho, “An Overview of Wireless Indoor Geolocation Techniques and Systems,” in *Lecture Notes in Computer Science*, 2000, vol. 1818, pp. 1–13.
[36] K. Pahlavan, Xinrong Li, and J. P. Makela, “Indoor geolocation science and technology,” *IEEE Communications Magazine*, vol. 40, no. 2, pp. 112–118, Feb. 2002.
[37] I. Sharp and K. Yu, *Wireless Positioning: Principles and Practice*. Springer, 2019.
[38] L. O. Krause, “A Direct Solution to GPS-Type Navigation Equations,” *IEEE Transactions on Aerospace and Electronic Systems*, vol. AES-23, no. 2, pp. 225–232, Mar. 1987.
[39] S. Bancroft, “An Algebraic Solution of the GPS Equations,” *IEEE Transactions on Aerospace and Electronic Systems*, vol. AES-21, no. 1, pp. 56–59, Jan. 1985.
[40] J. Yan, C. C. J. M. Tiberius, G. Bellusci, and G. J. M. Janssen, “A Novel Non-Iterative Localization Solution,” in *GLOBECOM 2009 - 2009 IEEE Global Telecommunications Conference*, Honolulu, HI, USA, 2009, pp. 1–6.
[41] C. T. Kelley, *Iterative Methods for Optimization*. Society for Industrial and Applied Mathematics, 1999.
[42] K. Levenberg, “A method for the solution of certain non-linear problems in least squares,” *Quart. Appl. Math.*, vol. 2, no. 2, pp. 164–168, 1944.
[43] R. E. Kalman and R. S. Bucy, “New Results in Linear Filtering and Prediction Theory,” *J. Basic Engineering*, vol. 83, no. 1, pp. 95–108, 1961.
[44] K. W. Cheung, H. C. So, W.- Ma, and Y. T. Chan, “Least squares algorithms for time-of-arrival-based mobile location,” *IEEE Transactions on Signal Processing*, vol. 52, no. 4, pp. 1121–1130, Apr. 2004.
[45] H. Wei, Q. Wan, Z. Chen, and S. Ye, “A Novel Weighted Multidimensional Scaling Analysis for Time-of-Arrival-Based Mobile Location,” *IEEE Transactions on Signal Processing*, vol. 56, no. 7, pp. 3018–3022, Jul. 2008.
[46] J. Yan, C. C. J. M. Tiberius, P. J. G. Teunissen, G. Bellusci, and G. J. M. Janssen, “A Framework for Low Complexity Least-Squares Localization With High Accuracy,” *IEEE Transactions on Signal Processing*, vol. 58, no. 9, pp. 4836–4847, Sep. 2010.
[47] R. J. Dippy, “Gee: a radio navigational aid,” *Journal of the Institution of Electrical Engineers - Part IIIA: Radiolocation*, vol. 93, no. 2, pp. 468–480, 1946.
[48] G. Hefley, *The Development Of Loran-C Navigation And Timing*. Washington : U.S. Dept. of Commerce, National Bureau of Standards : For sale by the Supt. of Docs., U.S. G.P.O., 1972.
[49] R. Yamasaki, A. Ogino, T. Tamaki, T. Uta, N. Matsuzawa, and T. Kato, “TDOA location system for IEEE 802.11b WLAN,” in *IEEE Wireless Communications and Networking Conference, 2005.*, New Orleans, LA, USA, 2005, vol. 4, pp. 2338-2343 Vol. 4.
[50] Y. Li, G. Qi, and A. Sheng, “Performance Metric on the Best Achievable Accuracy for Hybrid TOA/AOA Target Localization,” *IEEE Communications Letters*, vol. 22, no. 7, pp. 1474–1477, Jul. 2018.

[51] S. Galler, W. Gerok, J. Schroeder, Kyandoghere Kyamakya, and T. Kaiser, “Combined AOA/TOA UWB localization,” in *2007 International Symposium on Communications and Information Technologies*, 2007, pp. 1049–1053.
[52] R. Zekavat and R. M. Buehrer, “Wireless Local Positioning Systems,” in *Handbook of Position Location: Theory, Practice, and Advances*, IEEE, 2019, pp. 1263–1288.
[53] O. Kanhere and T. S. Rappaport, “Position Locationing for Millimeter Wave Systems,” in *2018 IEEE Global Communications Conference (GLOBECOM)*, 2018, pp. 206–212.
[54] A. Cidronali, G. Collodi, S. Maddio, M. Passafiume, and G. Pelosi, “2-D DoA Anchor Suitable for Indoor Positioning Systems Based on Space and Frequency Diversity for Legacy WLAN,” *IEEE Microwave and Wireless Components Letters*, vol. 28, no. 7, pp. 627–629, Jul. 2018.
[55] M. Gunia, Y. Lu, N. Joram, and F. Ellinger, “On the Precision of Common Individual or Hybrid Positioning Systems,” in *2019 International Conference on Localization and GNSS (ICL-GNSS)*, 2019, pp. 1–6.
[56] A. Noroozi and M. A. Sebt, “Algebraic solution of source location estimation using TDOA and AOA measurements,” in *2017 Iranian Conference on Electrical Engineering (ICEE)*, 2017, pp. 1609–1614.
[57] A. Noroozi and M. A. Sebt, “Algebraic solution for three-dimensional TDOA/AOA localisation in multiple-input–multiple-output passive radar,” *Sonar Navigation IET Radar*, vol. 12, no. 1, pp. 21–29, 2018.
[58] Chin-Der Wann, Yi-Jing Yeh, and Chih-Sheng Hsueh, “Hybrid TDOA/AOA Indoor Positioning and Tracking Using Extended Kalman Filters,” in *2006 IEEE 63rd Vehicular Technology Conference*, 2006, vol. 3, pp. 1058–1062.
[59] W. Wang, P. Bai, X. Liang, Y. Wang, and J. Zhang, “Optimal deployment of sensor–emitter geometries for hybrid localisation using TDOA and AOA measurements,” *IET Science, Measurement Technology*, vol. 13, no. 5, pp. 622–631, 2019.
[60] Y. Zhao, Z. Li, B. Hao, P. Wan, and L. Wang, “How to select the best sensors for TDOA and TDOA/AOA localization?,” *China Communications*, vol. 16, no. 2, pp. 134–145, Feb. 2019.
[61] H. Takshi, M. Nemati, E. Arvas, and T. Baykas, “A novel one-base station hybrid positioning method,” in *2017 IEEE International Black Sea Conference on Communications and Networking (BlackSeaCom)*, Istanbul, Turkey, 2017, pp. 1–5.
[62] M. Fowler and X. Hu, “Signal models for TDOA/FDOA estimation,” *Aerospace and Electronic Systems, IEEE Transactions on*, vol. 44, no. 4, pp. 1543–1550, 2008.
[63] A. Y. Ali and I. B. Jasim, “Tracking Mobile Emitter Using TDOA and FDOA Techniques,” *International Journal of Emerging Engineering Research and Technology*, vol. 3, no. 9, pp. 45–54, 2015.
[64] Z. Liu, Y. Zhao, D. Hu, and C. Liu, “A Moving Source Localization Method for Distributed Passive Sensor Using TDOA and FDOA Measurements,” *International Journal of Antennas and Propagation*, vol. 2016, p. 12, 2016.
[65] S. M. Kay, *Fundamentals of Statistical Signal Processing: Estimation Theory*. Upper Saddle River, NJ, USA: Prentice-Hall, Inc., 1993.
[66] R. Kaune, J. Hörst, and W. Koch, “Accuracy analysis for TDOA localization in sensor networks,” in *14th International Conference on Information Fusion*, Chicago, IL, USA, 2011, pp. 1647–1654.
[67] R. Kaune, “Accuracy studies for TDOA and TOA localization,” in *2012 15th International Conference on Information Fusion*, Singapore, 2012, pp. 408–415.

[68] A. Jasch, T. Feuerle, G. Scoor, and P. Hecker, “Geometrical siting considerations for wide area multilateration systems,” in *IEEE/ION Position, Location and Navigation Symposium*, 2010, pp. 1304–1308.
[69] C. S. Carrano, C. T. Bridgwood, and K. M. Groves, “Impacts of the December 2006 solar radio bursts on the performance of GPS,” *Radio Science*, vol. 44, no. 1, pp. 1–12, 2009.
[70] P. Das, J. Vilà-Valls, E. Chaumette, F. Vincent, L. Davain, and S. Bonnabel, “On the Accuracy Limit of Time-delay Estimation with a Band-limited Signal,” in *ICASSP 2019 - 2019 IEEE International Conference on Acoustics, Speech and Signal Processing (ICASSP)*, 2019, pp. 5282–5286.
[71] S. Kay and N. Vankayalapati, “Improvement of TDOA Position Fixing Using the Likelihood Curvature,” *IEEE Transactions on Signal Processing*, vol. 61, no. 8, pp. 1910–1914, Apr. 2013.
[72] N. Vankayalapati, S. Kay, and Quan Ding, “TDOA based direct positioning maximum likelihood estimator and the cramer-rao bound,” *IEEE Trans. Aerosp. Electron. Syst.*, vol. 50, no. 3, pp. 1616–1635, Jul. 2014.
[73] S. J. Julier and J. K. Uhlmann, “Unscented filtering and nonlinear estimation,” *Proceedings of the IEEE*, vol. 92, no. 3, pp. 401–422, Mar. 2004.
[74] R. Kaune, “Gaussian Mixture (GM) Passive Localization using Time Difference of Arrival (TDOA),” in *GI Jahrestagung 2009*, Lübeck, Germany, 2009, pp. 2375–2381.
[75] J. Yan, C. C. J. M. Tiberius, G. J. M. Janssen, P. J. G. Teunissen, and G. Bellusci, “Review of range-based positioning algorithms,” *IEEE Aerospace and Electronic Systems Magazine*, vol. 28, no. 8, pp. 2–27, Aug. 2013.
[76] J.-Y. Do, M. Rabinowitz, and P. Enge, “Performance of TOA and TDOA in a Non-homogeneous Transmitter Network Combining GPS and Terrestrial Signals,” in *Proceedings of the 2006 National Technical Meeting of The Institute of Navigation*, Monterey, CA, USA, 2006, pp. 642–649.
[77] P. J. G. Teunissen, “Nonlinear least squares,” *Manuscripta Geodaetica*, vol. 15, no. 3, pp. 137–150, 1990.
[78] W. H. Foy, “Position-Location Solutions by Taylor-Series Estimation,” *IEEE Transactions on Aerospace and Electronic Systems*, vol. AES-12, no. 2, pp. 187–194, Mar. 1976.
[79] D. J. Torrieri, “Statistical Theory of Passive Location Systems,” *IEEE Transactions on Aerospace and Electronic Systems*, vol. AES-20, no. 2, pp. 183–198, Mar. 1984.
[80] K. Kuttler, *Linear Algebra, Theory And Applications*. Bringham Young University,USA: Saylor Foundation, 2012.
[81] J. Yang, H. Lee, and K. Moessner, “Multilateration localization based on Singular Value Decomposition for 3D indoor positioning,” in *2016 International Conference on Indoor Positioning and Indoor Navigation (IPIN)*, 2016, pp. 1–8.
[82] H. Schau and A. Robinson, “Passive source localization employing intersecting spherical surfaces from time-of-arrival differences,” *IEEE Transactions on Acoustics, Speech, and Signal Processing*, vol. 35, no. 8, pp. 1223–1225, Aug. 1987.
[83] J. Smith and J. Abel, “Closed-form least-squares source location estimation from range-difference measurements,” *IEEE Transactions on Acoustics, Speech, and Signal Processing*, vol. 35, no. 12, pp. 1661–1669, Dec. 1987.

[84] J. Caffery, “A new approach to the geometry of TOA location,” in *Vehicular Technology Conference Fall 2000. IEEE VTS Fall VTC2000*, Boston, MA, USA, 2000, vol. 4, pp. 1943–1949 vol.4.
[85] B. Friedlander, “A passive localization algorithm and its accuracy analysis,” *IEEE Journal of Oceanic Engineering*, vol. 12, no. 1, pp. 234–245, Jan. 1987.
[86] B. T. Fang, “Simple solutions for hyperbolic and related position fixes,” *IEEE Transactions on Aerospace and Electronic Systems*, vol. 26, no. 5, pp. 748–753, Sep. 1990.
[87] Y. T. Chan and K. C. Ho, “A simple and efficient estimator for hyperbolic location,” *IEEE Transactions on Signal Processing*, vol. 42, no. 8, pp. 1905–1915, Aug. 1994.
[88] Z. Liu, D. Hu, Y. Zhao, and Y. Zhao, “An algebraic method for moving source localization using TDOA, FDOA, and differential Doppler rate measurements with receiver location errors,” *EURASIP Journal on Advances in Signal Processing*, vol. 2019, no. 1, p. 25, Apr. 2019.
[89] T. Le and N. Ono, “Closed-Form and Near Closed-Form Solutions for TDOA-Based Joint Source and Sensor Localization,” *IEEE Transactions on Signal Processing*, vol. 65, no. 5, pp. 1207–1221, Mar. 2017.
[90] M. D. Gillette and H. F. Silverman, “A Linear Closed-Form Algorithm for Source Localization From Time-Differences of Arrival,” *IEEE Signal Processing Letters*, vol. 15, pp. 1–4, 2008.
[91] A. Goldsmith, *Wireless Communications*, 1st edition. Cambridge,UK: Cambridge University Press, 2005.
[92] Y. Okumura, T. Kawano, K. Fukuda, and E. Ohmori, “Field Strength and Its Variability in VHF and UHF Land-Mobile Radio Service,” *Review of the Electrical Communications Laboratory*, vol. 16, no. 9–10, pp. 825–873, 1968.
[93] H. Kumar Sharma, S. Sahu, and S. Sharma, “Enhanced Cost231 W.I. Propagation Model in Wireless Network,” *IJCA*, vol. 19, no. 6, pp. 36–42, Apr. 2011.
[94] V. Erceg *et al.*, “An empirically based path loss model for wireless channels in suburban environments,” *IEEE Journal on Selected Areas in Communications*, vol. 17, no. 7, pp. 1205–1211, Jul. 1999.
[95] M. Gudmundson, “Correlation model for shadow fading in mobile radio systems,” *Electronics Letters*, vol. 27, no. 23, pp. 2145–2146, Nov. 1991.
[96] ITU, “Recommendation ITU-R P.1816-3. The prediction of the time and the spatial profile for broadband land mobile services using UHF and SHF bands.” ITU, 2015.
[97] J. G. Proakis and M. Salehi, *Digital Communications*, 5th edition. McGraw-Hill, 2008.
[98] B. Sklar, *Digital Communications: Fundamentals and Applications*, Second edition. New Jersey, USA: Prentice Hall P T R, 2017.
[99] M. Nakagami, “The m-Distribution—A General Formula of Intensity Distribution of Rapid Fading,” in *Statistical Methods in Radio Wave Propagation*, W. C. Hoffman, Ed. Pergamon, 1960, pp. 3–36.
[100] Hong Shen Wang and N. Moayeri, “Finite-state Markov channel-a useful model for radio communication channels,” *IEEE Transactions on Vehicular Technology*, vol. 44, no. 1, pp. 163–171, Feb. 1995.
[101] ITU, “Recommendation ITU-R P.1411-9. Propagation data and prediction methods for the planning of short-range outdoor radiocommunication systems and radio local area networks in the frequency range 300 MHz to 100 GHz.” ITU, 2017.

[102] J. Marcum, “A statistical theory of target detection by pulsed radar,” *IRE Transactions on Information Theory*, vol. 6, no. 2, pp. 59–267, Apr. 1960.
[103] S. Parl, “A new method of calculating the generalized Q function (Corresp.),” *IEEE Transactions on Information Theory*, vol. 26, no. 1, pp. 121–124, Jan. 1980.
[104] M. Z. Bocus, C. P. Dettmann, and J. P. Coon, “An Approximation of the First Order Marcum Q-Function with Application to Network Connectivity Analysis,” *IEEE Communications Letters*, vol. 17, no. 3, pp. 499–502, Mar. 2013.
[105] B. R. Mahafza, *Radar Signal Analysis and Processing Using MATLAB*, 1st edition. Boca Raton, FL, USA: Chapman & Hall/CRC, 2008.
[106] Neyman Jerzy, Pearson Egon Sharpe, and Pearson Karl, “IX. On the problem of the most efficient tests of statistical hypotheses,” *Philosophical Transactions of the Royal Society of London. Series A, Containing Papers of a Mathematical or Physical Character*, vol. 231, no. 694–706, pp. 289–337, Feb. 1933.
[107] S. M. Kay, *Fundamentals of Statistical Signal Processing: Detection theory*. Upper Saddle River, NJ, USA: PTR Prentice-Hall, 1993.
[108] K. Zhao, M. Zhu, X. Yang, and J. Zhang, “A New Method of Creating Minimal-Order Markov Set and Transition States of M/N Sliding Window,” *IEEE Access*, vol. 7, pp. 94350–94364, 2019.
[109] G. Dillard, “A moving-window detector for binary integration,” *IEEE Transactions on Information Theory*, vol. 13, no. 1, pp. 2–6, Jan. 1967.
[110] W. Pei and T. Bin, “Detection and estimation of non-cooperative uniform pulse position modulated radar signals at low SNR,” in *2013 International Conference on Communications, Circuits and Systems, ICCCAS 2013*, Chengdu, China, 2013, vol. 2, pp. 214–217.
[111] K. M. Hock, “Narrowband weak signal detection by higher order spectrum,” *IEEE Transactions on Signal Processing*, vol. 44, no. 4, pp. 874–879, Apr. 1996.
[112] M. Sanaullah, “A Review of Higher Order Statistics and Spectra inCommunication Systems,” *Global Journal of Science Frontier Research Physics and Space Science*, vol. 13, no. 4, p. 21, 2013.
[113] B. W. Parkinson and J. J. Spilker, *Global Positioning System: Theory & Applications (Volume One)*, 1st edition. Washington DC: American Institute of Aeronautics and Astronautics, Inc., 1996.
[114] Y. H. Chen, S. Lo, P. Enge, and S. S. Jan, “Evaluation comparison of ranging using Universal Access Transceiver (UAT) and 1090 MHz Mode S Extended Squitter (Mode S ES),” in *2014 IEEE/ION Position, Location and Navigation Symposium - PLANS 2014*, Monterey, CA, USA, 2014, pp. 915–925.
[115] M.-S. Huang, R. M. Narayanan, Y. Zhang, and A. Feinberg, “Tracking of Noncooperative Airborne Targets Using ADS-B Signal and Radar Sensing,” *International Journal of Aerospace Engineering*, vol. 2013, no. 11, p. 12, 2013.
[116] R. D. Clarke, “An application of the Poisson distribution,” *Journal of the Institute of Actuaries*, vol. 72, no. 3, pp. 481–481, 1946.
[117] C. R. Johnson Jr, W. A. Sethares, and A. G. Klein, *Software Receiver Design: Build your Own Digital Communication System in Five Easy Steps*. Cambridge University Press, 2011.
[118] A. Mohan, A. Mishra, M. Karthik, N. Padma, G. Prashanth, and R. Deepa, “A novel pre-distortion type adaptive channel equalisation technique for SISO systems,” in *2011 International Conference on Emerging Trends in Electrical and Computer Technology*, Nagercoil, India, 2011, pp. 1047–1050.

[119] N. Miroshnikova, “Adaptive blind equalizer for HF channels,” in *2017 Systems of Signal Synchronization, Generating and Processing in Telecommunications (SINKHROINFO)*, Kazan, Russia, 2017, pp. 1–5.
[120] Lang Tong, Guanghan Xu, B. Hassibi, and T. Kailath, “Blind channel identification based on second-order statistics: a frequency-domain approach,” *IEEE Transactions on Information Theory*, vol. 41, no. 1, pp. 329–334, Jan. 1995.
[121] A. Moussa, M. Frikel, M. Pouliquen, S. Bedoui, K. Abderrahim, and M. M’Saad, “Performance of a blind equalization algorithm for Rayleigh and Rician channels,” in *2016 17th International Conference on Sciences and Techniques of Automatic Control and Computer Engineering (STA)*, Sousse, Tunisia, 2016, pp. 685–690.
[122] H. Yan and Q. Zhaoyang, “Blind equalization for burst signals based on soft information of constellation,” in *2017 IEEE 2nd Advanced Information Technology, Electronic and Automation Control Conference (IAEAC)*, Chongqing, China, 2017, pp. 1656–1660.
[123] P. Puricer and P. Kovar, “ADS-B Reception at Airport Airside Areas using TDL-based Channel Modeling,” *IJAST*, vol. 5, no. 4, pp. 1–9, 2015.
[124] O. Jakubov, P. Kovar, P. Kacmarik, and F. Vejrazka, “The Witch Navigator - A Low Cost GNSS Software Receiver for Advanced Processing Techniques,” *Radioengineering*, vol. 19, no. 4, pp. 536–543, 2010.
[125] H. L. Van Trees, *Detection, Estimation, and Modulation Theory, Part I: Detection, Estimation, and Linear Modulation Theory.*, 1st edition. John Wiley & Sons, Ltd, 2001.
[126] nuand Inc., “bladeRF USB 3.0 Software Defined Radio.” [Online]. Available: https://www.nuand.com/bladeRF-brief.pdf. [Accessed: 22-Aug-2019].
[127] A. Csete, “Gqrx SDR – Open source software defined radio,” 2019. [Online]. Available: http://gqrx.dk/. [Accessed: 22-Aug-2019].
[128] S. Sanfilippo, *Dump1090 is a simple Mode S decoder for RTLSDR devices: antirez/dump1090*. 2019.
[129] F. Horlin and A. Bourdoux, *Digital Compensation for Analog Front-Ends*, 1st edition. Wiley Blackwell, 2008.
[130] “Gatwick Aviation Society.” [Online]. Available: http://www.gatwickaviationsociety.org.uk/modeslookup.asp. [Accessed: 23-Aug-2019].
[131] N. Petrochilos, G. Galati, and E. Piracci, “Separation of SSR Signals by Array Processing in Multilateration Systems,” *Aerospace and Electronic Systems, IEEE Transactions on*, vol. 45, pp. 965–982, 2009.

Bibliography

The publications listed below were realized and published during the work on the thesis.

The publications related to the topics of the thesis

Articles in impacted journals

Puričer, P.; Kovář, P.; Bárta, M. Modernized solar radio spectrograph in the L band based on software defined radio. Electronics. 2019, 8(8), 1-16. ISSN 2079-9292. DOI 10.3390/electronics8080861.(authors participation: uniform)

Articles in peer reviewed journals

Morong, T.; Puričer, P.; Kovář, P. Study of the GNSS Jamming in Real Environment. International Journal of Electronics and Telecommunications. 2019, 65(1), 65-70. ISSN 2300-1933. DOI 10.24425/ijet.2019.126284.(authors participation: uniform)

Puričer, P.; Kovář, P. ADS-B Reception at Airport Airside Areas using TDL-based Channel Modeling. International Journal of Applied Science and Technology. 2015, 5(4), 55-63. ISSN 2221-0997.(authors participation: uniform)

Publications with record in WoS

Kovář, P.; Puričer, P. Experimental SDR receiver for monitoring and processing of solar radio bursts. In: 22nd 2017 International Conference on Applied Electronics. 22nd International Conference Applied Electronics 2017, Pilsen, 2017-09-05/2017-09-06. Pilsen: University of West Bohemia, 2017. p. 83-86. ISSN 1803-7232. ISBN 978-80-261-0641-8. DOI 10.23919/AE.2017.8053588.(authors participation: uniform)

Puričer, P.; Kovář, P. Estimation of parameters for ground ADS-B radio channel model. In: Proceedings of 25th International Conference RADIOELEKTRONIKA 2015. Radioelektronika 2015 25th International Conference, Pardubice, 2015-04-21/2015-04-23. Pardubice: University of Pardubice, 2015. p. 199-202. ISBN 978-1-4799-8117-5. DOI 10.1109/RADIOELEK.2015.7129008.(authors participation: uniform)

Puričer, P.; Kovář, P. Empirical Model of the ADS-B Channel for Airport Area. In: 19th International Conference on Applied Electronics 2014. Pilsen, 2014-10-09/2014-10-10. Pilsen: University of West Bohemia, 2015. p. 255-258. ISSN 1803-7232. ISBN 978-80-261-0276-2. DOI 10.1109/AE.2014.7011714.(authors participation: uniform)

Other publications

Publications with record in WoS

Puričer, P.; Laifr, J.; Kovář, P.; Mikeš, J. Telemetry System of FIK III. Stratospheric Balloon. In: FLIEGEL, K. and S. VÍTEK, eds. 2018 28th International Conference Radioelektronika. 28th International Conference Radioelektronika 2018, Praha, 2018-04-19/2018-04-20. IEEE (Institute of Electrical and Electronics Engineers), 2018. p. 1-4. ISBN 978-1-5386-2485-2. DOI 10.1109/RADIOELEK.2018.8376394.(authors participation: uniform)

Puričer, P.; Kovář, P.; Mikeš, J.; Kákona, J. Telemetry system for research stratospheric balloon. In: 22nd 2017 International Conference on Applied Electronics. 22nd International Conference Applied Electronics 2017, Pilsen, 2017-09-05/2017-09-06. Pilsen: University of West Bohemia, 2017. p. 171-174. ISSN 1803-7232. ISBN 978-80-261-0641-8. DOI 10.23919/AE.2017.8053608.(authors participation: uniform)

Dobeš, J.; Grábner, M.; Puričer, P.; Vejražka, F.; Míchal, J.; Popp, J. A new assessment of pHEMT models by comparing relative errors of drain current and its derivatives up to the third order. In: MONEBHURRUN, V. and A. DOUYÈRE, eds. 2016 IEEE Radio and Antenna Days of the Indian Ocean (RADIO). IEEE Radio and Antenna Days of the Indian Ocean (RADIO), Saint-Gilles Les Bains, Réunion Island, 2016-10-10/2016-10-13. Piscataway, NJ: IEEE, 2016. ISBN 978-1-5090-2580-0. DOI 10.1109/RADIO.2016.7772016. Available from: http://ieeexplore.ieee.org/stamp/stamp.jsp?arnumber=7772016(authors participation: 50-10-10-10-10-10)

Kačmařík, P.; Kovář, P.; Roule, P.; Puričer, P.; Vejražka, F. Dual-frequency Tracking of Compass Signals: Compass Implementation to the Witch Navigator Receiver. In: International Symposium on GPS/GNSS 2012 Proceedings. International Symposium on GPS/GNSS 2012, Xi'an, 2012-10-31/2012-11-02. Xi'an: Chang'an University, 2012. p. 1-6.(authors participation: uniform)

Appendix A – The closed form of solution of hyperbolic equation

The simple closed form solution presented by [Fang1990] has been generalized here for arbitrary location of receivers. For simplicity reasons, the 2D position determination was chosen for demonstration of the method but it can be expanded to 3D case as well. For our case, the positions of the receivers and transmitter are at common plane in 3D with constant *z* coordinate. The transmitter position expressed in $(x, y) \in \mathbf{R}^2$ is related to the position on this plane.

The range distance between the transmitter $\boldsymbol{u}$ at (x_u, y_u) and chosen receiver $\boldsymbol{u}_i$ at $(x_i, y_i)$is

$$r_i = \sqrt{(x_u - x_i)^2 + (y_u - y_i)^2} \tag{A.1}$$

The difference in range distance between receiver $\mathbf{u}_i$ and chosen reference receiver $\mathbf{u}_k$ can be expressed as

$$r_{ik} = r_i - r_k \tag{A.2}$$

If we substitute (A.2) into (A.1) and square both sides of equation, we obtain

$$r_{ik}^2 + 2 r_{ik} r_k + r_k^2 = x_u^2 + y_u^2 + x_i^2 + y_i^2 - 2 x_u x_i - 2 y_u y_i \tag{A.3}$$

that can be further rewritten as

$$r_{ik}^2 + 2 r_{ik} r_k = x_i^2 + y_i^2 - 2 x_u x_{ik} - 2 y_u y_{ik} - x_k^2 - y_k^2 \tag{A.4}$$

where $x_{ik} = x_i - x_k$ and $y_{ik} = y_i - y_k$.

If we consider system of M=3 receivers $\boldsymbol{u}_i\ (x_i, y_i)$, $\boldsymbol{u}_j\ (x_j, y_j)$, $\boldsymbol{u}_k\ (x_k, y_k)$ the (A.4) provides set of $M-1$ equations

$$\begin{aligned} 2 r_{ik} r_k + 2 y_u y_{ik} &= x_i^2 + y_i^2 - x_k^2 - y_k^2 - 2 x_u x_{ik} - r_{ik}^2 \\ 2 r_{jk} r_k + 2 y_u y_{jk} &= x_j^2 + y_j^2 - x_k^2 - y_k^2 - 2 x_u x_{jk} - r_{jk}^2 \end{aligned} \tag{A.5}$$

Considering results in form of

$$y_u = g\,x_u + h \tag{A.6}$$

we obtain from combination of (A.5) and (A.6)

$$g = \frac{x_{ik}\,r_{jk} - x_{jk}\,r_{ik}}{y_{jk}\,r_{ik} - y_{ik}\,r_{jk}} \quad , \quad h = \frac{(x_k^{\,2} + y_k^{\,2})\,r_{ji} + (x_j^{\,2} + y_j^{\,2})\,r_{ik} - (x_i^{\,2} + y_i^{\,2})\,r_{jk} + r_{ik}^{\,2}\,r_{jk} - r_{jk}^{\,2}\,r_{ik}}{2\,(y_{jk}\,r_{ik} - y_{ik}\,r_{jk})} \tag{A.7}$$

We can then substitute (A.6) into the first of equations (A.5) and we get following result in the form of quadratic equation for signle unknown parameter x_u

$$d\,x_u^{\,2} + e\,x_u + f = 0 \tag{A.8}$$

where

$$\begin{aligned} d &= 1 + g^2 - \frac{(x_{ik} - g\,y_{ik})^2}{r_{ik}^{\,2}} \\ e &= -2\,x_k - 2\,g\,(y_k - h) + \frac{1}{r_{ik}^{\,2}}\,(g\,y_{ik} - x_{ik})\,(x_i^{\,2} + y_i^{\,2} - x_k^{\,2} - y_k^{\,2} - 2\,h\,y_{ik} - r_{ik}^{\,2}) \\ f &= x_k^{\,2} + (y_k - h)^2 - \frac{1}{4\,r_{ik}^{\,2}}\,(x_i^{\,2} + y_i^{\,2} - x_k^{\,2} - y_k^{\,2} - 2\,h\,y_{ik} - r_{ik}^{\,2}) \end{aligned} \tag{A.9}$$

We can then easily solve this quadratic equation and obtain two values of target (transmitter) x coordinate $\hat{x}_{ua}$ and $\hat{x}_{ub}$. The remaining values $\hat{y}_{ua}$ and $\hat{y}_{ub}$ we obtain using (A.6).

Appendix B – The error parameters for ADS–B message start detection simulation

The values of means and standard deviations for errors in detection fo ADS–B signal start in scenario 2: channel with multipath.

Impulse response A

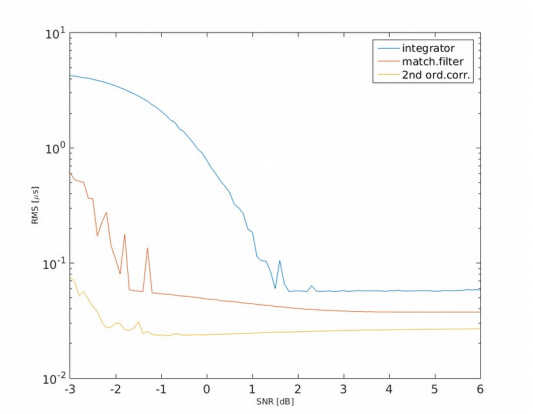

(1)

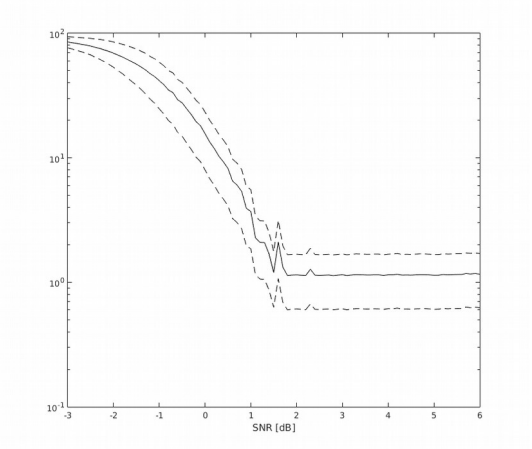

(2)

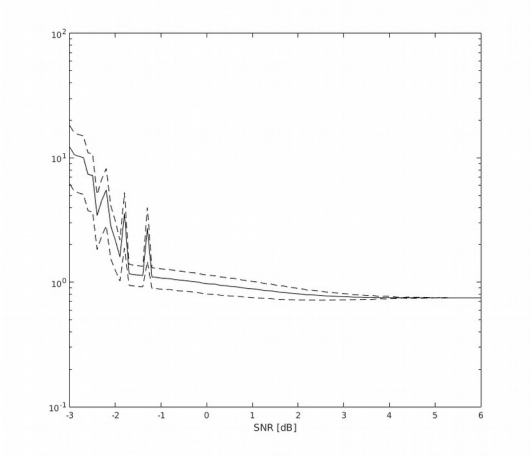

(3)

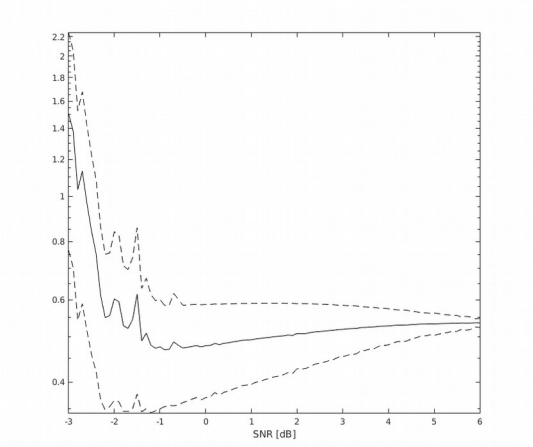

(4)

RMS error for all detectors (1) and Mean (solid) and standard deviation (dashed) of error in samples for integrator detector (2), matched filter (3) and second order correlator (4) for impulse response A in scenario 2

Impulse response B

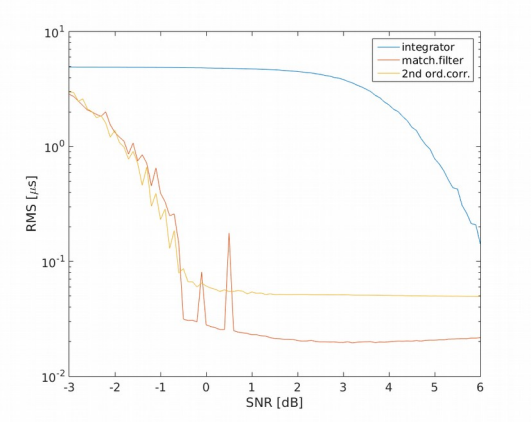

(1)

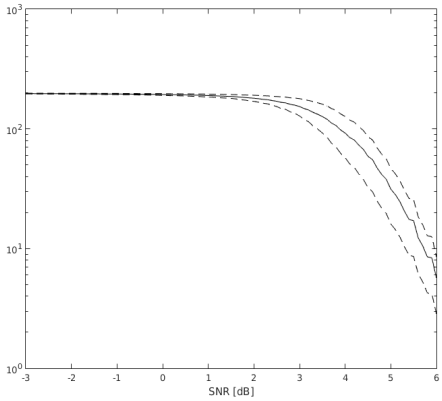

(2)

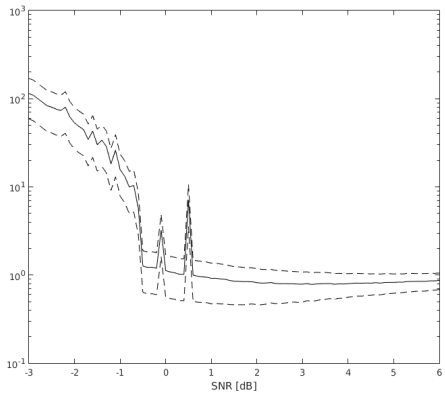

(3)

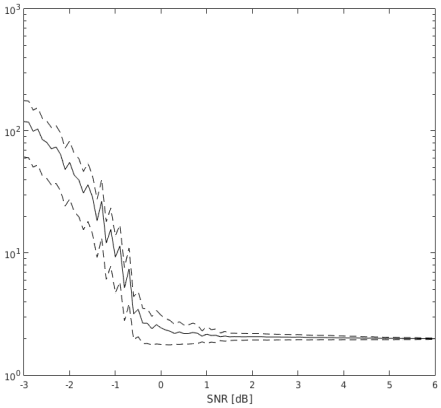

(4)

RMS error for all detectors (1) and Mean (solid) and standard deviation (dashed) of error in samples for integrator detector (2), matched filter (3) and second order correlator (4) for impulse response B in scenario 2

Impulse response C

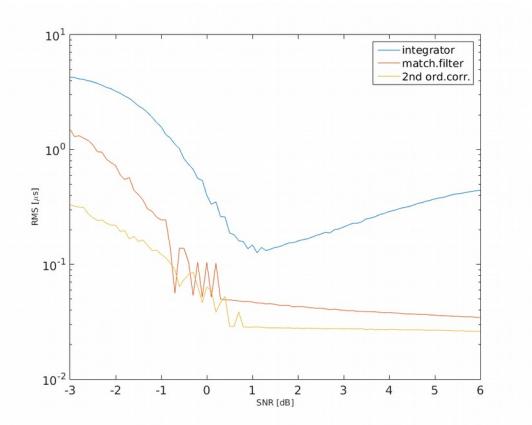

(1)

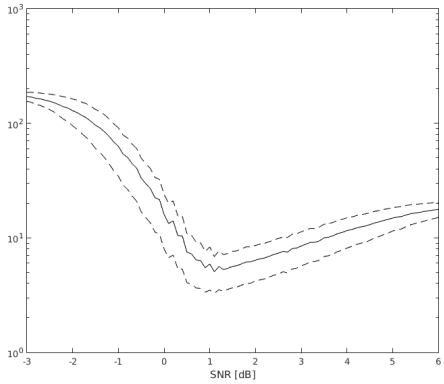

(2)

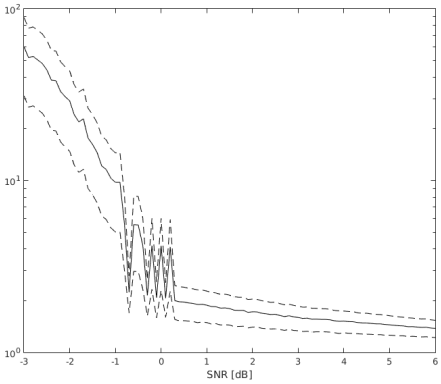

(3)

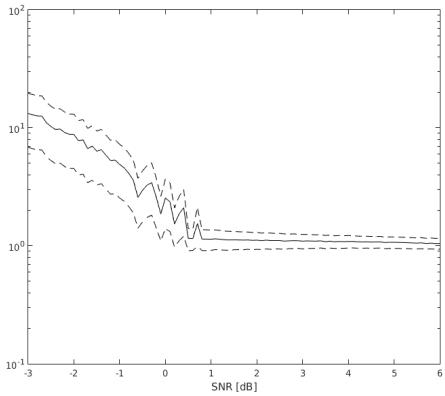

(4)

RMS error for all detectors (1) and Mean (solid) and standard deviation (dashed) of error in samples for integrator detector (2), matched filter (3) and second order correlator (4) for impulse response C in scenario 2

Appendix C – the combinations of values producing minimal BER

The following table shows values of equalizer length and delay producing minimal BER for simulations with impulse response (B).

SNR [dB]	δ [number of samples]	Equalizer length [no of taps]	SNR [dB]	δ [number of samples]	Equalizer length [no of taps]
-2	8	20	0.1	4	15
-1.9	7	18	0.2	4	15
-1.8	9	20	0.3	4	15
-1.7	7	18	0.4	3	14
-1.6	9	20	0.5	3	14
-1.5	8	19	0.6	7	17
-1.4	9	20	0.7	8	18
-1.3	8	19	0.8	3	13
-1.2	6	17	0.9	4	14
-1.1	7	18	1	4	14
-1	5	16	1.1	3	13
-0.9	5	16	1.2	7	17
-0.8	7	18	1.3	6	16
-0.7	6	17	1.4	2	12
-0.6	4	15	1.5	3	13
-0.5	6	17	1.6	2	12
-0.4	3	14	1.7	2	12
-0.3	5	16	1.8	1	11
-0.2	3	14	1.9	2	12
-0.1	3	14	2	2	12
0	3	14			

Appendix D – The characteristics of band pass filter Teroz 519

The band pass filter tuned to frequency 1090 Mhz. No possibility of power supply throughput for active antenna. Insertion loss: 2 dB.

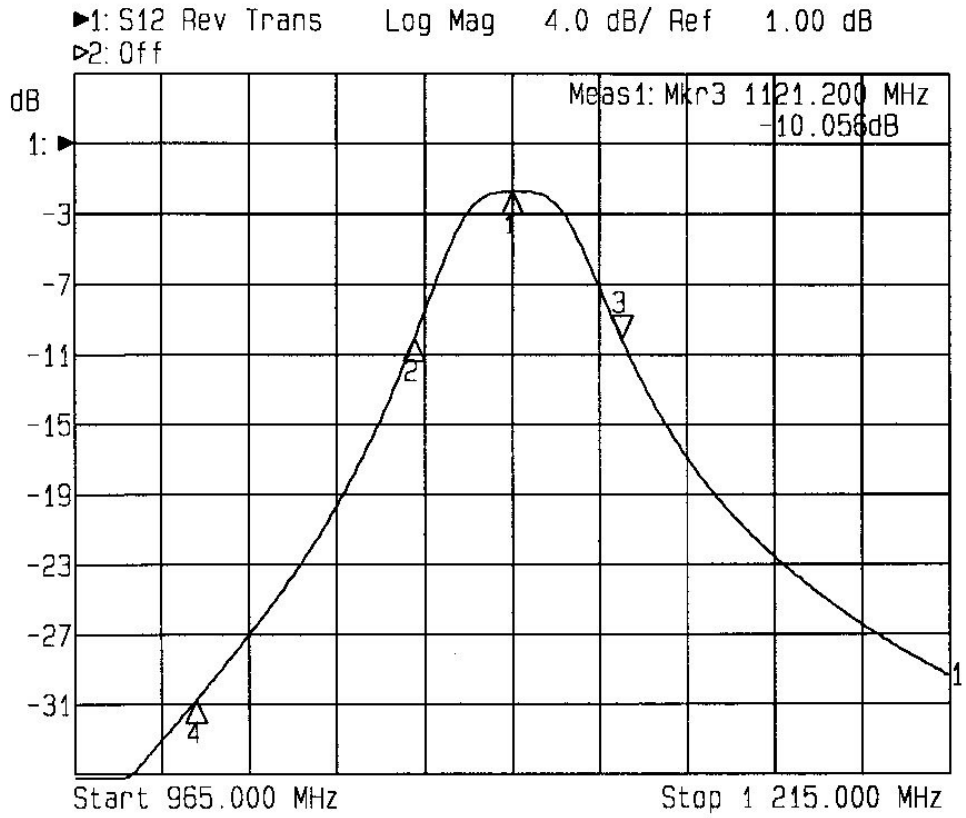

1: Mkr (MHz)	dB	2: Mkr (MHz)	dB
1: 1090.0000	-1.698		
2: 1062.1333	-10.073		
3> 1121.2000	-10.056		
4: 1000.0000	-30.782		